Manipulating Thermoacoustic Streaming

Measuring the Synergy of Laser-induced Temperature Gradients and Ultrasonic Pressure Fields in Acoustofluidic Microchannels

Martens, Franziska

2026

Document Version:
Publisher's PDF, also known as Version of record

Manipulating Thermoacoustic Streaming

Measuring the Synergy of Laser-induced Temperature Gradients and Ultrasonic Pressure Fields in Acoustofluidic Microchannels

Franziska Martens
Department of Biomedical Engineering
Faculty of Engineering | LTH | Lund University

Manipulating Thermoacoustic Streaming

Measuring the Synergy of Laser-induced Temperature Gradients and Ultrasonic Pressure Fields in Acoustofluidic Microchannels

Franziska Martens

LUND
UNIVERSITY

Doctoral Dissertation

by due permission of the Faculty of Engineering, Lund University, Sweden.

To be defended in E:1406, Ole Römers väg 3, Lund

February 6th, 2026, at 9:00

Faculty opponent
Dr. Jörg König
Engineering Thermodynamics Group, Technical University Ilmenau

Organization: LUND UNIVERSITY
Document name: Doctoral Dissertation **Date of issue:** 2026-01-13

Author(s): Franziska Martens

Sponsoring organization: Swedish Foundation for Strateegic Research (Grants No ICA16-0002 and No. FFL18-0122) and European Research Council (ERC) under the European Union's Horizon 2020 Research and Innovation Programme (Grant Agreement No 852590)

Title and subtitle: Manipulating Thermoacoustic Streaming *Measuring the Synergy of Laser-induced Temperature Gradients and Ultrasonic Pressure Fields in Acoustofluidic Microchannels*

Abstract:
In Acoustofluidics, sound pressure waves can cause a force field on the liquid in a microfluidic channel. The forces depend on density and compressibility of the medium as well as the pressure and velocity amplitude of the sound. The forces lead to a steady flow in the bulk of the fluid, namely acoustic streaming. If a localized change in temperature introduces a gradient in compressibility and density, the force landscape changes accordingly. As a consequence, thermoacoustic streaming arises and replaces the acoustic streaming in velocity and shape.

In the experiments for this thesis, a laser beam with a diameter of a third of the microchannel's width creates a localized temperature hot spot through absorption of the light, resulting in a temperature gradient. In the first study, the thermoacoustic streaming effects of such a gradient are classified in 3D. Firstly, the setup, that was built specifically for the experiments in this thesis is introduced. The shape of the temperature gradient is varied through the amount of absorbed light across the channel height z and the position of the laser spot in x and y. A simulation is shown to support our understanding of the effect. In the second study, the time scales for the build-up and decay of the thermoacoustic streaming are investigated through imaging at a high frame rate and the temperature gradient is measured using a temperature sensitive fluorophore. A video is included, in the second study, to demonstrate how toggling of the ultrasound with pre-established temperature gradient can deflect single particles from their original position in the channel, demonstrating the effects potential for sorting applications. For the third study, we introduce Dimethyl Sulfoxide to the channel. Its compressibility changes with increasing temperatures such that a reversal of the thermoacoustic streaming takes place in the temperature range of 20-50°C. By controlling those quantities, compressibility and density, through the background temperature of the whole channel, the acoustic force landscape and the resulting thermoacoustic flow is manipulated. The temperature gradient originating from the laser remains the same and we show through varying concentrations of the substance and by changing the background temperature, that the acoustic body force landscape can be manipulated in a way that the direction of the streaming reverses. A video shows how the streaming slows down, changes direction and speeds up again, during a gradually increasing background temperature for unchanged laser- and ultrasound actuation.

The aims of this thesis work are: to classify the newly found thermoacoustic streaming for a localized, laser-induced temperature gradient, to show how rapid the response of an acoustofluidic system is, to demonstrate how the phenomenon can be shaped and manipulated and to present an outlook on application possibilities for future studies.

Key words: Ultrasonics, Microfluidics, Acoustofluidic, Laser Heating, Acoustic Forces, Thermoacoustic Streaming, Laser Optics, Cell Sorting

Language: English, German **Number of pages**: 195

ISSN and key title: ISRN: LUTEDX/TEEM-1150-SE, Report No. 1/26

ISBN: 978-91-8104-812-4 (print) 978-91-8104-813-1 (electronic)

Signature Date 2026-01-12

Public defence
February 6th, 2026, at 9:00 in E:1406, E-building, LTH, Ole Römers väg 3, 223 63 Lund, Sweden.

Supervisors
Professor Per Augustsson
Dept. of Biomedical Engineering, Lund University, Sweden
Assistant Professor Wei Qiu
Dept. of Biomedical Engineering, Lund University, Sweden
Associate Professor Andreas Ehn
Dept. of Combustion Physics, Lund University, Sweden

Faculty opponent
Dr. Ing. Jörg König
Group of Engineering Thermodynamics, Technische Universität Ilmenau, Germany

Examination board
Professor Magnus Andersson
Docent at Dept. of Physics, Biophysics and Biophotonics Group, Umeå University, Sweden
Professor Karin Maria Tenje
Dept. of Materials Science and Engineering, Uppsala University, Sweden
Professor Veikko Sariola
Microsystems in Cell and Tissue Technology, Faculty of Medicine and Health Technology, Tampere University, Finland
Deputy member: Associate Professor Nina Reistad
Dept. of Physics, Lund University, Sweden

Chairman
Professor Thomas Laurell
Dept. of Biomedical Engineering, Lund University, Sweden

Cover illustration
Aquarelle abstraction exploring the interplay of light, temperature and ultrasound as swirling thermoacoustic streaming vortices
Illustration by: Franziska Martens

ISBN: 978-91-8104-812-4 (print)
ISBN: 978-91-8104-813-1 (electronic)
Report No. 1/26
ISRN: LUTEDX/TEEM-1150-SE
Printed at Tryckeriet, E-building, Faculty of Engineering, Lund University, Lund, Sweden

To
Mama & Papa,
and Simon & Selma,
to Kimchi and to coffee.

Popular science summary

Ultrasound consists of pressure waves that are too fast to be perceived by human hearing. But just because we cannot hear them doesn't mean they aren't powerful: small entities like polystyrene particles or biological cells can "hear" them and even make them visible for us! If a cell, like a blood cell, is submerged in a liquid, ultrasound can move the cell inside the liquid. It pushes the cell around until it reaches an area without pressure, the pressure node. Of course, for this to work, a lot of conditions need to be fulfilled. One of them is that the liquid, the cells, and the sound are in a microchannel with hard walls, which can reflect the sound back and forth. A vibrating pressure landscape builds up with valleys and hills (antinodes) and flat regions (pressure node). But not only do the cells perceive the sound and move with it, but also the liquid itself. It flows around inside the channel in the form of a circular streaming pattern.

Let's dive into the microchannel: imagine you are a small, round particle, about 1 µm in diameter, drifting through a closed microchannel, filled with green water. Around you, you feel ultrasonic beating, powerful enough to cause the liquid you are submerged in, to stream. Of course, you don't stand still. Being a particle that small, you join the liquid and get dragged with it! You stream in circular patterns, that are determined by the pressure highs and lows of the ultrasonic field, pulsing around you. You are doing one loop after the other, a bit like in a mosh pit at a concert (cirle pit to be precise), just without the beer and sweat. As you stream around in the channel, you suddenly notice a bright light column in front of you. As you get closer, it is getting warmer and warmer around you.
As you approach the red, warm light column, you feel that the liquid, that has been dragging you around, now starts to move differently. Instead of the previous circular patterns, you are now getting dragged faster and faster towards the heat source! For a split second, you think you can see a PhD student with laser googles and white lab

coat staring at you, but you move at 200 µm/s, so too fast to be sure. As you swirl away from the heat source, you slow down. What a ride!
What you (the particle) experienced is the heating effect of a near-infrared point-laser source. The red light is absorbed by the green liquid, and the common acoustic streaming (so-called Rayleigh streaming), that moved the particle around at first (before the laser light was switched on) is replaced by the thermoacoustic streaming pattern, that is the topic of this thesis.

This thesis deals with how to create, manipulate, and make use of thermoacoustic streaming patterns. The results are presented to the research world in three articles:
The first publication classifies what the streaming looks like for different heat source positions in the channel and how it behaves for different amounts of heat. The laser was positioned in two different positions in the channel and in another experiment, the amount of green colouring (called ICG) in the liquid was increased step by step to increase the amount of absorbed laser light. We looked at the resulting videos in 3D and found out that, compared to regular streaming, the new, thermoacoustic streaming is not only of a different shape, it is also about 10 times faster.
Next, we were curious how much time it takes for the streaming to appear and disappear. Consequently, in another study, we took many images in a shorter amount of time while switching the system on and then off. We could see that it takes less than 50 ms for the streaming pattern to appear and disappear fully and less then 2 ms for a first appearance. 50 ms is less than a half the time it takes for you to blink your eye (approximately, unless you blink very fast, then it might be as fast as that). We measured the temperature, which is very difficult on such a small scale. We used a special dye for this, that would shine less bright, the hotter it gets, and we found out that the laser increases the temperature in the channel by about 15°C. In this publication, we also included a video to demonstrate that the phenomenon can be used to move tiny objects in the microchannel. The video shows a particle being deflected from the side of the channel to the center, while a particle that is nearby remains in its position.
In a third publication, we investigate the effect that a special molecule has on the force landscape that causes the thermoacoustic streaming. That molecule has the ability to change how the liquid reacts to the ultrasound. Since the forces, moving the liquid, depend on both the sound and the temperature landscape, we could show that the vortex, the particle in the channel flows in, reverses. Instead of going clock-wise, the particle would now move anti-clockwise inside the channel and we could choose the direction by changing the temperature or the amount of the molecules.

The experiments in this thesis give an idea about our understanding of the phenomenon thermoacoustic streaming. They show how the liquid and particles in the channel

behave and how we can manipulate that behaviour to make use of it. We could demonstrate, that moving specific 1 µm small objects in the channel is possible under the right conditions and we envision that the technology could be used to sort micro- or nano-objects in the future.
The results inspire new research ideas for the project. Modifying the laser beam shape could lead to new streaming patterns. Using longer wavelengths of light to induce the temperature gradient directly in water, without the need for an absorbing dye, could facilitate sample preparation and avoid potentially harming biological cells. Finally, a question remains about how thermoacoustic streaming in acoustofluidic microchannels can be harnessed for applications in biotechnology.

Populärwissenschaftliche Zusammenfassung

Ultraschall besteht aus Schalldruckwellen, die zu schnell sind, um vom menschlichen Gehör wahrgenommen zu werden. Doch nur weil wir ihn nicht hören können, heißt das nicht, dass er nicht kraftvoll ist: kleine Objekte wie Polystyrolpartikel oder biologische Zellen können ihn "hören" und sogar für uns sichtbar machen! Eine biologische Zelle, wie zum Beispiel eine Blutzelle, die in einer Flüssigkeit schwebt, kann vom Ultraschall bewegt werden. Er schiebt die Zelle hin und her, bis sie in einem Bereich ankommt, in dem sie von dem Schalldruck nichts mehr merkt: an einem Druckknoten. Damit das funktioniert, müssen natürlich viele Voraussetzungen erfüllt sein. Eine davon ist, dass sich Flüssigkeit und Zellen in einem Mikrokanal mit harten Wänden befinden, die den Schall konstruktiv zwischen sich hin und her reflektieren. Es entsteht eine vibrierende Drucklandschaft mit Tälern und Hügeln (Bäuchen) und flachen Bereichen (Druckknoten). Doch nicht nur die Zellen nehmen den Schall wahr und bewegen sich mit ihm, sondern auch die Flüssigkeit selbst. Sie fließt in Form eines kreisförmigen Strömungsmusters im Mikrokanal.

Tauchen wir hinein: Stell dir vor, du bist ein kleines, rundes Teilchen mit einem Durchmesser von etwa 1 µm. Du treibst in einem geschlossenen, mit grünem Wasser gefüllten Mikrokanal. Um dich herum spürst du Ultraschallwellen, die stark genug sind, um die Flüssigkeit, in der du schwimmst, zum Strömen zu bringen. Natürlich stehst du nicht still. Als so kleines Teilchen machst du es der Flüssigkeit nach und strömst mit ihr umher! Du strömst in kreisförmigen Mustern, die durch die Druckhöhen und -tiefen des Ultraschallfelds bestimmt werden, das um dich herum pulsiert. Du drehst eine Runde nach der anderen, ein bisschen wie in einem Moshpit bei einem Konzert (Circle Pit um genau zu sein), nur ohne das Bier und den Schweiß. Während

du im Kanal umherströmst, bemerkst du plötzlich eine Lichtsäule vor dir. Je näher du ihr kommst, desto wärmer wird es um dich herum.
Als du dich der roten, warmen Lichtsäule näherst, bemerkst du, dass sich die Flüssigkeit, die dich bisher mitgerissen hat, nun anders bewegt. Statt dem kreisförmigen Muster zu folgen wirst du nun immer schneller zur der Wärmequelle gezogen! Für den Bruchteil einer Sekunde glaubst du, eine Doktorandin mit Laserschutzbrille und weißem Laborkittel zu erkennen, die dich anstarrt, aber du bewegst dich mit 200 µm/s – zu schnell, um dir sicher zu sein. Als du dich von der Wärmequelle entfernst, wirst du wieder langsamer. Was für ein Trip! Was du (das Teilchen) erlebt hast, ist der wärmende Effekt, den eine infrarote, punktförmige Laserlichtquelle auf die strömende Flüssigkeit in einem Schalldruckfeld hat. Das rote Licht wird von der grünen Flüssigkeit absorbiert und die akustische Strömung (die sogenannte Rayleigh-Strömung), die das Teilchen zunächst bewegte bevor das Laserlicht eingeschaltet wurde, wird durch das thermoakustische Strömungsmuster ersetzt, das das Thema dieser Arbeit ist. Meine Dissertation befasst sich mit der Erzeugung, Manipulation und Nutzung des thermoakustischen Strömungsmusters in akustofluidischen Mikrokanälen.

Die Ergebnisse werden der Forschungswelt in drei Artikeln vorgestellt: der erste Schritt war das Klassifizieren, wie genau das Strömungsmuster erzeugt wird, wie es aussieht und wie sie sich bei unterschiedlichen Laserlichtmengen verhält. Dazu wurde der Laserstrahl zu zwei verschiedenen Positionen im Kanal gelenkt und außerdem die Menge des grünen Farbstoffs in der Flüssigkeit (wir nennen ihn ICG), schrittweise erhöht. Die Menge an Farbstoff bestimmt, wie viel Laserlicht von der Flüssigkeit aufgenommen wird, also wie warm es im Kanal wird. Die Videos wurden so analysiert, dass man Bilder in 3D erhielt. Wir fanden heraus: die neue thermoakustische Strömung hat im Vergleich zur bereits bekannten Strömung nicht nur eine andere Form, sondern ist auch mindestens 10-mal schneller, je nach experimentellem Aufbau.
Als nächstes wollten wir herausfinden, wie lange das Strömungsmuster braucht, um zu entstehen und wieder zu verschwinden. Dazu haben wurden in einer zweiten Studie viele Bilder in kurzer Zeit aufgenommen, während das System an- und wieder ausgeschaltet wurde. So fanden wir heraus, dass das Entstehen und Abklingen nicht mal 50 ms dauert! Die Zeit, bis man das Strömungsmuster zum ersten Mal erkennen kann, kann, je nach Messkonstellation, sogar noch kürzer sein, nämlich nur 2 ms. 50 ms ist weniger als ein halbes mal Blinzeln (ungefähr, es sei denn man blinzelt sehr schnell). Wir haben auch die Temperatur gemessen, was in einem so kleinen Maßstab sehr schwierig ist. Dafür benutzten wir einen speziellen Farbstoff, der bei höheren Temperatur schwächer leuchtet als bei niedrigen. So fanden wir heraus, dass der Laser die Temperatur der Flüssigkeit um etwa 15 °C erhöht. Diese Veröffentlichung enthält ein Video, das demonstriert, wie das Phänomen genutzt werden kann, um winzige Objekte im Mikrokanal gezielt zu positionieren. Das Video zeigt, wie ein Teilchen,

nach kurzem Anregen des Systems, vom Rand des Kanals in die Mitte gelenkt wird, während sich ein benachbartes Teilchen nicht wegbewegt.
In einer dritten Veröffentlichung untersuchten wir, wie ein besonderes Moleküls, wir nennen es DMSO, die Kraft beeinflussen kann, die das thermoakustische Strömen antreibt. Das DMSO ändert die Eigenschaften der Flüssigkeit im Kanal, die sich auf die Ultraschalllandschaft auswirken. Und wenn sich das Schalldruckfeld ändert, ändert sich auch das thermoakustische Strömungsmuster. Wir konnten zeigen, dass sich die Richtung der Strömung des Teilchens umkehrt. Anstatt im Uhrzeigersinn bewegte sich das Teilchen nun gegen den Uhrzeigersinn und wir konnten die Richtung durch Änderung der Temperatur oder der Molekülmenge bestimmen.

Die Experimente in dieser Arbeit geben einen Einblick in unser Verständnis von thermoakustischen Strömungen in Mikrokanälen. Es wird untersucht, wie sich Flüssigkeit und Teilchen im Kanal verhalten und wie man das Verhalten beeinflussen können, um es für den Bereich der Biotechnologie nutzbar zu machen. Wir konnten zeigen, dass das gezielte Ablenken von Teilchen im Kanal unter den richtigen Bedingungen möglich ist. Das Projekt inspiriert neue Forschungsfragen für die Zukunft darüber wie man die Form des Laserspots verändern kann um andere Strömungsmuster zu erzeugen, ob es andere Stoffe, wie das DMSO, gibt, mit interessanten Effekten im Schalldruckfeld. Außerdem könnte man Licht einer anderen Wellenlänge benutzen, das direkt von Wasser absorbiert wird, sodass man sich den potentiell zellschädigenden Farbstoff (ICG) sparen kann. Abschließend besteht die Frage, wie man sich die thermoakustischen Strömungen in akustischen Mikrokanälen für Anwendungen in der Biotechnologie zu Nutze machen kann.

Abstract

In Acoustofluidics, sound pressure waves can cause a force field on the liquid in a microfluidic channel. The forces depend on density and compressibility of the medium as well as the pressure and velocity amplitude of the sound. The forces lead to a steady flow in the bulk of the fluid, namely acoustic streaming. If a localized change in temperature introduces a gradient in compressibility and density, the force landscape changes accordingly. As a consequence, thermoacoustic streaming arises and replaces the acoustic streaming in velocity and shape.
In the experiments for this thesis, a laser beam with a diameter of a third of the microchannel's width creates a localized temperature hot spot through absorption of the light, resulting in a temperature gradient.
In the first study, the thermoacoustic streaming effects of such a gradient are classified in 3D. Firstly, the setup, that was built specifically for the experiments in this thesis, is introduced. The shape of the temperature gradient is varied through the amount of absorbed light across the channel height z and the position of the laser spot in x and y. A simulation is shown to support our understanding of the effect.
In the second study, the time scales for the build-up and decay of the thermoacoustic streaming are investigated through imaging at a high frame rate and the temperature gradient is measured using a temperature sensitive fluorophore. A video is included, to demonstrate how toggling of the ultrasound with pre-established temperature gradient can deflect single particles from their original position in the channel, demonstrating the effects potential for sorting applications.
For the third study, we introduce a substance called Dimethyl Sulfoxide (DMSO) to the channel. Its compressibility changes with increasing temperatures such that a reversal of the thermoacoustic streaming takes place in the temperature range of 20-50°C. By controlling those quantities, compressibility and density, through the background temperature of the whole channel, the acoustic force landscape and the resulting thermoacoustic flow is manipulated. The temperature gradient originating

from the laser remains the same and we show through varying concentrations of the substance and by changing the background temperature, that the acoustic body force landscape can be manipulated in a way that the direction of the streaming reverses. A video shows how the streaming slows down, changes direction and speeds up again, during a gradually increasing background temperature for unchanged laser- and ultrasound actuation.
The aims of this thesis work are: to classify the newly found thermoacoustic streaming for a localized, laser-induced temperature gradient, to show how rapid the response of an acoustofluidic system is, to demonstrate how the phenomenon can be shaped and manipulated and to present an outlook on application possibilities for future studies.

List of publications

I. Configurable thermoacoustic streaming by laser-induced temperature gradients.
Franziska Martens, Wei Qiu, Ola Jakobsson, Christian Cierpka, Andreas Ehn, Per Augustsson
Published in: Physical Review Applied, Vol. 23, 024043, 18th February 2025

The author designed, built and set up the laser beam line and modified the microscope visualising the acoustofluidic microchip. The author performed the streaming experiments. The author processed images using open-source code and modified scripts from a co-author. The author took part in analysing the results and writing the manuscript.

II. Temporal evolution of thermoacoustic streaming around spatially confined temperature gradient.
Franziska Martens, Enrico Corato, David van Assche, Ola Jakobsson, Wei Qiu, Per Augustsson
Under Review at: Physical Review Applied

The author modified the setup. The author performed the streaming experiments and assisted the temperature measurements. The author processed images using open-source code and modified scripts from a co-author. The author took part in analysing the results and writing the manuscript.

III. Reversal of thermoacoustic streaming direction through compressibility and density tuning.
Franziska Martens, Ola Jakobsson, Wei Qiu and Per Augustsson
Manuscript

The author performed the streaming experiments. The author processed images using open-source code and modified scripts from a co-author. The author took part in analysing the results and writing the manuscript.

Related work

The work has been presented at the following conferences.

I. **Effects of a Laser-induced Thermal Gradient on the Acoustic Streaming Field**
Franziska Martens, Wei Qiu, Andreas Ehn, Per Augustsson
Presented at Acoustofluidics Conference 2021

II. **Thermoacoustic Streaming Induced by Asymmetric Laser Heating**
Franziska Martens, Wei Qiu, Per Augustsson
Presented at Acoustofluidics Conference 2022

III. **Acoustic Streaming Manipulated by Laser-induced Thermal Gradient**
Franziska Martens, Wei Qiu, Per Augustsson
Presented at SMILS 2023 Swedish Microfluidics Network

IV. **On the charaterization of the velocity and temperature fields in an acoustically driven microchannel with non-uniform temperature distribution**
Franziska Martens*, Wei Qiu, Per Augustsson, Christian Cierpka
Presented and written by Christian Cierpka at Fachtagung "Experimentelle Strömungsmechanik 2023"

V. **Transient buildup and decay of thermoacoustic streaming**
Franziska Martens*, Wei Qiu, Ola Jakobsson,Per Augustsson
Presented and written by Per Augustsson at Acoustofluidics Conference 2024

VI. **Laser Induced Streaming in Acoustofluidic Microchannel**
Franziska Martens
Presented at Workshop and Conference of Chemical and Biological Micro Laboratory Technology, Ilmenau, 2024

Acknowledgments

MANY many people have contributed to this thesis project. The first person I want to thank is my supervisor, **Per**. The story of me starting this journey very much starts with you because you gave me the opportunity to do this. When you decided that I seemed suitable for this endeavour, I had not quite finished my master thesis, had zero experience with microfluidics and it was the beginning of the pandemic where no one even knew if I was going to make it into the country. And yet you decided to let me try. You wrote me a letter to show the police and customs at the boarders saying that I needed to get to Sweden so that I could do "interesting and important research". That line has unintentionally become somewhat of a mantra for me in situations when I wonder why I am doing all of these things, like improving a conference abstract on my first day of summer vacation, crying over Matlab errors or writing this thesis on a Saturday at midnight. (Okay to be honest, I also thought of that phrase whenever an expensive coolLED got destroyed, when laser-curtain materials went up into flames and when we build a sauna to enclose the setup). I want to thank you not only for the opportunity but also for not giving up on me in the process. During my academic life, even starting in High School, there have been many teachers and unrequested advisors who did not believe in me, who made me think it was not possible for whatever reason (mostly gender-related idiocy I assume) and yet here we are. You are not like them, you helped me so much and you taught me so much. I admire your undisguised curiosity about research and your serene persistence to improve. We made it! The only thing I am unhappy about is that you never played trumpet for us PhD students. Maybe I can wish for that as a defence gift.

Next, I have to thank **Wei**, who co-supervised this thesis project. I want to thank you for always being critical and even though I have not been good at asking you questions about the complicated physics we have had to deal with, I know you were there to answer them. Thank you for reading all those manuscripts, for the long discussions

in all those meetings and even dealing with my data plots when I couldn't figure out what the code was meant to do.
Thank you **Andreas**, for co-supervising the optical aspects of this thesis.
Ola, how would I have ever measured anything or plotted a single plot without you. You have not only dealt with my rebellious equipment but you also took care of all kinds of data processing and analysis and plotting and I think many experimental researchers would agree that that is one of the worst parts of the job. Thank you for keeping the spirits up when they were low and please take care of yourself when you go out on the water. I hope I will have time this summer to get the dust of my kite and improve my skills, maybe Ill even run you over in Lomma!
Next I want to thank the biggest Oompa-Loompa of them all, **Enrico**. You know it: there is a good chance this thesis would never have been written if it wasn't for you. You are denying it now but I believe it and who are you to judge my believe. Hope I triggered you a little there. I have to thank you for all the conversations and discussions we had, you are a good teacher. But I have to thank you even more for being the happiest pessimistic monkey I have ever met. I hope you will find what makes you fulfilled and happy and that you manage to recognise it as that when you see it.
Now I also need to thank the rest of the gang. Thank you **Megan**, for always being cheerful. And thank you for still being my friend after all the things I (allegedly!) did to you. Like letting you bike after one gin tonic or going on a snowboarding trip together. I was glad Achilles was there for the kayaking trip so whatever would have happened could have been blamed on him. Thank you **Achilles**, for taking care of Megan! I am looking forward to an exciting next summer, I hope there will be a lot of painting and trips to the beach! **Felix**, it has been so much fun and I really hope the States will kick you out soon so that you are not that far away. I am very happy for you and **Amanda**. Who could have come up with that 5 years ago! It is student house magic. Thank you for all the German (and non-german) Fikas, for being PhD student representative with me, for your insights about spice organisation, graphic making and also for the kayaking trip for which you are the reason that we even came up with the idea. I also want to thank **Richard**, it has been fun meeting someone from Bavaria and seeing them pretending to be a normal person doing day-to-day business. I hope the Bob-Ross painting session wont have been our only joint project because I still think we can write that paper. Thank you **Qing** for being a great office mate, aquarelle painting mate and thank you introducing us all to hotpot! I hope we can have some more this year. Thank you **Xing** for being such happy company and thank you also for all the amazing pictures you take. Thank you **Jules and Livia** for keeping the PhD representative activities alive! The BME (& IEA & TG) PhD student crowd is lucky to have you two. Next I want to thank **Alex & Azin** for being in the DOKT board with me. It has been such fun to be the project coordinator and that is also due to you two

at my side for support, creative inspirations but help in practical matters. Thanks for keeping it alive, PhD students need a community and even if it sometimes feels like its only a handful people that are interested, for that handful it makes a huge difference. Thanks, **Leo**, for being my co-student representative! It has been fun and I think we did good.
There are a lot of other BME colleagues that have made my time here special. I want to start with **Ulrika**, thank you for always having a good mood even though you need to deal with so much and with stuff that me and most of us researchers would not be able to handle. Thank you for always trying everything you possibly could to make my life a little easier. Special thanks also to **Johan Gran**, you have not only given me advice on how to buy a house but also taught me my first (and actually only) Swedish swearword. I will not write it here, I think you know which one it is. Thank you **Pelle**, you are probably the most kind and dedicated teacher I have ever had. The students are truly lucky to have you! I want to thank **Johan Nilsson**, who has always had an open ear, even if I didn't know it was needed. Thank you **Ingrid, Christian, Ammi**, for explaining patiently all the numbers during board meetings. Thank you **Axel Tojo**, for fun conversations, making the impossible possible and distracting Enrico from milling the E-house to the ground. Thanks to all the BMC people, **Thomas, Thierry, Michael, Andreas and Cecilia** in the far-away land on the other side of the road for all the critical questions, inspiring conversations and fun conference trips! And an extra thanks to **Axel Broman**, for tips on parental leave.
I also want to thank **Christian Cierpka** for a fun and educational collaboration, the applied microfluidics conference and exchange of research culture.
Lastly, I want to thank my family.
First, **my South-African Family**! Thank you, **Aunty Vee and Uncle Ricky**, my second Mom and Dad. You have taught me how important education and the right priorities are. I am immensely grateful that I can call you my family. I am starting to understand how difficult it is to be a parent and I admire the selflessness and love you showed when you took me in and made me your daughter from other parents. **Mona and Nicole**, thank you for being the best third and fourth sisters I could have imagined. I want to thank all of the Naicker and Pillay family, for not only teaching me English but also some important life skills to tackle this thesis (and of course how to cook Durban Indian food to survive it all): **Eugene Mama and Auntie Seshnie, Logan Mama and Auntie Loanne, Rajen Mama and Auntie Julie, Auntie Marlene** and of course **Mervin Mama**.
Mange tak, to the **Rejkjær family** for being such a wonderful, chaotic distraction that helped to escape all of this for a little while.
Danke an meinen **Onkel Stephan** und meinen Cousin **Alexander**, die immer Bier geliefert haben, wenn es am dringendsten nötig war und mich stets auf meinem Weg begleitet haben, egal wo der hingeführt hat.

Mama und Papa, ich muss euch eigentlich für so viele Dinge danken, dass ich gar nicht weiß wo ich anfangen soll. Ihr habt mich immer unterstützt, auf jede erdenkliche Art und Weise. Diese Arbeit hat viel Durchhaltevermögen gekostet und ich habe es euch zu verdanken, dass ich da durchgekommen bin.
Mama, du hast mal zu mit gesagt, ich soll immer mein Bestes geben. Manchmal klappe es am Ende nicht, das könne mal passieren, aber dann hätte ich es wenigstens mit aller Kraft versucht. Das ist schon einige Jahre her, ich hatte vielleicht gerade erst auf dem Gymnasium angefangen, aber ich hab es nicht vergessen. Dass du das gesagt hast hat mich viele Hürden überwinden lassen, an die ich mich sonst nicht herangetraut hätte.
Papa, du hast mir beigebracht neugierig zu sein, kritisch zu hinterfragen ob etwas wirklich so stimmen kann und du hast uns, deinen Töchtern, nie das Gefühl gegeben, dass wir in Naturwissenschaften irgendeinem männlichen Mitmenschen in irgendwas nachzustehen haben. Auch wenn das selbstverständlich sein sollte, empfinde ich es in der Gesellschaft, in der wir leben nicht so; zu Hause, bei dir und Mama, allerdings schon! Es braucht Stärke diese Gleichstellung so in seinem Alltag zu verankern, dass alle drei (!) Töchter sich in technische und naturwissenschaftliche Berufe wagen ohne das Gefühl zu haben, dass das etwas außerordentliches ist. Gut gemacht!
Jule, danke für die Crystallography Summerschool (wie ist das eigentlich passiert?), danke für die physikalischen Exkurse, fürs zusammen in der Unibib arbeiten und fürs auf Selma aufpassen. Du bist fast mit deinem Studium fertig und ich frage mich ob ich dir empfehlen würde einen PhD zu machen.
Sophia, danke dafür, dass du uns allen beibringst, dass jeder anders ist, auf seine spezielle Art und Weise, und das man trotzdem miteinander eine Familie sein kann. Und natürlich Danke für alle Autoteile, Reparaturen und den damit verbundenen Nervenverlust. Ich bin richtig froh, dass ich mich darum in der Endphase dieser ganzen Sache hier nicht auch noch kurz nebenbei noch kümmern musste.
Lastly, thank you **Simon**, for so many things. You know the best, from all the people in this long list, how much of a struggle it was. Thank you for helping me with almost every aspect of this work, for coding, for talking physics, for fixing the cover page, for making sure I don't eat only egg everyday, for all the diaper changes and hours spent taking care of our daughter so I could finish this whole thing eventually. You are the best!
Danke meine liebe, kleine **Selma**, du liest das erst in ein paar Jahren, und am Ende war das alles hier für dich.


Franziska Martens
Lund, 2026.

Considerations about research ethics

The research presented in this thesis is of fundamental nature which aids the avoidance of typical ethical dilemmas of biotechnology.
An important aspect that comes to mind is research integrity. It is essential that we are transparent with our methods to ensure that experiments are reproducible by other researchers. While this is a difficult goal, as the precise description of every element of an experiment is probably impossible, trying to be as clear as possible is our goal. Similarly important is that we do not exaggerate the importance of our findings or embellish results. Drawing conclusions from such results prevents future endeavours in answering a supposedly resolved research question or others could continue the research based on false assumptions. It is important to be transparent with unresolved questions and not remove results that do not match the hypothesis. We discuss unexplained effects and depict them as such.

No biological cells were used for the experiments of this thesis, but the proposed application idea is aimed for working with cells. The research with cells is inevitably connected to the use of animal products, either for culture media or for the retrieval of cells themselves. Alternatives exist but because of the characteristic of research, that protocols are written once and rarely ever changed after that, these alternatives are not as popular as they could be. Researchers need to test their protocols for the use of animal-free culturing media. From an environmental aspect, culturing cells in a sterile environment is a highly waste-producing process, where materials are never reused unless absolutely necessary. Other means of ensuring clean cell culture, with recyclable materials and the corresponding cleaning devices are desirable. While culturing cells in an inevitable part of biomedical research, its execution should be reformed with environmental aspects in mind.

Declaration concerning the use of generative Ai

During the preparation and writing of this PhD thesis, AI-based tools were used in a limited and supportive capacity. The primary tools employed were OpenAi's ChatGPT accessed via M365 Copilot and Consensus academic search engine as well as Gemini via NotebookLM. The use was intermittent and focused on non-critical tasks. No AI tools were used for generating scientific ideas, designing experiments, collecting data, performing data analysis, or interpreting results. All research design, methodology, and conclusions were developed independently by the author and co-authors of the respective publications. The use of AI was limited to editorial assistance and did not influence the originality or integrity of the research. This statement was formulated with the help of Ai.

List of Abbreviations

DMSO Dimethyl Sulfoxide

ELISA Enzyme-Linked Immunosorbent Assay

GDPT General Defocused Particle Tracking

ICG Indocyanine Green

SLM Spatial Light Modulator

List of Materials and Devices

470-nm LED LED (Thorlabs, SOLIS LED) equipped with excitation filter (FESH0500) to excite the fluorescent tracer particles.

785-nm Laser Light Source near-infrared, continuous-wave laser (Toptica, IBEAM-SMART-785-S) to generate the thermal gradient through optical absorption.

Adhesive Loctite Super Glue to permanently attach the piezoelectric transducer to the glass slide of the chip.

Analog Discovery 2 Digilent device to handle system timing and generate electrical signals for the piezoelectric transducer.

BCECF Thermosensitive fluorophore dissolved in the sample to measure the magnitude and characteristic time for temperature gradient buildup and decay.

CMOS Camera Hamamatsu OrcaFusion BT camera.

COMSOL Multiphysics v. 6.1 Software for 3D numerical modelling of heat transfer and flow within the microchannel.

Cylindrical Lens plano-convex lens with a 300-mm focal distance (Thorlabs, LJ1558RM) to facilitate 3D defocus tracking of particles.

Dichroic Mirror Thorlabs hot mirror (M254H45) to reflect the laser light onto the channel while passing visible light to the camera.

DMSO Dimethyl Sulfoxide to dissolve BCECF and ICG dye stock solutions and for density and compressibility tuning in publication III

Emission Filter Chroma ET519/26m emission filter avoid any light coming from the LED other than for fluorescence excitation of micro-beads.

Fluid Handling Tools Teflon tubes and Luer connectors to connect the chip to a syringe for the injection of sample liquids.

Microscope Adapted inverted fluorescence microscope, Olympus CKX41SF.

Function Generator To actuate the transducer with a specific amplitude and frequency sweep to create the acoustic field in publication I, after that, the Analog Discovery was used

Indocyanine Green (ICG) Laser-grade absorbing dye (Thermo Fisher, IR-125) dissolved in MilliQ filtered water.

LabView software Software interface to coordinate triggers for, the syringe pump, the camera, the laser and the valve.

MasterGel Pro v2 thermal paste Conductive paste applied at each interface to ensure good thermal contact between components.

MATLAB & DefocusTracker Computational platform to process particle data using the DefocusTracker algorithm.

Microfluidic Chip Straight single-inlet–single-outlet channel (GeSim Bioinstruments and Microfluidics GmbH) constructed from anodically bonded glass-silicon-glass layers.

neMESYS syringe pump Cetoni GmbH pump to supply the sample mixture to the microchannel.

Optical Power Meter Thorlabs PM100D meter with sensors (S245C or S425C) to measure the intensity and transmission of the laser light through the channel and absorbed fraction of light by ICG dye in paper I.

Peltier elements Two CP40136 components placed in contact with the chip to maintain a constant background temperature in the channel

Piezoelectric Transducer Pz26 actuator (Ferroperm piezoceramics, Meggit A/S) glued to the chip to generate a 2-MHz standing-wave field.

Resistance temperature detector Pt1000 sensor glued close to the metal plates touching the chip to provide temperature feedback to the controller.

Stop Valve Valve connected to the outlet tubing to ensure stop-flow conditions.

Thermoelectric cooler controller Meerstetter Engineering TEC-1123 device to drive Peltier elements for precise temperature regulation.

Tracer Particles 1.1 µm and 1.9 µm-diameter fluorescent particles (Thermo Fisher, Fluoro-Max Dyed Green) used to map the streaming flow

WaveForms software Computational tool to control the Analog Discovery device

Contents

Part I

Introduction

Chapter 1

Opportunities of Laser Induced Temperature Gradients in Acoustofluidics

1.1 Introduction

Microfluidics depicts an interesting tool for biomedical research because of its low sample volumes and its small size, making it ideal for point-of-care applications. Well-known, everyday life application examples are COVID tests, pregnancy tests [1] or the paperfluidics newborn screening (heel prick test). One subfield of Microfluidics is Acoustofluidics, where an ultrasound transducer is attached to a microfluidic channel. The transducer sends ultrasound waves into the channels to move or analyse objects, like biological cells, microparticles or mixtures of different components such as blood [2], sperm [3] or cerebrospinal fluid [4].
For those applications, using ultrasound is an elegant approach: the sound waves are reflected at the channel walls and, if in resonance, create a sound pressure field similar to the interference patterns of waves made visible in a wave tank. A sound pressure landscape builds up within a few hundred microseconds for an actuation in the low MHz range [5]. The exerted forces and resulting temperatures can be kept within a range compatible with biological samples, making it ideal for the biomedical field. Two main phenomena in acoustofluidic devices are acoustic focusing of cells or particles and acoustic streaming of the liquid. Manipulating the latter is the main goal of this thesis.
Acoustic streaming refers to a flow of the fluid in the channel, driven by the ultrasound. It arises within the fluid due to energy dissipating in the boundary liquid layer at the channel walls. The shape of acoustic streaming patterns depends on different factors such as density and compressibility of the fluid and therefore, indirectly, on the

temperature distribution in the channel.
The temperature in a microchannel can be altered in different ways, for example through Peltier elements [6], through resistive heating of electrodes or optically through light absorption in the liquid, as in this thesis. Qiu et al. [7] produced a thermal gradient by absorbing light from a focused LED in a water-dye mixture in an acoustofluidic channel. Building on their work, the results of this thesis are created with a laser light source. The laser depicts a more confined heat source, with more possibilities to alter the temperature distribution in the channel compared to an LED.
To summarize, the experiments in this thesis aim to use sound and light to move liquid in a structure that is merely the thickness of a few human hairs. The results might aid the biomedical field concerning cancer research via (rare-) cell sorting by controlling the motion of the liquid and the objects in it. Considering that both sound and light are a type of wave, it is intriguing to think that we are trying to move objects in a fluid. I like to imagine that the particles are dancing to the beat of the ultrasound bouncing around in the microchannel. The temperature gradients in this scenario create "hot spots" like a moshpit at a concert. Different kinds of moshpits mean different kinds of temperature gradients, shuffling the fans around. As soon as the music ends (the laser and ultrasound turns off), everyone stops moving and so does the liquid in the channel.

1.2 Research Questions

These research questions are going to be addressed:

- How can laser light be used to heat the microfluidic cavity?
- How do different temperature gradients influence the acoustic streaming field and in what way can they be varied?
- How fast does the temperature field build up?
- How large is the temperature difference inside the channel?
- In what way can we manipulate the liquid's properties to modify thermoacoustic streaming?
- Can we move individual particles in the acoustic field and what are the options for future applications?

1.3 Thesis Structure

After this short introduction and motivation, the thesis frame begins with a chapter about sound and light waves. The concepts of sound, resonance and a materials interaction with it will be introduced. After that, we focus on light: What makes laser light special, how does absorption work and how is it useful for this thesis.
Chapter three focuses on the third defining concept, microfluidics. It starts with a general perspective on microfluidics in our everyday life, followed by a short look into an application example of acoustofluidics and lasers: optical tweezers in microfluidics. After that, we dive deeper into microfluidic research, thinking about laminar flow, Reynolds number, Peclet number and viscosity.
Chapter four contains the juice of the thesis frame: Acoustofluidics. Here, the driving principles are explained: acoustic body force and how temperature gradients affect it as well as time scales of the two. A short historical overview is given and the thesis project placed within the field.
Chapter five gives an overview of experimental methods, explains the setup, designed for this thesis in detail, and outlines data analysis methods and simulation details.
Chapter six contains summaries of each paper.
Chapter seven discusses limitations and future possibilities for the project to give some final food for thoughts.
Thank you for being curious and happy reading!

Part II

Thesis Frame

Chapter 2
Waves of Sound and Light

Waves are a neat way of physics to explain both sound and light. Kundt showed with his dust-tube experiment (Kundt's tube), that the propagation of sound can be described as a wave [8]. Huygens described light as a wave with his wave-front construction method (Huygens principle), based on its reflection and refraction behaviour at interfaces and the observations of it being double refracted in a calcite crystal. In a fluid, sound propagates longitudinally as compressions and rarefactions of the liquid molecules. Sound needs a medium to compress to travel, there is no sound in a vacuum. Light, on the other hand, does not require a medium since it is electromagnetic fields that propagate.
This thesis describes the effects of the interplay of the two types of waves with matter, observing outcomes of these interactions: the interplay of heat due to absorption of electromagnetic waves in the fluid with the motion of the fluid due to interaction with the sound pressure waves. How is it possible, that these two oscillations have such different effects?

2.1 What are waves of sound, what is resonance?

The crucial differences of the two types of waves, sound and light, are the way they propagate and the amount of energy they transfer. Longitudinal (sound pressure) waves move parallel to the particle oscillation direction. The net movement of the molecules transferring the pressure as density changes is zero. Transversal waves require shear elasticity. Water is not elastic and can therefore not transfer transversal waves, making sound waves purely longitudinal in fluids. One might wonder how water, often being considered an incompressible fluid, can transmit pressure waves, that compress and decompress the water. That is because water is only nearly incompressible, as

all materials known to mankind, nothing is absolutely incompressible. However, in physics it is allowed to make assumption and neglect certain aspects of reality and often get pretty close to the truth with that (like describing a ballet dancer as a rotating cylinder without hands or legs but still being able to correctly estimate her angular momentum as she spins and spins [9, 10]). Short fun fact, before we start thinking about light: in solids, like the ground, sound waves can have both transversal and longitudinal components. And it turns out, that it is due to this fact, that we know that the earth has a liquid core: by measuring the transmitted waves of an earthquake, the scientists found that in certain directions no transversal waves were transmitted because the liquid core "swallowed" them.
Light can be described as a transversal wave, propagating perpendicular to its oscillation direction. It comprises a magnetic and an electric field standing perpendicular to each other. Unlike sound, no molecules are necessary to compress or relax to transmit light. We can see the electromagnetic waves in vacuum but we cannot hear sound. Light is in the order of 10^3 to 10^6 faster than ultrasound, which is in the range of 20 kHz to GHz, and the visible wavelength range is about 350 to 750 nm. For $c_{\text{light}} = 3 \cdot 10^6$ m/s that corresponds to a frequency of 860 to 400 THz.
A substance can be heated through absorption of light, most efficiently at an absorption line of the substance. In this thesis, the substance is water spiked with ICG (Indocyanine Green) dye and the light source a 785 nm near infrared laser. The water itself would not absorb the laser light of that wavelength efficiently enough to generate the necessary heating effects, since its nearest absorption peaks are at 1.5 µm and 3 µm (fig. 2.1). The use of those wavelengths for heating is discussed in the outlook (sec. 7).
Coming back to the wave character of sound and light, we need to understand the importance of resonance for the presented research. Also here, it is a curiosity that the absorption of light can be considered a type of resonance. From a (simplified) quantum mechanics perspective, the absorption of a material relates to its energy levels. Only photons with a wavelength (or frequency, hence energy) that matches the material's energy gap can be absorbed, which makes the absorption lines of a spectrum a visible indications of the materials resonance with the photons.
In terms of resonance of a microfluidic system, the relevant dimensions are much larger (despite it being "micro" and us needing a microscope to observe it) and we (luckily) do not need to wrap our heads around quantum mechanics. For resonance to take place, the channel dimensions need to match some multiple of the frequency (or wavelength) of the sound. In this case, a frequency of 2 MHz at $c_{\text{sound in water}} = 1500$ m/s has a wavelength of $750 \cdot 10^{-6}$ m $= 750$ µm. For these parameters, a half standing wave fits just nicely into our 375 µm x 150 µm sized microchannels.

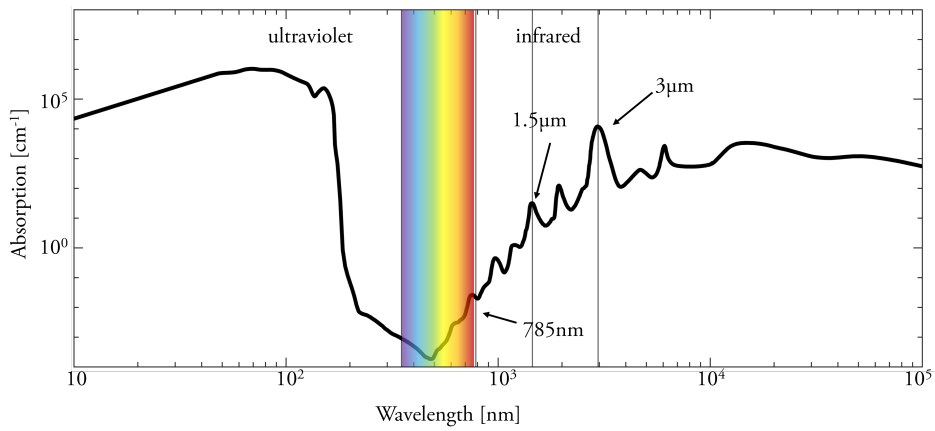

Figure 2.1: Absorption spectrum of water. Many people have measured the absorption spectrum of water. Scott Prahl [11] has compared several sources and found that most of them agree well. We can see that the absorption in the visible range is low. One often used absorption peak is at 1.5 µm because it is used in communication technology (so those lasers have become cheap and off-the-shelve available). At 3 µm wavelength, water absorbs even better. This data was taken from D. J. Segelstein [12], who gathered data in 1981 from other sources to create an extensive absorption spectrum of water.

2.2 Propagation of Sound in a medium

Sound waves move through a medium as oscillations of molecules. If we record sound, we record how the molecules are compressed and expanded with respect to each other as compressions and rarefactions. We can assume the propagation of sound as an adiabatic process as the temperature changes are small enough that we can neglect them. Laplace added the adiabatic assumption in 1819 to Newton's explanation from 1687 and with this created the Newton-Laplace equation for the speed of sound in a medium, that we are using today. It states that the speed of sound c in a medium is equal to 1 over the square root of the adiabatic compressibility of the medium κ_{med} and density of the medium ρ_{med}:

$$c_{\text{medium}} = \frac{1}{\sqrt{\kappa_{\text{med}} \cdot \rho_{\text{med}}}} \tag{2.1}$$

Similar to the effect of a straw in a water glass that appears bent, an interface of two media with different compressibility κ and density ρ affects how sound propagates. The sound, just as the light, has different speeds in the different media and boundary effects appear. The ones we can observe in our everyday life are for example reflection of sound in a tunnel, creating an echo (reflection at a dense wall) or trying to talk to

someone under water compared to on land (propagation in media with different speeds of sound). Mathematically, we use plane wave equations to describe the oscillating pressure field p_1 and velocity field $\mathbf{v}_1$ in 1D:

$$p_1 = p_\mathrm{a} \cdot \cos(k_y y) \tag{2.2}$$

$$\mathbf{v}_1 = i\frac{p_\mathrm{a}}{c_0 \rho_0} \cdot \sin(k_y y)\mathbf{e}_y \tag{2.3}$$

with: p_a = pressure amplitude, $k_y = 2\pi/\lambda$ wave vector, y = location across the channel width with $y = 0$ being one of the channel walls, c_0 = speed of sound in the liquid, ρ_0 = density in the liquid and $\mathbf{e}_y$ the unit vector in the y-direction.

2.3 Sound pressure in the microchannel

The sound pressure waves oscillate between the hard channel surfaces. Resonance takes place both in the channel but also in the chip itself. Rune Barnkob [13] simulated resonance in a channel structure, similar to the ones used here, that shows resonance in the entire system (fig. 2.2). Inside the cavity of the microchannel, the sound

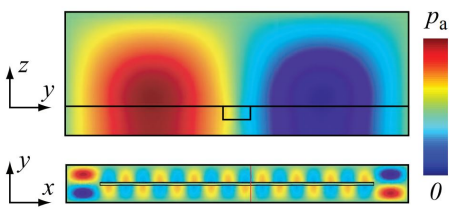

Figure 2.2: Simulated pressure field inside a microchannel with piezo attached to the bottom surface. Cross-sectional view (z-y) and top view (y-x). Taken from Per Augutsson's PhD thesis [14] who modified it from Rune Barnkob Master thesis [13]

waves are reflected at the interface between water and silicon. To achieve constructive interference of the sound pressure waves, any channel dimension d that is a multiple n of the sound's wavelength λ_s would work.

$$d_w = n \cdot \frac{\lambda_s}{2} \tag{2.4}$$

A half standing wave fits across the width of the channel.

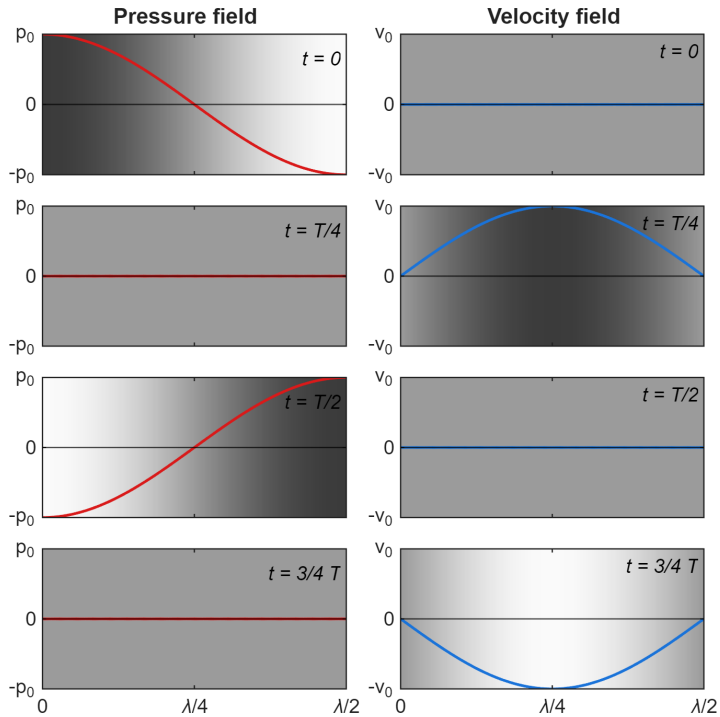

Figure 2.3: Pressure (left, red) and velocity (right, blue) oscillate between minimum and maximum values between the channel walls. The velocity is the derivative of the pressure so they are out of phase by a quarter period. The shading indicates the amplitude: at $t = 0$, the pressure maximum is on one side of the channel, the velocity, being the second order effect, is 0. At $t = T/4$, the pressure is 0 as its even across the channel, while the velocity has its maximum in the center. A quarter period later at $t = T/2$, the pressure maximum is at the right side of the channel while the velocity is 0. At $3T/4$, the velocity is maximal again, in opposite direction, while the pressure is 0. Transferring this to the resonating cavity, the oscillation process happens with a frequency of 2 MHz. Looking at it over a long time, the pressure at the side walls is maximal, while it is 0 in the center and the velocity maximal in the center and 0 on the sides.

2.4 Laser light, why is it so special?

Laser is an acronym that stands for Light Amplification by Stimulated Emission of Radiation. The juice in that lengthy term is in the stimulated emission. One photon stimulates the drop of an electron in an atom from a higher to a lower energy level. The dropping electron emits a photon of the same characteristics (phase relationship, energy and amplitude) that it was stimulated with. A cavity resonates the emitted photons

back and forth through the laser medium to stimulate more and more emissions, the medium in the cavity lases. Photons which are not in phase or in other ways different from the desired wavelength are filtered out by the geometry of the laser cavity. The produced light is powerful and well manipulable because of its coherence in time and space. Other light sources like LEDs do not fulfil the coherence criteria and the possibilities to focus them or interfere them with each other are limited because of their lack of order. The theoretical limits for focusing laser light are dependent on its wavelength λ and the numerical aperture NA of the system. The minimal beam diameter d is [15]:

$$d = 2\omega_0 = \frac{2\lambda}{\pi \cdot \mathrm{NA}} \tag{2.5}$$

The numerical aperture is a property determined by the component used for focusing and can be calculated with the refractive index n and the opening angle α of the optical element:

$$\mathrm{NA} = n \cdot \sin(\alpha) \tag{2.6}$$

The laser used in the presented experiments has a wavelength of $\lambda = 785\,\mathrm{nm}$, and the objective a numerical aperture of 0.4, leaving us with a theoretically minimal beam diameter of:

$$d = 2\omega_0 = \frac{(2 \cdot 785 \cdot 10^{-9}\,\mathrm{m})}{(\pi \cdot 0.3)} \approx 1.66 \cdot 10^{-6}\,\mathrm{m} = 1.66\,\mu\mathrm{m} \tag{2.7}$$

2.5 Absorption of light, its timescales and its heating effects

Simplified, absorption of light means that a photon with suitable frequency ν is absorbed by an atom's electron with matching energy gap $h\nu = E_2 - E_1$, h being Planck's constant. The electron is excited from a lower energy state E_1 to a higher state E_2. The states can be rotational, vibrational or electronic. These differ by the amount of energy transferred: rotational states require frequencies in the microwave range, $\approx 10^{-3}\,\mathrm{eV}$, vibrational states are in the infrared range with energies of about $\approx 0.01 - 0.5\,\mathrm{eV}$ and electronic states in the UV and visible range with $\approx 1 - 10\,\mathrm{eV}$. In the case of ICG dye absorbing 785 nm wavelength laser light, we are looking at the vibrational and electronic regime. These energy states are unstable and eventually (in the atto- to femtosecond time scale [16, 17]), the electron will relax back to its previous state. In the process, it releases energy either radiative or nonradiative. Radiative means that photons are emitted and we can observe phosphorescence or fluorescence.
The ICG dye we are using to absorb the laser light is a fluorescent dye, so some energy is lost due to radiative transfer. The filters and the camera in the setup were chosen

purposefully to avoid visualizing the ICG emission. Its fluorescence would interfere with observing the emission of the particles and in the case of paper II, where we use a temperature sensitive fluorophore, it would have disturbed the temperature measurements. Other than through fluorescence, the decaying electron can transfer energy non radiatively.
Nonradiative decay is the transfer of energy to nearby atoms as kinetic energy through collision and other intermolecular interactions. The time that it takes is slightly slower than the absorption, in the femto- to picosecond range. The collisions that transfer the energy to surrounding molecules is where the energy is transferred from the dye molecule, that absorbed the laser light, to the water, which does not absorb the chosen laser wavelength of 785 nm. With that, we have reached the macroscopic range of the heating process, the temperature of the water molecules increases and creates a (literal) hot spot in the microchannel [18]. Its safe to say, that the absorption of the light in the liquid and the time it takes for that energy to be transformed into a local temperature change, is the fastest time scale discussed in this thesis. How fast the liquid heats up, despite the atto- to picoseconds it takes for the energy from the photons to be converted into heat, depends on more graspable quantities: the amount of liquid, its thermal conductivity, the absorption efficiency (in this thesis that is the amount of dye and its ability to absorb the light), the laser spot size and its power.

2.6 Temperature transport

One of the prerequisites for the thermoacoustic streaming, as presented in this thesis, is the presence of a temperature gradient. Different mechanisms can transfer heat and for this work we need to consider thermal diffusion as well as radiative heat transfer due to laser light absorption.

Thermal diffusion is a comparably slow process. Assuming a distance of 375 µm, which is the channel width and a thermal diffusion coefficient of water with $\alpha = 1.5 \cdot 10^{-7} \frac{\mathrm{m}^2}{\mathrm{s}}$ we can calculate [19]:

$$t_{\text{diff}} = \frac{L^2}{4\alpha} \tag{2.8}$$

$$= \frac{(375 \cdot 10^{-6}\mathrm{m})^2}{4 \cdot 1.5 \cdot 10^{-7}\,\mathrm{m^2 s^{-1}}} = 0.23\,\mathrm{s} \tag{2.9}$$

For the radiative heat transfer, we can estimate how much time it takes for a water column with the diameter of the laser spot, d =50 µm and the height of the channel h =150 µm to heat up: We need the volume and mass of the water column (density

water: $\rho = 997\,\frac{\mathrm{kg}}{\mathrm{m}^3}$, specific heat capacity: $c = 4186\,\frac{\mathrm{J}}{\mathrm{kg}\,^\circ\mathrm{C}}$):

$$V = \pi r^2 h = \pi \left(\frac{d}{2}\right)^2 h \tag{2.10}$$

$$= \pi(25 \cdot 10^{-6})^2 \cdot 150 \cdot 10^{-6} \approx 2.95 \cdot 10^{-13}\,\mathrm{m}^3 \tag{2.11}$$

$$\tag{2.12}$$

$$m = \rho V \tag{2.13}$$

$$= 997 \cdot 2.95 \cdot 10^{-13} \approx 2.94 \cdot 10^{-10}\,\mathrm{kg} \tag{2.14}$$

Calculate how much energy it takes to heat that mass by $\Delta T = 20\,^\circ\mathrm{C}$:

$$Q = mc\Delta T \tag{2.15}$$

$$= 2.94 \cdot 10^{-10} \cdot 4186 \cdot 20 \approx 2.46 \cdot 10^{-5}\,\mathrm{J} \tag{2.16}$$

Calculate how much energy the laser delivers per second with its $P = 10\,\mathrm{mW}$ power and $\eta_{\mathrm{abs}} = 30\,\%$ absorption efficiency:

$$P_{\mathrm{absorbed}} = \eta_{\mathrm{abs}} P = 0.30 \cdot 0.01 = 0.003\,\mathrm{W} \tag{2.17}$$

And finally compare how long it would take to deliver the energy to heat up the column:

$$t_{\mathrm{heat}} = \frac{Q}{P_{\mathrm{absorbed}}} = \frac{2.46 \cdot 10^{-5}}{0.003} \approx 0.0082\,\mathrm{s} \tag{2.18}$$

To heat the full column takes about 8 ms. The thermoacoustic streaming will start building up before then but cannot reach a stable state. We will come back to these numbers when thinking about time scales for the buildup with respect to publication II.

Chapter 3
Fluidics at the Micro-scale

Microfluidics can be found all around us. Trees transport their water using microfluidics, as the water evaporates from the leaves, creating a negative pressure to pull water up from the roots.
The blood in our body is a non-Newtonian fluid, which means that its viscosity decreases under shear stress. You might have seen an experiment where a water-cornstarch mixture is filled in a bowl or pool and if pressure is applied to it by pressing the fluid or jumping on it, it seems to become solid. Our blood behaves similarly, and (weirdly) so does ketchup.
We can observe the Marangoni effect after swirling a glass of wine (fig.3.1). On the glass walls, a thin wine layer of liquid forms. The alcohol in the liquid will evaporate, creating a higher surface tension at the top of the liquid layer. Liquid from below is pulled up to the top and forms a droplet due to gravity. When this droplet eventually flows down, we can see the typical tears of wine flowing down the glass.

Microfluidics is especially useful for biomedical tests because, as the name says, it does only require small liquid volumes. A famous example is the Enzyme-Linked Immunosorbent Assay (ELISA) test, where a pregnancy indicative hormone, called hcg (human chorionic gonadotropin), is detected using enzymes and antibodies. The urine flows through different areas of the test. If hcg is present, two different antibodies are used as markers to detect it in the fluid and cause a colour change that tells us the result of the test.

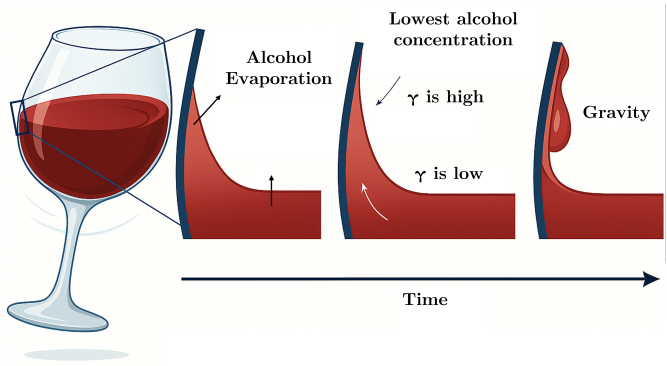

Figure 3.1: The Marangoni effect can be observed at the walls of a wine glass. After the glass has been swirled, the alcohol evaporates from the thin liquid layer, causing a higher surface tension at the top of the layer than at the reservoir in the glass. Wine is being pulled up the walls and gathers as droplets at the top. The droplets run down in "tears". Adapted from [20]

3.1 Optical Tweezers and Microfluidics

A good example of how laser light and microfluidics can be combined are optical tweezers [21, 22, 23]. In optical tweezers, a focused laser beam can trap and move particles or cells with optical forces (fig.3.2). The laser light needs to be focused and the laser power sufficiently high. Typically, the wavelength range is infrared. Optical tweezers require the refractive index of the object to be higher than the surrounding medium because as the light is refracted through the particle or cell, the photon momentum creates as inward force trapping the particle. It should be kept in mind, that heating effects can happen depending on the liquids and wavelengths used. The surrounding liquid can heat the microobject, so it can come to a temperature increase even if the object itself does not absorb the light [18].

Even though the system used for this thesis resembles an optical tweezer setup, such effects cannot be achieved. The laser would need to be focused to a much smaller size, to reach the necessary optical forces [24]. An objective with higher numerical aperture, so a better focusability could allow trapping due to optical tweezing. However, a smaller focus and higher numerical aperture means a shallower depth of focus. As it is built now, the distance during which the laser beam maintenance approximately the same diameter is large enough that the laser beam can be considered invariant throughout the sample. With an objective with higher numerical aperture, that length would decrease and the channel floor and ceiling would be heated less and in a larger area than the channel center. The use of smaller focused light is discussed in the outlook ch.7.

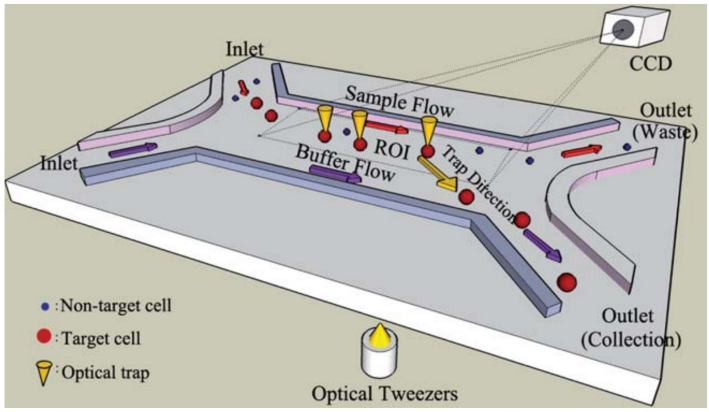

Figure 3.2: An optical tweezer can be used to sort specific cells from a population. Here, mixtures of yeast cells and particles or embryonic stem cells and other cells are flown through a microfluidic system and the target cells separated from the other objects. After a detection step, they are guided to the collection outlet with optical forces. Reproduced, with permission, from Wang et al. [23]

3.2 Laminar flow and Reynolds number

Laminar flow is a central concept of microfluidics. The small dimensions of the microchannels result in a highly ordered and therefore deterministic flow pattern. In contrast to chaotic, turbulent flows (e.g. in rivers), laminar flow will follow nonrandom paths and objects submerged in it will follow a predictable path. External forces can be imposed on it and modify that path, such as magnetic, electric, optical or acoustic fields. To find out if a system will be in the turbulent or laminar regime, we can calculate the Reynolds number:

$$\mathrm{Re} = \frac{uL}{\nu} = \frac{\rho u L}{\eta} \tag{3.1}$$

with: ρ = fluid density, u = flow speed, L = characteristic length, η = dynamic viscosity, ν = kinematic viscosity.
It compares inertia which is related to turbulence ($\rho u L$) to viscous friction which stabilizes the flow (η). Reynolds numbers far below 1 are considered as creeping flow and inertial effects can be neglected. Reynolds numbers up to $Re \lessapprox 2000$ are in the laminar regime. Numbers larger than that, $Re \gtrapprox 2000$, mean that turbulences are present. The equation tells us that high flow speeds, large dimensions and high density can lead to turbulent flows. The higher the viscosity, the larger chance of laminar flow. The Reynolds number for a 150 µm deep microchannel and water with a kinematic

viscosity of $\nu = 1 \cdot 10^{-6}\,\mathrm{m}^2/\mathrm{s}$ as used in this thesis is:

$$\mathrm{Re} = \frac{2 \cdot 10^{-4}\,\mathrm{m/s} \;\cdot\; 150 \cdot 10^{-6}\,\mathrm{m}}{1 \cdot 10^{-6}\,\mathrm{m}^2/\mathrm{s}} = 0.03 \tag{3.2}$$

for a flow speed of $200\frac{\mu\mathrm{m}}{\mathrm{s}}$, which is at the top end of the measured thermoacoustic streaming. Therefore, the experiments in this thesis are in the creeping regime.

3.3 Peclet number

The Peclet number is used in microfluidics to relate advective to diffusive transport i.e. transport due to bulk motion of the fluid versus transport due to molecular motion. It is defined as:

$$\mathrm{Pe} = \frac{\text{advective transport}}{\text{diffusive transport}} = \frac{uL}{D} \tag{3.3}$$

with: u = characteristic flow velocity, L = characteristic length scale, D = diffusion coefficient.
An example is the H-filter (fig.3.3), where differently sized molecules are filtered according to their diffusion coefficients [25]. Larger molecules take more time to diffuse from the sample liquid to the other liquid. If the flow speed is chosen accordingly, the small molecules will diffuse into the other half of the middle section, from where they exit through the top outlet of the filter. The slower diffusing molecules remain in their half and exit through the other outlet. The Peclet number can be calculated by comparing how long it takes for molecules to diffuse across the width of the channel to how long it takes to pass through the length of the channel due to advection (bulk motion), because it compares how fast molecules diffuse to how fast they flow due to advection. If the Peclet number is high, it means that for that molecule at that specific flow rate, advection will dominate diffusion and vice versa. The Peclet number can also be used to describe heat transfer if the diffusion coefficient D is replaced with thermal diffusivity α.
Thermal diffusivity α is a material property and describes how quickly heat conducts through the material relative to its ability to store heat.

$$\alpha = \frac{k}{\rho \cdot c_p} \tag{3.4}$$

with k = thermal conductivity, c_p = specific heat capacity and ρ = density. It is thus a property that characterizes thermal diffusion, which describes the process of heat spreading through a material due to a temperature gradient.
Another way to look at thermal diffusivity is as the rate at which a temperature gradient

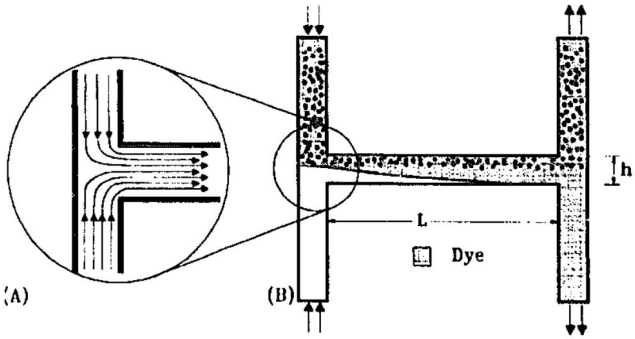

Figure 3.3: The H-filter makes use of diffusive transport to separate molecules or particles with a lower diffusion coefficient from a mixture with objects of a higher diffusion coefficient. It was first published in 1997. Reproduced, with permission, from Brody et al. [25].

smooths out over time. The diffusion of molecules shows to be similar to the diffusion of temperature if we look at Fick's second law of diffusion and the thermal diffusivity as it is used in the heat equation:

$$\text{Fick: } \frac{\partial \varphi}{\partial t} = D\nabla^2\varphi \tag{3.5}$$

$$\text{heat equation: } \frac{\partial T}{\partial t} = \alpha\nabla^2 T \tag{3.6}$$

φ = molecular concentration, t = time, $\frac{\partial \varphi}{\partial t}$ = rate of molecular concentration change over time, $\frac{\partial T}{\partial t}$ = rate of temperature change over time,$\nabla^2\varphi$ = curvature of concentration distribution (how it evolves in space), $\nabla^2 T$ = curvature of temperature distribution, α = thermal diffusivity.
Both the molecular diffusion and the thermal diffusivity describe the evolution of a gradient over time with a constant and the curvature of the gradient.
In microsystems, diffusion plays a more important role compared to macroscale systems, due to their small size. While in a bathtub, diffusion takes a long time and advection is more important, in a microchannel, the relevant length scales are overcome comparably quickly by diffusion.

3.4 Viscosity

An experiment visualising viscosity is to place a fluid in between two plates and then move the top plate with a constant velocity in one direction. If we look at the fluid's

motion, we notice, that its velocity at the still plate is zero while at the moving plate, it has the same velocity as that plate [26]. Between the fluids we have a linear velocity distribution in case of a Newtonian fluid (fig.3.4).

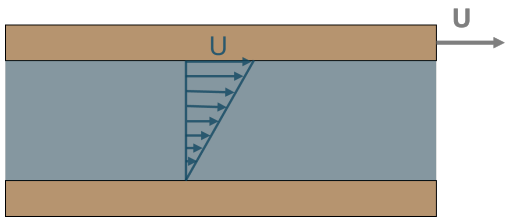

Figure 3.4: Two plates, with a fluid in between: if one plate moves with velocity U while the other plate remains still, the fluid in between will move with the same velocity at the moving plate but have zero velocity at the other plate. In between, the velocity decreases linearly.

An interesting phenomenon of viscosity and ultrasound, related to thermoacoustic effects, was presented here by Li et al. They investigated thermoacoustic streaming in differently viscous droplets [27]. Surface acoustic waves are used to heat droplets of a water and glycerol directly through absorption of the ultrasound. The increased viscosity (compared to water), leads to absorption in the liquid causing an increase in temperature. They found that higher viscosity leads to lower streaming velocities, resulting in a smaller mixing effect of the temperature gradient.

Chapter 4
Acoustofluidics

Acoustofluidics is a field in Microfluidics, where sound fields are used to actuate particles or liquid inside a microchannel. Some advantages of acoustic actuation in microchannels are its biocompatibility [28, 29], its non-invasive operation and the quick response time, e.g. in the configuration presented in paper II (sec. 6.2) it takes less than 1 ms for the sound pressure field to buildup or decay completely. Acoustic actuation of microchannels has been demonstrated for cell biology applications because it utilises the cell's intrinsic characteristic for labelfree sorting, contactless and gentle handling and low sample volumes.
This chapter will:

- give a short historical overview of acoustic streaming
- come back to the present and outline application examples of acoustic effects in microfluidics, ending with the gap, this thesis is addressing
- introduce the acoustic radiation force to find a critical radius with respect to the acoustic body force
- explain Schlichting and Rayleigh streaming
- place this thesis in the field of thermoacoustics
- explain the acoustic body force and its changes due to a temperature gradient
- talk about the time scales, with publication II in mind

4.1 Historical background of acoustic streaming

The research about sound took a leap in 1787, when Ernst F. F. Chladni proved that sound was travelling through air as waves and discovered resonance modes [30]. He

vibrated a plate using a violin bow and observed sand gathering at the nodal and antinodal areas of the plate, forming what we now call Chladni figures (Fig.4.1 and 4.2a).

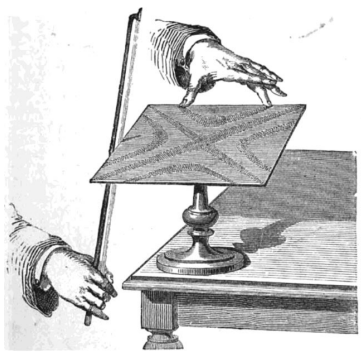

Figure 4.1: Chladni's experimental setup, proving that sound travels as waves, revolutionizing physics [30, 31]. Using a bow to vibrated the plate with sand on it, he observed that the sand gathered in lines, according to actuation frequency, at nodal and antinodal lines. For the first time, he was able to visualise, that the sound we hear, travels as waves.

He described his observation in a paper which was the basis for Savart's discovery of rotational resonance modes, 40 years later, showing that resonance and sound in vibrating bodies are more complex than anticipated [32]. Specifically, he observed that in a similar system, finer sand would not gather in the lines that Chladni described but instead in what he called secondary lines. This transport was later proposed by Faraday [33] to be caused by currents of air. A bit later, about 80 years after Chladni had presented his figures, Kundt showed the resonance in the famous Kundt's tube, measuring the speed of sound in air for the first time by visualizing resonance modes through dust figures inside the vibrating tube (Fig.4.2b), that was actuated with a tuning fork of known resonance frequency [8]. Almost another 20 years later, Lord Rayleigh revisited Kundt's experiment and the hitherto unexplained vortices first observed by Dvorak, by the dust particles in the tube. He published his findings and a mathematical description of this bulk flow which laid the basis for acoustic streaming research [34]. Schlichting, in 1932, investigated the boundary layer of the vibrating wall, that Rayleigh had neglected in his mathematical considerations [35]. He found streaming vortices in the oscillating Stokes boundary layer [36], that had not been described before.

Later, important contributions have been made by Faraday, who likely first observed acoustic streaming in vibrating plate experiments [33, 37], by Eckart, who described bulk viscous dissipation leading to Eckart streaming [38], and by Nyborg, who provided a theoretical framework and governing equations for acoustic streaming [37]. Lighthill further advanced the understanding by formulating acoustic streaming in terms of nonoscillatory Reynolds stresses using the Navier–Stokes equations [39].

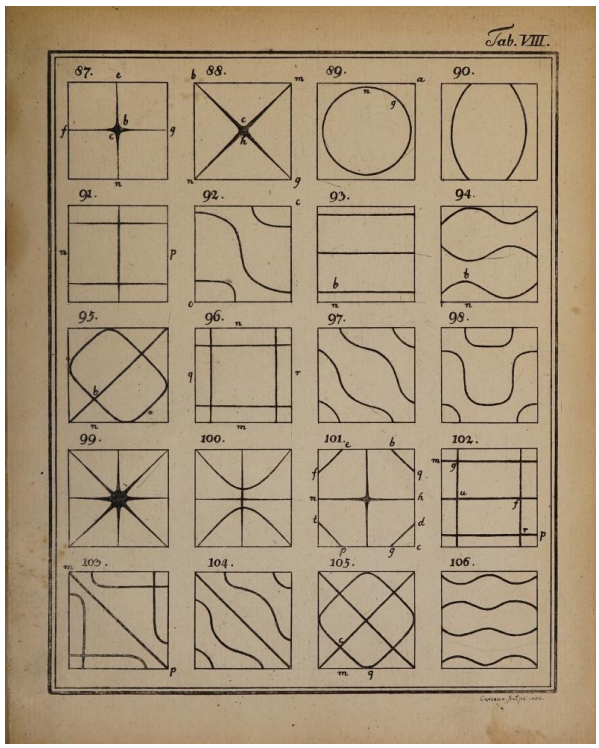

(a) Chladni figures, as shown in his book "Discovery about the Theory of Sound" from 1787 [30].

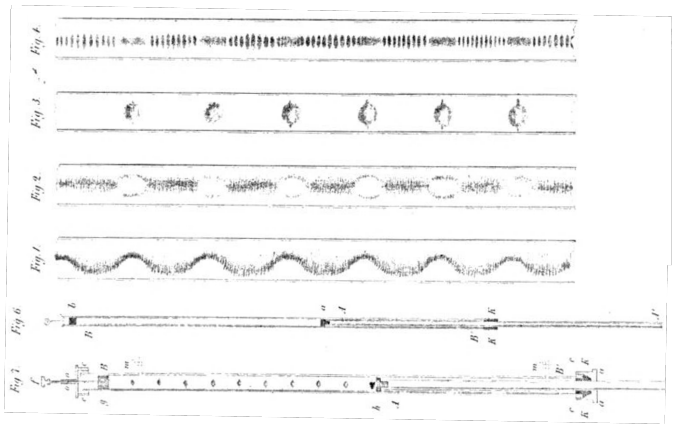

(b) In 1866, Kundt observed dust gathering at nodes and antinodes in a tube, that he actuated at a known frequency. From that he was able to, for the first time, calculate the speed of sound [8].

4.2 Applications of Acoustofluidics

More than 200 years of research have led to some exciting applications of acoustofluidics in biotechnology. A small selection of them will be outlined next with the purpose of showing how versatile and useful the technology is and to place this work in its niche of the bigger context. For a full overview of the field, there are excellent review papers available [40, 41, 42].

Acoustic effects in microfluidics are aimed at trapping, separating and sorting of cells, particles, bacteria or other biomarkers from body fluids, e.g. blood [43], sperm [44, 45], saliva or breast milk [40, 46]. The technology is popular because of it's contactless manner. It exerts relatively low shear forces compared to other cell- or biomarker handling methods as well as the fact that often harmful stains and dyes are not needed [47, 48, 49].

Acoustic trapping is a method to capture cells or particles as they flow through a localized acoustic field. The forces of drag due to streaming, gravity, buoyancy and a retention force to withstand the drag are balanced, so that cells are trapped in the pressure node while the liquid around them can be replaced, e.g. as a means of washing [50, 51, 52]. This can even be accomplished for biological nanoparticles (0.1 - 1 µm) such as extracellular vesicles using seed particles [53, 54, 55]. Gerlt et al. recently presented an acoustofluidic trapping and chromatography platform to trap nanoparticles [56].

Separation and sorting seem like the ideal tasks for acoustofluidics and sometimes when I hear researchers from other fields talk about separating or handling microobjects in a liquid, I wonder if acoustofluidics, could solve all their problems if they were introduced to the field. Cells or particles with different intrinsic characteristics, as density, compressibility and size, will react differently when exposed to a sound pressure field. A detailed explanation will follow in chapter 4.3. Consequently, the cells or biomarkers can be split into different groups corresponding to these properties. A good example for this is Per Augustsson's publication on isoacoustic focussing, where a density gradient in an acoustofluidic microchannel is used to align cells according to their density to measure their acoustic impedance [57]. Enriching, separating and isolating cancer cell from blood is an often targeted application [58, 59, 60] to study circulating tumour cells and learn about their behaviour in blood. Antfolk et al. presented an on-chip concentration and analysis system, where circulating tumour cells (CTC's) from enriched blood samples are concentrated using acoustophoresis (separation with the means of acoustofluidics) to be analysed on chip with dielectrophoresis [61]. Wu et al. separated exosomes (biomarkers in the nanometre size range, found in almost all body fluids) from blood by using surface acoustic waves to split the nano vesicles from the blood cells and other vesicles in a two-step process on chip [62]. He et al. addressed the problem of slow, sedimentation based urine analysis by presenting an automated

system, concentrating the urine using acoustic focussing [63]. Acoustofluidic devices have also proven their use for male fertility research by filtering sperm samples. Gai et al. have shown a selection procedure where sperm is selected according to size and motility using surface acoustic waves [64]. Recently, Abbasi et al. have presented a similar platform and observed a new effect, that they named acoustotaxis, where highly motile sperm swim against the propagation direction of the surface acoustic wave. They use this behaviour to select sperm with high motility and without the use of a pump [65]. Microfluidic fluorescence based activated cell sorting is another example of how ultrasound can be used to move microobjects [66, 67]. For example, surface acoustic waves can be used to align and deflect cells in a microfluidic fluorescence based activated cell sorter (μFACS) [68]. Many of these applications utilize the acoustic radiation force which can be described with the Gor'kov potential (sec.4.3).
In applications of acoustofludics, the presence of acoustic streaming is often an unwanted side effect due to the fact that it drags along small particles [69, 70]. Efforts have been made to suppress it using impedance gradients [71, 72] or through inhomogeneous fluids, specifically density and compressibility gradients [73]. However, other studies show its usability for micromixing [74, 75], for cell sorting [76] or for chemical signal enhancement [77].

4.3 Acoustic Radiation force

The experiments in this thesis do not deal with acoustic focussing, and the only reason that it is not observed is the choice of particle size. The acoustic radiation force arises when ultrasound is scattered at an object in the sound pressure field. It causes particles to move to the pressure node or antinode of the sound pressure field, depending on the material properties of the particle and the suspending liquid. The particle becomes a scattering monopole, if its compressibility is different from the surrounding liquid. In addition, a difference in density compared to the liquid leads to dipole scattering due to a phase shift relative to the incoming wave [14].
The force can be described by the Gor'kov potential $U_{\text{Gor'kov}}$ [78, 79]: Additionally to the pressure $\langle p^2 \rangle$ and velocity $\langle \boldsymbol{v}^2 \rangle$ of the acoustic field (timeaveraged over one period), the potential depends on the acoustic contrast in compressibility κ and density ρ between fluid and particle (contrast factors f_1, f_2).

$$U_{\text{Gor'kov}} = \frac{4\pi a^3}{3} \left(\frac{1}{2} f_1 \langle p^2 \rangle - \frac{3}{4} f_2 \rho_{\text{fluid}} \langle \boldsymbol{v}^2 \rangle \right) \tag{4.1}$$

with

$$f_1 = 1 - \frac{\kappa_{\text{particle}}}{\kappa_{\text{fluid}}} \tag{4.2}$$

and

$$f_2 = \frac{2(\frac{\rho_{\text{particle}}}{\rho_{\text{fluid}}} - 1)}{\frac{2\rho_{\text{particle}}}{\rho_{\text{fluid}}} + 1} \tag{4.3}$$

As mentioned, where particles are displaced to depends on their contrast factor: Particles with a negative contrast factor would move to the pressure antinode (maximum pressure, here that is near the channel walls) while particles with a positive contrast would move to the pressure node (minimal pressure, here the centre of the channel). The Acoustic radiation force $\boldsymbol{F}_{\text{rad}}$ is the force given by the gradient $\boldsymbol{\nabla}$ of the potential. So the slope of the potential determines how strong the radiation force is, while the steepest gradient determines the direction.

$$\boldsymbol{F}_{\text{rad}} = -\boldsymbol{\nabla} U_{\text{Gor'kov}} \tag{4.4}$$

The focusing behaviour, for which the gradient of the potential $\boldsymbol{\nabla} U$ provides the direction and force $\boldsymbol{F}_{\text{rad}}$ that moves a particle, is only valid for particles of a radius a much smaller than the wavelength of the sound.

As in the second chapter, we will assume a plane timeharmonic wave with pressure p_1 and velocity $\boldsymbol{v}_1$:

$$p_1 = p_{\text{a}} \cos(k_y y) \tag{4.5}$$

$$\boldsymbol{v}_1 = i \frac{p_{\text{a}}}{c_0 \rho_0} \sin(k_y y) \mathbf{e}_y \tag{4.6}$$

with: p_{a} = pressure amplitude, $k_y = 2\pi/\lambda$ wave vector, y = location across the channel width with $y = 0$ being one of the channel walls, c_0 = speed of sound in the liquid, ρ_0 = density in the liquid and $\mathbf{e}_y$ the unit vector in y-direction.
Inserting that in equation 4.4 and with 4.1 we can describe the acoustic radiation force as:

$$\boldsymbol{F}_{\text{rad}}(y) = 4\pi \left(\frac{f_1}{3} + \frac{f_2}{2} \right) a^3 \, k_y \, E_{ac} \sin(2k_y y) \, \mathbf{e}_y \tag{4.7}$$

with E_{ac}, the acoustic energy density:

$$E_{\text{ac}} = \frac{p_{\text{a}}^2 \, \kappa_{\text{fluid}}}{4} \tag{4.8}$$

Stokes drag from the liquid surrounding the particle counteracts the radiation force which is why it needs to be considered when determining the focussing velocity. To receive the velocity a particle focuses with, we balance $\boldsymbol{F}_{\text{rad}}$ and $\boldsymbol{F}_{\text{drag}}$ and solve for velocity $\boldsymbol{u}_{\text{rad}}$. We note, that the focussing velocity scales with the radius to the power

of 2, making it quite sensitive to particle's size. $\boldsymbol{F}_{\text{drag}}$ is the drag force, that the liquid exerts on a moving particle:

$$\boldsymbol{F}_{\text{drag}} = 6\pi\ a\ \eta\ \boldsymbol{u}_{\text{rad}} \tag{4.9}$$

with $a =$ particle radius and $\eta =$ dynamic viscosity. We set $\boldsymbol{F}_{\text{rad}} = \boldsymbol{F}_{\text{drag}}$ and solve for $\boldsymbol{u}_{\text{rad}}$:

$$\boldsymbol{u}_{\text{rad}} = \frac{2}{3\eta}\left(\frac{f_1}{3} + \frac{f_2}{2}\right) a^2\ k_y\ E_{\text{ac}}\ \sin(2k_y y) \tag{4.10}$$

We can now investigate if $\boldsymbol{u}_{\text{rad}}$ is large or small compared to any type of streaming that may be present in the fluid. To find the critical particle radius for streaming as opposed to focussing, we can calculate the ratio of the magnitudes of the two velocities:

$$\frac{|\boldsymbol{u}_{\text{str}}|}{|\boldsymbol{u}_{\text{rad}}|} > 1 \tag{4.11}$$

If the quotient is substantially larger than 1, the particle follows the streaming, if its substantially smaller than 1, it will get focused by the radiation force.
The maximum velocity magnitude of Rayleigh-type acoustic streaming along the floor and ceiling (details on that in sec.4.4.1) can be expressed [14, 34]:

$$\boldsymbol{u}_{\text{str}} = -\frac{3}{2}\frac{E_{\text{ac}}}{\rho_o c_o}\sin(2k_y y)\mathbf{e}_y \tag{4.12}$$

leading to the ratio:

$$\frac{|\boldsymbol{u}_{\text{str}}|}{|\boldsymbol{u}_{\text{rad}}|} = \frac{9\eta}{8\pi\ \Phi\ a^2\ \rho_0\ f} \tag{4.13}$$

For an acoustofluidic system like the one in this thesis, we insert:

- $\eta = 0.001\,\text{Pa}\cdot\text{s}$, dynamic viscosity of water
- $\Phi = \frac{f_1}{3} + \frac{f_2}{2}$, acoustic contrast factor
- $f_1 = 1 - \frac{\kappa_{\text{polyst}}}{\kappa_{\text{water}}}$
- $f_2 = \frac{2(\rho_{\text{polyst}}/\rho_{\text{water}})-1}{(2\rho_{\text{polyst}})/\rho_{\text{water}}+1}$
- $\kappa_{\text{water}} = 4.589\cdot 10^{-10}\,\text{Pa}^{-1}$, compressibility of water
- $\kappa_{\text{polyst}} = 2.5\cdot 10^{-10}\,\text{Pa}^{-1}$, compressibility of polystyrene
- $\rho_{\text{water}} = 998.2\,\text{kg/m}^3$, density of water
- $\rho_{\text{polyst}} = 1050\,\text{kg/m}^3$, density of polystyrene
- $a = 0.4, 0.5, 0.7369, 1, 1.5\cdot 10^{-6}\,\text{m}$, particle radius

- $E_{ac} = 10\,\mathrm{J/m^3}$, acoustic energy density

For a particle diameter $d < 1\,\mu\mathrm{m}$, streaming dominates over radiation. At $d \approx 1.47\,\mu\mathrm{m}$, the ratio is close to 1 which depicts the turning point. For 2 µm and 3 µm the ratio is smaller than 1 and the radiation force dominates.

Particle diameter	$\mathbf{u_{ustr}}/\mathbf{u_{rad}}$
0.8 µm	3.39
1 µm	2.17
1.4738 µm	1.0001
2 µm	0.54
3 µm	0.24

Table 4.1: Ratio of $|\boldsymbol{u}_{str}|$ to $|\boldsymbol{u}_{rad}|$ for different particle diameters

The critical radius for Rayleigh streaming is not the same as for thermoacoustic streaming. When comparing their velocities, we see that $|\boldsymbol{u}_{str}|$ is about 10 times slower than $|\boldsymbol{u}_{thstr}|$, allowing for larger particles to be streaming dominated. Experimentally this can be seen in paper I, fig.6 showing temperature and streaming velocity for different concentrations of DMSO. In that work, 2 µm large particles were used to trace the streaming recorded in water to compare it to thermoacoustic streaming at different Indocyanine Green (ICG) dye concentrations. We could not observe pure Rayleigh streaming in fig. 6(B) because the critical particle radius had been exceeded. However, thermoacoustic streaming appeared when ICG was added to the liquid, absorbing the laser light and creating the temperature gradient. Thus, to register thermoacoustic streaming, the 2 µm particles were a reasonable compromise between fluorescence brightness and ability to register the streaming flow.

4.4 Boundary effects and Acoustic Streaming

As outlined in sec.4.1, there are several kinds of acoustic streaming. In the acoustofluidic system used here there are Schlichting streaming and as a consequence also Rayleigh streaming, apart from the thermoacoustic streaming. Even though Schlichting/Rayleigh streaming and thermoacoustic streaming seem very similar, they are based on different physical phenomena. To understand the similarities and differences, I will broadly outline some theoretical background for both.

4.4.1 Rayleigh- and Schlichting streaming

Schlichting streaming appears in the viscous boundary layers near the walls, fig.4.3, and causes Rayleigh streaming in the bulk of the fluid. The Schlichting streaming

appears in the Stokes boundary layer at the channel walls which has a thickness δ of:

$$\delta = \sqrt{\frac{2\nu}{\omega}} = \sqrt{\frac{\nu}{\pi f}} \tag{4.14}$$

It depends on the kinematic viscosity ν of the fluid as well as the actuation frequency f or the angular frequency $\omega = 2\pi f$. For this work, that is a thickness of:

$$\delta = \sqrt{\frac{1.0035 \cdot 10^{-6}\,\mathrm{m^2/s}}{\pi \cdot 2 \cdot 10^{6}\,\mathrm{Hz}}} = 3.996 \cdot 10^{-7}\,\mathrm{m} \approx 0.4\,\mu\mathrm{m} \tag{4.15}$$

While it is not possible for us to visualize the Schlichting streaming in the viscous boundary layer due to its small size, we can instead observe its effect, the Rayleigh streaming. The force driving the Rayleigh streaming can be derived from the com-

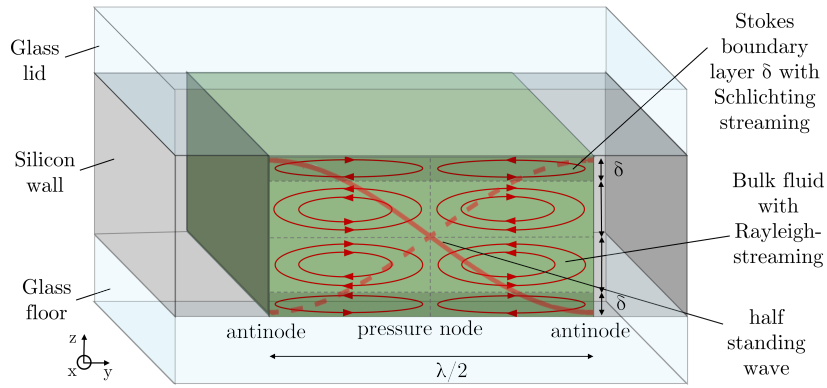

Figure 4.3: Schlichting streaming is found in the viscous boundary δ layer at the channel wall (not to scale, its much smaller than indicated here). It drives the Rayleigh streaming, which occurs in the bulk of the fluid. The sound pressure field is 0 in the center (node) and maximal on the sides (antinodes). For the half standing wave to resonate in the channel, the distance between the hard silicon walls needs to be half the sound's wavelength λ.

pressible Navier-Stokes equation:

$$\rho\left(\frac{\partial \boldsymbol{u}}{\partial t} + \boldsymbol{u}\cdot\boldsymbol{\nabla}\boldsymbol{u}\right) = -\boldsymbol{\nabla}p + \mu\boldsymbol{\nabla}^2\boldsymbol{u} + (\mu_b + 3\mu)\boldsymbol{\nabla}(\boldsymbol{\nabla}\cdot\boldsymbol{u}) \tag{4.16}$$

with: ρ = fluid density, $\boldsymbol{u}$ = spatial fluid velocity, t = time, p = oscillatory pressure of the sound wave, μ and μ_b = dynamic and bulk viscosity.
The pressure p in the microchannel that fits a half standing wave is zero in the center

and maximal at the sides (fig.4.3). The dynamic or shear viscosity μ dominates close to the walls, where there is friction between the liquid and the wall. Bulk viscosity is unintuitive (to me). It is associated with irreversible energy dissipation during timedependent compression and expansion of a fluid, like it those of the sound pressure field, which leads to damping. It acts on the divergence of the velocity $\boldsymbol{\nabla}(\boldsymbol{\nabla}\boldsymbol{u})$. To come to the point, the first term of the Navier Stokes equation $\rho\frac{\partial \boldsymbol{u}}{\partial t}$ represents the acceleration of the fluid particles and is important for the oscillatory acoustic motion. The convective term $\rho(\boldsymbol{u}\cdot\boldsymbol{\nabla}\boldsymbol{u})$ is the most important for Rayleigh streaming and will be discussed in the next paragraph. The equation also includes the pressure gradient $\boldsymbol{\nabla}p$ and viscous terms both for the boundary layer $\mu\boldsymbol{\nabla}^2\boldsymbol{u}$ and the bulk of the fluid $(\mu_b+3\mu)\boldsymbol{\nabla}(\boldsymbol{\nabla}\cdot\boldsymbol{u})$, as mentioned before. We will only have a closer look at the nonzero time averaged oscillatory velocity component of the (long and scary) equation because it represents the convection of momentum, which is essential to explaining Rayleigh streaming.
The nonlinear term

$$\boldsymbol{u}\cdot\boldsymbol{\nabla}\boldsymbol{u}\neq 0 \tag{4.17}$$

means that the interaction of the oscillatory velocity component $\boldsymbol{u}$ of the fluid, with itself inside the space of the channel is not zero. When averaged over time, the selfinteraction of $\boldsymbol{u}$ and $\boldsymbol{\nabla}\boldsymbol{u}$ produces a net force.
Coming back to my moshpit-at-a-concert example from the introduction, there is an analogy for this term: The crowd, loosely squeezed in the area in front of the stage, starts moving in an oscillatory motion (maybe they are all physicists and want to celebrate harmony). If they all were moving perfectly back and forth, there would be no net force, just the oscillatory movement. However, if some people, for example the ones at the wall due to friction with the wall, stand still and the ones next to them move slower than the ones closer to the center and so forth, the oscillatory motion will be disturbed. Averaged over time, the disturbance, caused by the people close to the wall, will increase until everyone in the crowd can notice that some people were not oscillating harmonically. That is where the netforce, driving the flow comes from, from the terms that do not disappear when we average the oscillatory field over time. In summary that means that there is oscillatory movement in the system, the nonlinear interactions of that with itself creates a steady force which leads to a streaming flow but only if there is a viscous boundary layer on the side that initiates it all.

4.5 Thermoacoustic Streaming

Thermoacoustic streaming is a variation of acoustic streaming that appears when the temperature in the resonator changes locally. Creating such temperature gradients can be achieved with different kinds of heat sources. The ultrasound itself can have heating

effects, as Li et al. showed [27] where a droplet was heated with surface acoustic waves. An example, that is closer related to the experiments presented in this work is the publication from my research group here in Lund, by Enrico Corato et al. [6]. They used Peltier elements, attached to aluminium plates at the channel sides to create a linear temperature gradient. The thermoacoustic streaming pattern and velocity were compared to acoustic streaming for an even temperature distribution. The linear gradient, spread 30°C over a distance of 375 µm and increased the convection or flow velocity from 6 to 11 µm/s (barely measurable) with only temperature gradient or only ultrasound, to 160 µm/s for heating and ultrasound combined. They observed, that the acoustic streaming pattern was suppressed and replaced with a pattern similar to the one they observe for thermal convection. They presented a COMSOL model which aided the explanation of the streaming pattern which appeared distorted due to an uneven sound pressure field. Furthermore, they found that the heat transfer due to the streaming liquid had a significant effect on the temperature distribution. In conclusion, the thermoacoustic streaming proved to be dominant over acoustic streaming or thermal convection and 15 to 30 times faster.

The origin of my thesis project lies in Wei Qiu et al.'s publication using an LED and an absorbing dye to heat an acoustofluidic microchannel [7]. The experiment was to shine a focused, blue LED onto a channel that was filled with water and an orange dye to achieve absorption of the light in the channel. 1.1 µm fluorescent tracer particles added so that the streaming was visible to the camera. The channel was twice as large compared to the one used in this thesis, which results in an actuation frequency of about 1 MHz to create the half standing wave in the channel. The authors found that the thermoacoustic streaming replaced the Rayleigh streaming visible without the presence of a temperature gradient. For a temperature gradient of 10°C/mm, this new, thermoacoustic streaming was nearly 100 times faster than that of the boundary driven Rayleigh streaming. A model was developed that showed a good match between experiment and simulation. The paper opened up a new research questions: How can the findings be used for transient or steady control of local flows in microchannels? At this point, this thesis picks up, replacing the LED with a focused laser beam in a similar acoustofluidic system, investigating time scales of the thermoacoustic streaming, experimenting with different temperature gradients as well as temperature induced density and compressibility changes. To understand how the potential of the thermoacoustic streaming was researched, some theoretical background will be introduced next.

4.6 Acoustic Body Force & temperature effects

So far in this chapter, we had a historical overview as well as an acoustofluidics application overview. Acoustic focussing and the radiation force were discussed and compared to acoustic streaming for different particle sizes. After that, Schlichting and Rayleigh streaming were discussed. Then the origins of this project were explained with literature in thermoacoustic microfluidics. Now it is time for thermoacoustic streaming, the core of this thesis.
In a nutshell, we use a laser and an absorbing dye, diluted in water, to heat an acoustofluidic microchannel. Without the created temperature gradient, we see Rayleigh streaming in the channel for particles smaller than 1 µm and acoustic focusing (due to the radiation force) for larger particles. The laser-induced temperature gradient leads to thermoacoustic streaming. The material properties of the liquid are temperature dependent, which influences the forces acting on the bulk of the liquid in the channel and changes shape and velocity of the acoustic streaming. The thermoacoustic streaming is a visual documentation of the interaction of ultrasonic pressure field and a laser-induced temperature gradient in an acoustofluidic cavity. To understand this interaction, we will look at the acoustic body force, driving the motion of the liquid. The acoustic bodyforce in acoustofluidic systems stem from spatial inhomogeneities in the compressibility or density of the fluid. It was first observed in systems having gradients in solute molecular gradients by Johansson et al and Deshmukh et al. [80, 81] and later described theoretically by Karlsen et al. [82]. The force landscape describing the thermoacoustic streaming can be described with the acoustic body force $\boldsymbol{f}_{\text{ac}}$ equation:

$$\boldsymbol{f}_{\text{ac}} = -\frac{1}{4}|p_1|^2\boldsymbol{\nabla}\kappa_{s,0} - \frac{1}{4}|\boldsymbol{v}_1|^2\boldsymbol{\nabla}\rho_0, \tag{4.18}$$

$$= -\frac{1}{4}\Big[|p_1|^2\Big(\frac{\partial\kappa_s}{\partial T}\Big)_{T0} + |\boldsymbol{v}_1|^2\Big(\frac{\partial\rho}{\partial T}\Big)_{T0}\Big]\boldsymbol{\nabla}T_0 \tag{4.19}$$

with $|p_1|^2$ being the pressure of the acoustic standing wave and $|\boldsymbol{v}_1|^2$ the velocity. It is also derived from the Navier-Stokes equation, like the Rayleigh streaming, but it additionally considers temperature induced inhomogeneities in density $\frac{\partial\rho}{\partial T}$ and compressibility $\frac{\partial\kappa}{\partial T}$.

Thinking of the concert-analogy, the thermoacoustic streaming depicts hot spots (or mosh pits), in a group of enthusiastic fans that get exceptionally excited. When the music plays, the group dances wildly, disturbing the harmonically moving rest of the crowd. In this example, it is not all the fans at the wall like it was for Rayleigh streaming, but maybe only a group in the center, or a few maniacs at the side of the crowd. Their disturbance remains throughout the concert and causes everyone else to have shifted their position, unlike a purely harmonically fan-base would. They drag

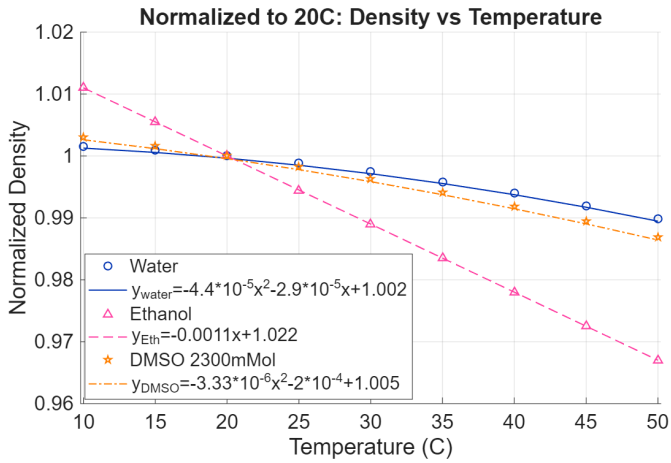

Figure 4.4: Density of water (blue o), and ethanol (pink △) and DMSO-water mixture (yellow ☆). The DMSO-water solution was measured as explained in publication III. The ethanol and water data was gathered from references [83, 84, 85, 86, 87, 88].

harmonically moving people with them, spin them around and release some at other points. Their hot spot remains, but the people that are moved around by it change.

Density and compressibility are temperature dependent and material-specific quantities. If the temperature of water increases from 10°C to 50°C, its density decreases by $\approx 2\%$ and its compressibility by $\approx 9.5\,\%$ (fig.4.4, 4.5).

For ethanol, the difference is even more drastic which would make it interesting to study for non-biomedical application since it is obviously not biocompatible. As Winckelmann et al. found out theoretically, with ethanol as a fluid, the acoustic radiation force direction seems to be reversible for polystyrene particles for a temperature increase of 1°C [89]. Due to its non-biocompatibility, ethanol was not considered an option for the experiments in this thesis.

We are keeping the temperature sensitivity of compressibility and density in mind, when looking at the body force equation. The force depends on the squared pressure and velocity of the acoustic field. Here we notice, that with a usual value around 10^5 Pa, the pressure has a much larger numerical value than the velocity which is in the range of 20-200 m/s. Consequently, the term including pressure will have a stronger influence on $\boldsymbol{f}_{\mathrm{ac}}$ than the velocity of the acoustic pressure wave. Taking the centred (also referred to as symmetric) laser spot position of publication I as an example, we can attempt to understand the acoustic streaming motion. With the pressure term dominating, and the acoustic body force pointing in the direction of the heat source, liquid is pushed from the side of the channel to the center, where the heat source is.

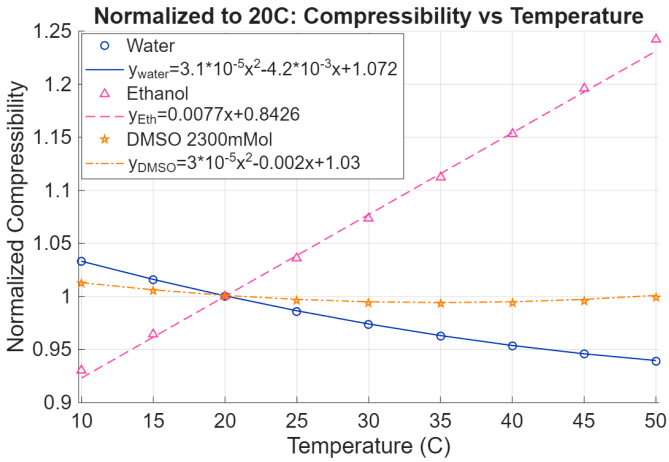

Figure 4.5: Compressibility of water (blue o), and ethanol (pink △) and DMSO-water mixture (yellow ☆). The DMSO-water solution was measured as explained in publication III. The ethanol and water data was gathered from references [83, 84, 85, 86, 87, 88].

In the center, however, the pressure drops to 0. Since water is mostly incompressible, the liquid that streams to the heat source then escapes through the center and away from the heat source, being pushed by the incoming liquid from the sides. Away from the heat source, the liquid is cooled by the channel walls and surrounding, cold liquid and is then moved towards the heat source again, by the acoustic body force. The result are streaming rolls, faster than the previously described boundary driven acoustic streaming. In publication I, the offcentered (or asymmetric) scenario depicts a different combination of acoustic field and temperature gradient. Here, the heat source is moved to the side of the channel, where the pressure is maximal. For this case, the liquid along the walls of the channel is accelerated towards the heat source by the body force. It moves the liquid at the heat source out of its way, towards the center of the channel, where the pressure, and consequently the acoustic body force, is lower. As the liquid cools down away from the heat source, the circle repeats and we can observe streaming patterns with only two vortices, instead of four as for the centred (symmetric) case.

In this first publication, the topic was to measure and classify the thermoacoustic streaming. The third publication is concerned with modifying the density and compressibility of the liquid even more, to play with the force balance of the acoustic body force equation. For that, we compare these properties for water, ethanol and Dimethyl Sulfoxide (DMSO). For water, a temperature change of 40°C affects the

compressibility 10 times more than it affects the density (fig.4.4 and 4.5). Ethanol has similarly drastic change in compressibility compared to density as the temperature increases with a factor of 7. One research question for this project was, in what way we can play with the liquid properties to manipulate the thermoacoustic streaming. For this, DMSO was studied because of its compressibility and density behaviour in the biocompatible temperature range. A 2.3 mol DMSO and water solution has a minimum in compressibility at 35°C. The slope, depicted by the term $\left(\frac{\partial \kappa}{\partial T}\right)$, changes sign from negative to positive at that temperature, while the density of DMSO, depicted by the term $\left(\frac{\partial \rho}{\partial T}\right)$ remains mostly unchanged. To compare what outcome that has on the power struggle in the body force equation, we summarize the compressibility term and the density term, while also considering velocity and pressure, as two forcing components:

$$\mathcal{F}_\kappa = -\tfrac{1}{4}|p_1|^2\left(\frac{\partial \kappa_s}{\partial T}\right)_{T_0} \tag{4.20}$$

$$\mathcal{F}_\rho = -\tfrac{1}{4}|\mathbf{v}_1|^2\left(\frac{\partial \rho_s}{\partial T}\right)_{T_0} \tag{4.21}$$

$$\mathcal{F} = \mathcal{F}_\kappa + \mathcal{F}_\rho \tag{4.22}$$

This enables to focus on the terms disconnected from the temperature gradient to compare their relative influence rather than all at once. To win the power struggle over the acoustic body force direction, a sign change of $\mathcal{F}_\kappa$ can lead to a reversal in thermoacoustic streaming pattern if the term is "positive" or "negative enough" to outweigh $\mathcal{F}_\rho$. The sign change can be achieved by changing the compressibility of the fluid, which is tunable in the whole channel through the background temperature. While in this work, the laser was specifically installed to create a local, spatially confined temperature gradient, the overall background temperature was set through Peltier elements on both sides of the chip. This temperature control allowed to tune the properties of the liquid in all areas, not only where the laser light is absorbed. Nevertheless, we have seen that the compressibility and density of water only decreases in the biocompatible temperature range but never increases. To achieve a sign change of the compressibility in the liquid, the temperature would need to be higher than 50°C to reach a minimum compressibility and then increase further to achieve a change in sign of the $\mathcal{F}_\kappa$ term and switch the direction of the acoustic streaming. The solvent Dimethyl Sulfoxide (DMSO) has its minimum compressibility at around 35°C for a concentration of 2.3 mol, when dissolved in water (cf. fig.4.5).

In publication III (sec. 6.3), we investigate experimentally how different concentrations of DMSO or different background temperatures at a specific DMSO concentration, in combination with the laser-induced temperature gradient, cause a reversal in the thermoacoustic streaming direction. Fig 4.6 and 4.7 show how $\mathcal{F}_\rho$

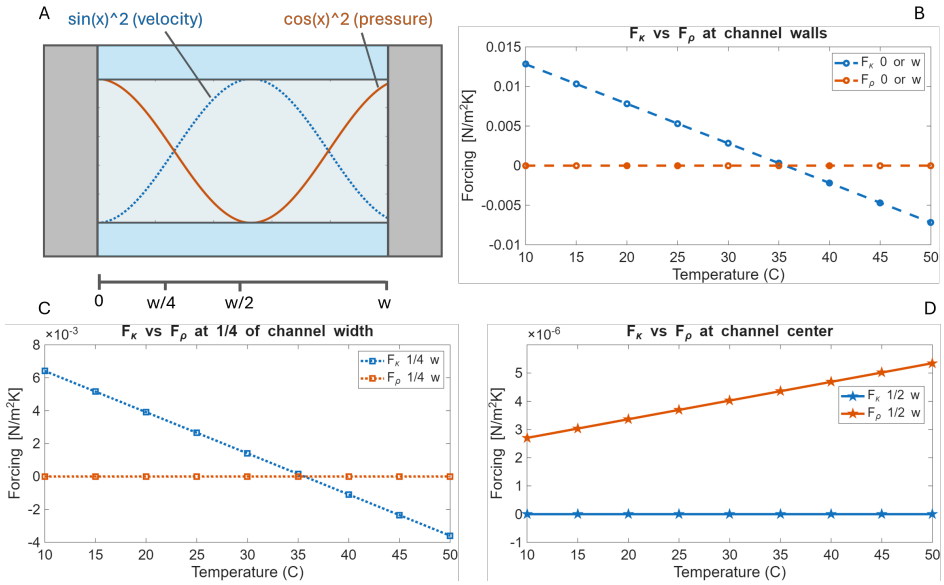

Figure 4.6: Forcing contributor comparison for different channel positions for a DMSO concentration of 2.3 mol. At the channel wall (B) and a quarter of the width into the channel (C), the compressibility term $\mathcal{F}_\kappa$ undergoes a sign change. At the center (half the width), $\mathcal{F}_\kappa$ becomes 0 because the pressure in the channel center is 0. However, the magnitude of $\mathcal{F}_\rho$ at the center is so too low to have a significant influence on the overall forcing. It is clear, that $\mathcal{F}_\kappa$ contributes much more than $\mathcal{F}_\rho$ to the forcing $\mathcal{F}$.

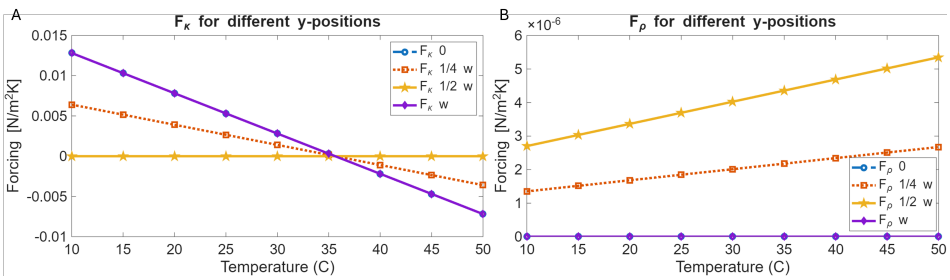

Figure 4.7: Comparing $\mathcal{F}_\rho$ (A) and $\mathcal{F}_\kappa$ (B) for different channel positions (as indicated in fig.4.6 (A)). $\mathcal{F}_\rho$ has an overall smaller magnitude than $\mathcal{F}_\kappa$. Positions 0 and w are the channel walls, which is why the curves are overlaying each other.

and $\mathcal{F}_\kappa$ change with temperature and compare their magnitude at different channel positions. Overall, $\mathcal{F}_\kappa$ is the stronger term while it also changes more drastically than $\mathcal{F}_\rho$. $\mathcal{F}_\rho$, in the range of 10^{-6}, is only ever equal or larger than $\mathcal{F}_\kappa$ around the turning point, where the density term changes sign. From the plots we can see, that the term worth focussing on is the compressibility term with $\mathcal{F}_\kappa$. However, the relative influence of the density term increases closer to the channel center as the pressure approaches zero. Hence, near the center, both terms become small compared to at the channel sides. To calculate the acoustic body force from it, we would need to consider the temperature gradient.
For publication III, simulations were performed calculating the resulting bodyforce, taking the temperature gradient into account, as will be discussed in the paper summary.

4.7 Time scales of Thermoacoustic Streaming

One major topic of the second publication is the timescales of buildup and decay of thermoacoustic streaming. Four aspects come into mind for time scales of the effect: light absorption, acoustic pressure and velocity field, the thermoacoustic streaming velocity itself and temperature transport.
From fast to slow, the time it takes for light to be absorbed is in the atto- to femtosecond timescale. For the purpose of the experiments we assume that to be instantaneous.
Similarly, the acoustic pressure field builds up in less than 1 ms. This can be estimated with the frequency $f = 2\,\mathrm{MHz}$ and Q-value [5]:

$$t_{\mathtt{sound}} = \frac{Q}{2\pi f} \tag{4.23}$$

$$= \frac{416}{\pi \cdot 2 \cdot 10^6} = 3.31 \cdot 10^{-5}\,\mathrm{s} = 0.031\,\mathrm{ms} \tag{4.24}$$

Assuming, conservatively, that 1000 cycles are necessary to build up the standing wave acoustic pressure field, that is still fast enough that it can be assumed instantaneous.

Acoustic streaming requires a sound pressure field and builds up about 10 times slower [5], assuming a Q-factor of 416. It can be calculated as the momentum diffusion time using the channel height $h = 150\,\mu\mathrm{m}$ and the kinematic viscosity $\nu = \eta/\rho_0 \approx 9 \cdot 10^{-7}\,\mathrm{m}^2/\mathrm{s}$ (shear viscosity $\eta = 8.9 \cdot 10^{-4}\,\mathrm{Pa\,s}$ and mass density

$\rho_0 = 9.971 \cdot 10^2\,\mathrm{kg\,m^3}$ of water).

$$\tau_\nu = \frac{1}{2\nu}\left(\frac{h}{8}\right)^2 \tag{4.25}$$

$$= 1.98 \cdot 10^{-4}\,\mathrm{s} = 0.198\,\mathrm{ms} \tag{4.26}$$

Thermal diffusion is a slow process, compared to the other ones at work, with approximately a quarter of a second across a 375 µm wide microchannel filled with water with thermal diffusivity in 2D of $\alpha_{\text{water}} = 1.5 \cdot 10^{-7}\,\mathrm{m^2/s}$:

$$t_{\text{diff}} = \frac{L^2}{4\alpha} \tag{4.27}$$

$$= \frac{(375 \cdot 10^{-6})^2}{6 \cdot 10^{-7}} \approx 0.23\,\mathrm{s} \text{ or } 230\,\mathrm{ms} \tag{4.28}$$

In sec. 2.6, the time for the water to fully heat up was calculated to be $t_{\text{heat}} = 13\,\mathrm{ms}$. For thermoacoustic streaming to be visible the water does not need to be fully heated up but it is still clear that it is one of the slowest contributors to the phenomenon.

To sum up, we expect the buildup time of thermoacoustic streaming to be highly influenced by the establishment of the temperature field due to the relatively slow thermal diffusion. Another important question, related to paper 2, has been to what extent the thermal diffusion can dominate over the generated thermoacoustic streaming. Is the generated temperature field affected by the advective flow? We observed in experiments that the measured temperature field is somewhat affected by the presence of the thermoacoustic streaming, but we could not capture this effect in the numerical model. This discrepancy is still unresolved.

Chapter 5
Setup and Data analysis

The setup, specifically built for this thesis project, had to be adaptable enough to accommodate a broad scope. There were only a few requirements but many possibilities and research questions. The one basic requirements was that there needed to be a laser, focused to a size significantly smaller than the LED used in the study by Qiu et al. [7] and that its light would be absorbed by the liquid in the microchannel to create a temperature gradient in an acoustofluidic cavity. Questions were manifold: how much power do we need, what wavelength should be used, how small do we want the spot to be? And the essential ones: will it work, will we even see anything? But also: how do we continue if it works? After a year and a half, during which various version of the setup had been built, rejected and improved, we could see the first laser-induced thermoacoustic streaming patterns and track the motion with particles. However, to be able to analyse the images in 3D and quantify the effect, the image quality needed to be improved. Artefacts caused by reflections of the laser were disturbing the imaging and the tracer particles were not bright enough in comparison. Nevertheless and simultaneously, new questions arose: how hot is it inside the channel, how quickly does the streaming build up exactly (we could see it was fast), can we pattern the light to change the effect and what would happen if the laser would scan over the sample? Most importantly, how can we improve the optics so that the data is trackable in 3D? And: how can we explain what is happening?
Three and a half years later, we have answers to most of the questions and we gained them with the setup that is presented in the following section.

5.1 The setup

To get an overview, we will continuously come back to the graphic of the setup in fig.5.1. In the figure, the setup is divided into six units (marked with letters A to F).

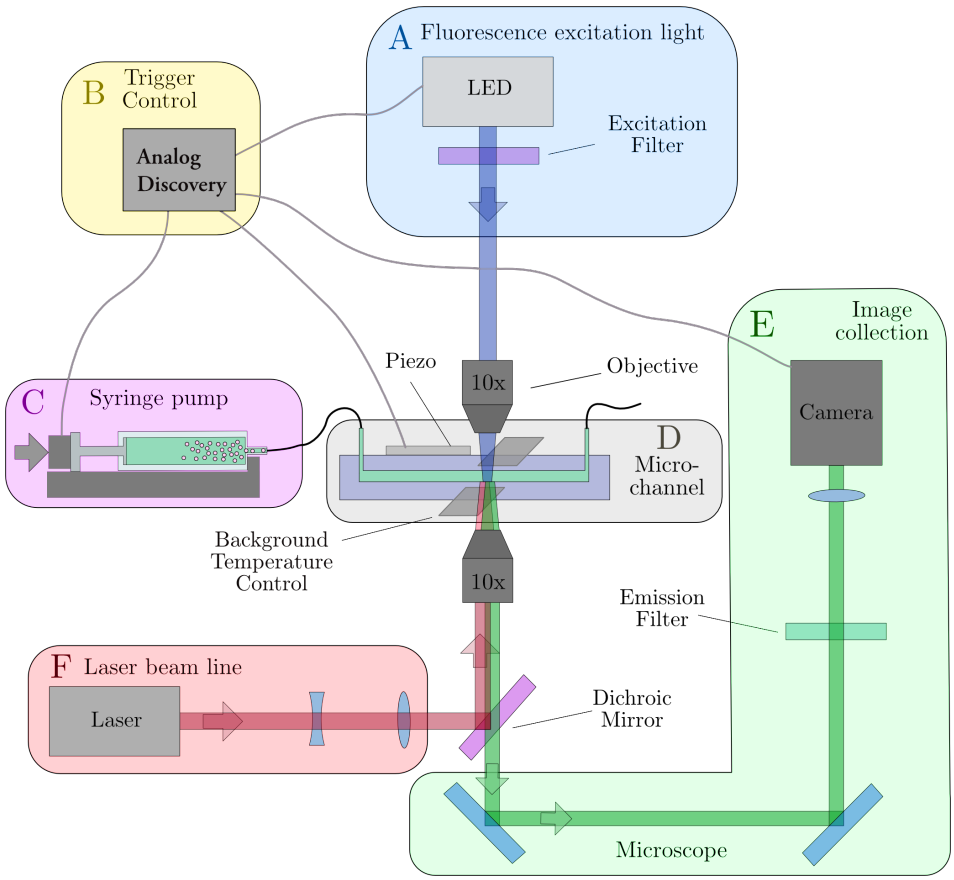

Figure 5.1: Overview figure of all components of the setup.

Each is described in its own subsection. A list with components and specifications is added at the very end of the thesis. The image analysis, data processing and simulations are outlined briefly at last, however details vary depending on research question and publication.

5.1.1 [A] Fluorescence excitation light

The blue-light LED is used to excite the fluorescence of the 1.1 µm or 1.9 µm sized tracer particles (fig.5.2). Its light is filtered with an excitation filter to avoid other wavelengths disturbing the imaging. The LED itself is mounted on a 3D translation stage for easy alignment so that the background illumination is as even as possible. The

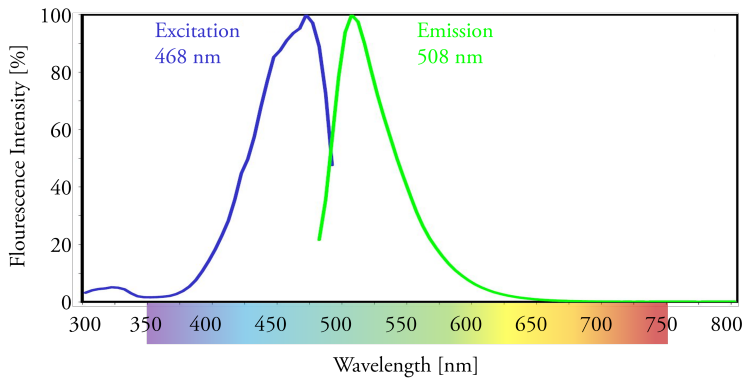

Figure 5.2: Absorption and emission spectrum of green fluorescent beads. The beads are 1.1 µm small (1.9 µm in paper I) and are used in the water-ICG solution to visualize the streaming and enable the tracking to quantify the streaming. Their fluorescence is excited with a blue LED. Data provided by manufacturer [90].

light wavelength is 470 nm. To blink the LED for paper II (transient thermoacoustic streaming), it was connected to the Analog discovery (referred to as trigger control), run with its Waveforms software. The LED was blinked because the fluorophore used for the temperature measurements photo-bleached to a degree where it was unusable after 10 ms. Therefore, unnecessary illumination was avoided by turning the light off between measurements.

5.1.2 [B] Trigger & Ultrasound Control and Automation

The trigger control and automation was managed with an analog discovery device. The analog discovery combined the functions of a waveform generator, power supply and for digital input and output for turning devices on and off at specific time points. Starting from the top of the graphic, it triggered the LED to blink for the temperature measurements or turn on and off during data acquisition of large data sets. It controlled the piezoelectric transducer, with the use of an amplifier in between. It gave a trigger signal to the camera to ensure an exact frame rate. It automated the workflow by: opening the valve, flushing with the syringe pump, closing the valve, triggering the LED at the same time as the camera for imaging and switched the ultrasound on and off between experiments.

5.1.3 [C] Syringe pump and flow

All experiments were conducted in stop-flow with exception of the sorting application example video in paper II. For this, a valve was installed to be able to flush the channel while being able to stop the flow quickly. The syringe pump and valve were automatized so that data could be recorded automatically: the valve would be opened, channel flushed, usually with about double its volume, and after a wait time of a few seconds the valve would be closed again.

5.1.4 [D] Microchannel, Piezoelectric transducer & Temperature Control

The channel used in all experiments is a single-inlet single-outlet straight microchannel. It is a made from a silicon layer anodically bonded to glass, in which the structure is etched with deep reactive-ion etching. A glass lid is anodically bonded on top, closing the cavity. On the top of the glass, a piezoelectric transducer is glued near the cavity but not covering it so that light can pass through. The background temperature is set through Peltier elements, which are connected to metal plates, touching the side of the glass channel. Thermal paste is used to improve temperature transfer. At the tip of the metal plates, PT100 temperature sensors are installed to read out the temperature of the plate. A custom made chip holder allows for precise alignment of Peltier elements, metal plates and chip in the microscope.

5.1.5 [E] Image Collection & Microscope

The microscope is an adapted, inverted Olympus miscroscope, where everything except for the objective holder, a lens underneath it two mirrors reflecting the light to the camera and the structural components were removed. That made space for the dichroic mirror, emission filters and a cylindrical lens to aid the particle tracking, as described in sec.5.3.

5.1.6 [F] Laser light

The laser is a 785 nm, circular polarized, near infrared light source with an output beam diameter of 1 mm and a maximum power of 250 mW, often used for Raman spectroscopy. For the experiments, is was focused to a size of 50 µm and run at 10 mW power. It is purely used for creating the temperature gradient, not illumination. The fluorescent dye, ICG, has an absorption peak at that wavelength and emits at about 820 nm (fig.5.3). The choice of laser and dye was based on the fact that they

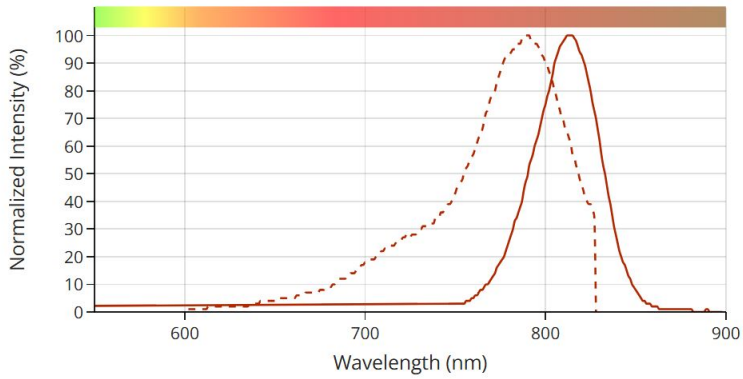

Figure 5.3: Absorption and emission spectrum of ICG [91]. The absorption fits well with the 785nm laser light. The emission is beyond what the camera can detect and consequently does not interfere with the imaging of the tracer particles, which emit at 508nm (c.f.5.2).

both operate outside the optical range of the particles and dyes commonly used in comparable experiments in the field and this specific research group. Moreover, even though the laser is near infrared, it is still visible to the human eye, which facilitates the alignment. The laser undergoes an inverted telescope lens setup, to increase its focusability when passing the objective in the microscope. In the beginning of the project, the laser was positioned where the LED is in the current constellation, leading to artefacts of the laser light in the sensitive camera. The use of suitable laser line filters could not filter the light sufficiently which is why the camera and LED position were changed. The dichroic mirror reflects the laser light to the objective at an angle of 45°while transmitting the emission light from the fluorescent tracer particles, that allow us to see the streaming. Its linear polarization would facilitate beam shaping experiments with an Spatial Light Modulator (SLM) since that requires polarized light (discussed in the outlook).

5.2 Simulations

The numerical models were created using COMSOL Multiphysics [92], simulating a 1 mm long section of the chip in 3D. The following description is based on publication I. The models and simulations of the other publications vary slightly from that, but the essential strategies are the same. The geometries and boundary conditions are highlighted in figs. 5.4 and 5.5. The parameters are listed in fig.5.6. For the material properties, the COMSOL inbuilt values for the respective materials were used.

We create the chip geometry as a cuboid with width W_{chip}, height H_{chip} and length L_{chip} and material properties of borosilicate glass. In the center of that, we place a silicon slab with height H and the same width and length as the glass. Centred in the silicon layer is the channel with width W, Heigh H and length L_{chip}. The resonator cavity consists of three parts: a centred, water-filled region of interest in the middle as well as a block of water on either side of it depicting inlet and outlet. With the geometry and materials in place, the laminar flow and heat transfer modules are applied.

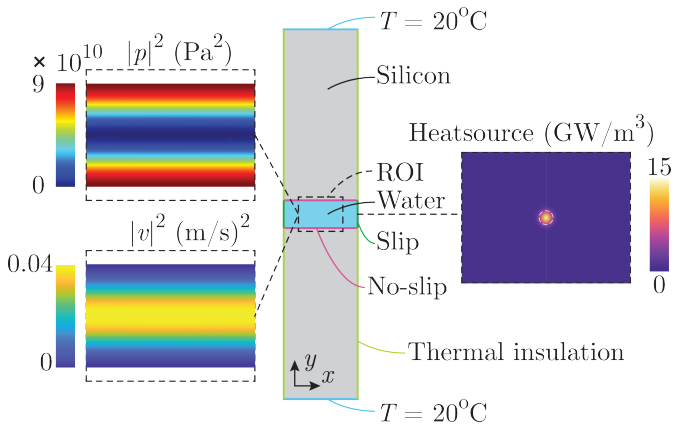

Figure 5.4: Topview, of COMSOL model as described in paper I. In this example, the laser spot is positioned in the center of the channel. Reproduced, with permission, from [93].

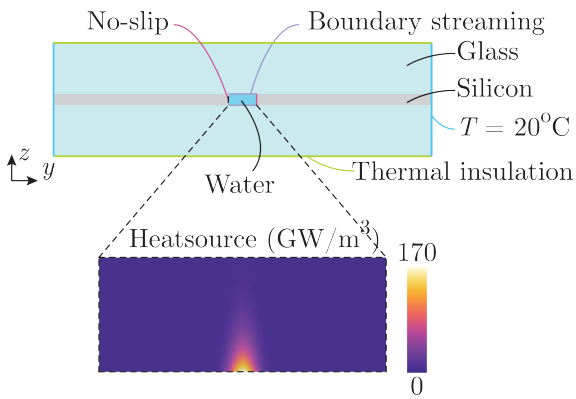

Figure 5.5: Sideview, of COMSOL model as described in paper I. Reproduced, with permission, from [93].

A no-slip condition is applied to the interface between water and silicon, i.e. the channel walls. The acoustic streaming is defined by imposing a velocity on the floor and ceiling through a sliding wall boundary condition with with velocity:

$$u_{\mathrm{w}} = \frac{3}{8} \cdot \frac{v_A^2}{c_0} \cdot \sin(2k_y y) \tag{5.1}$$

The inlet and outlet are approximated by perfect slip condition. The pressure and velocity of the sound are defined as $v = v_{\mathrm{A}} \cos(k_y y)$ and $p = p_{\mathrm{A}} \sin(k_y y)$ as in fig.5.6, respectively, and are used to calculate the bodyforce on the liquid applied in the entire channel volume. The temperature dependency of the density, compressibility and viscosity is taken into account by coupling the temperature field of the heat transfer module to the laminar flow module. It is important to note that the acoustic field is not modelled but assumed to be a perfect 1D plane wave across the channel. That is a weakness but it decreases the complexity and computational time of the model and seems to deliver sufficiently accurate results.

Gravity is included to mimic reality as close as possible even though volume effects play a minor role on the microscale compared to the macro scale. Introducing gravity to the simulation did not lead to a change in the results, except if the sound field is turned off.

Further, we define heat transfer starting with an overall initial temperature T_{bnd} of 20°C. The fluid's thermal conductivity is defined by the inbuilt material properties. The advection is taken from the velocity field solved for in the laminar flow module and thus the model is fully coupled. All outside walls of the cuboid are defined as insulating, except the outer side walls of the chip that are set to T_{bnd}, which is the only areas through which heat can escape. The heat source (Q)is modelled as a 2D Gaussian heat source, defined by the diameter of the laser beam and the attenuation coefficient, centred, or off-centred, entering through the channel floor. Its volumetric power density is given by:

$$Q = P_{laser} \cdot 2/(\pi\omega_0^2) \cdot a \cdot \mathrm{gauss2D}(x, y) \cdot \exp(-az) \tag{5.2a}$$

$$\mathrm{gauss2D}(x, y) = \exp(-2 \cdot [(x - x_{\mathrm{laser}})^2 + (y - y_{\mathrm{laser}})^2]/\omega_0^2) \tag{5.2b}$$

For paper III, where DMSO is added to the water to tweak its compressibility and density, the density and compressibility of the different fluids were determined experimentally and inserted into the simulation by polynomial fitting. We assume that the ICG dye does not change the thermal conductivity of the liquid which is reasonable considering the relatively low molar concentration of if in the sample, but including that in the model could increase the accuracy.

The mesh is a free tetrahedral, that is finest in and around the laser absorption area. To implement that, a cylinder is placed in the fluid domain at the laser point of incidence (at the middle of the channel floor), with the same height as the channel.
Variations of the simulation, apart from the DMSO compressibility and density properties in paper III, are the different absorptivities as well as a shifted laser spot location in papers I and II.

Name	Expression	Value	Description
Lchip	1 [mm]	0.001 m	Chip length
Lview	625e-6 [m]	6.25E-4 m	ROI length
Wchip	5 [mm]	0.005 m	Chip width
Hchip	1.5 [mm]	0.0015 m	Chip height
W	375 [um]	3.75E-4 m	Channel width
H	150[um]	1.5E-4 m	Channel height
xLaser	0 [m]	0 m	Laser x-location
yLaser	0 [m]	0 m	Laser y-location
Plaser	5.8 [mW]	0.0058 W	Laser power
Wlaser	50 [um]	5E-5 m	Laser beam diameter
w0	Wlaser/2	2.5E-5 m	Laser beam radius
Trm	0.9	0.9	Transmittance coefficient
A	-log(Trm)	0.10536	Absorbance
a	A/H	702.4 1/m	Attenuation coefficient
Tbnd	20[degC]	293.15 K	Ambient temperature
Eac	10[J/m^3]	10 J/m^3	Acoustic energy density
ky	pi/W	8377.6 1/m	Wave vector
kappa0	1/1000/1500^2 [Pa]	4.4444E-10 1/Pa	Compressibility of fluid
rho0	1000 [kg/m^3]	1000 kg/m^3	Density of fluid
c0	1500 [m/s]	1500 m/s	Speed of sound
pA	sqrt(4*Eac/kappa0)	3E5 J/m^3	Pressure amplitude, sound
vA	pA/rho0/c0	0.2 m/s	Velocity amplitude, sound
R	1e-6 [m]	1E-6 m	Particle radius PS beads
Phi	0.2	0.2	Acoustic contrast PS beads

Figure 5.6: Parameters for COMSOL simulation of publication I, laser position in the center. For the other studies certain properties like laser position (paper I, case II) or compressibility and density of the fluid (paper III) were modified.

5.3 Measuring streaming velocity fields

The images collected with the setup are processed using an image-defocusing-based 3D particle-tracking method, also referred to as General Defocused Particle Tracking (GDPT) [94, 95, 96]. Particles at different heights, i.e. different distances to the focal plane of the objective, appear differently defocused (see fig.5.7).

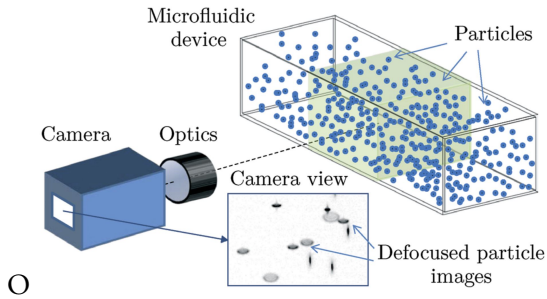

Figure 5.7: A camera is imaging a volume filled with spherical particles. Depending on the distance of the objectives focal plane to the particle, it appears differently defocused. Reproduced, with permission, from [95]

A calibration stack is recorded, comprising images of a particle positioned at a known height, over a distance z along the depth, to create a height-reference for the defocused particle images (fig.5.8). Then, the sample images can be cross-referenced with the calibration stack to find the position of the particles in the sample.

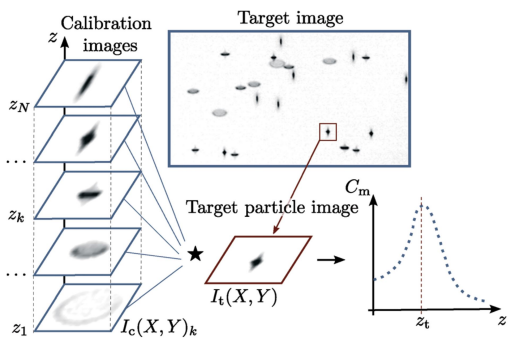

Figure 5.8: A calibration stack of a particle at known height, often sedimented to the channel floor, functions as a reference and the height position (z) of each particle in the volume can be determined. Reproduced, with permission, from [95]

With a cylindrical lens, the accuracy of the method improves as the distortion at different z-heights is clearer (fig.5.9).

An ideal spherical lens would deliver the same image of a round particle at equal distance above or below the focal plane. The particles appear different because of aberrations, so lens imperfections. The focal point of a lens is shifted, depending on how far away from the optical axis the light passes through it. This imperfection is taken advantage of in GDPT.

The x-, y- and z-position of each particle is determined using the MATLAB program DefocusTracker [97, 98]. The volume is divided into volume blocks or areas (depending on if the analysis is in 2D or 3D) and then the average velocity of the particles registered in each block or area is computed.

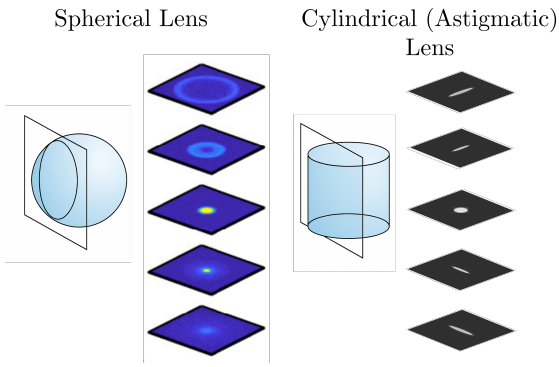

Figure 5.9: The defocused images of round objects, such as polystyrene particles, of a spherical and a cylindrical lens are different due to their in focal axes: The cylindrical lens only focuses along one axis while the spherical lens focuses in x- and y. Adapted, with permission, from [96, 99]

5.4 Measuring temperature

Measuring the temperature in acoustofluidic microchips is a challenge due to the small dimensions, that exclude large temperature probes, their in-transparency for deep infrared light and the fact that any object in the cavity affects the resonance and consequently the acoustic field.
We approached this challenge by measuring temperature with probes as close to the chips walls as possible, to be used as a reference for the fluorescence of a temperature sensitive fluorophore, here BCECF (paper II). The recorded images were smoothed with a Gaussian filter and uneven background illumination was accounted for with a pixel-wise calibration. The relation between the intensity I and T_{set} was fitted to a line as $I(x,y) = m(x,y)T_{\text{set}} + q(x,y)$. After capturing the experimental images (I_{exp}), at the desired time points, we used the inverted formula $T(x,y) = [I_{\text{exp}}(x,y) - q(x,y)]/m(x,y)$. Thus we could obtain a temperature map for the whole field of view at every frame. However, BCECF is fast bleaching and one volume in the ROI could only be used for a single frame with an illumination time of less than 10 ms. Moreover, measuring the temperature on the outside of the channel leaves room for inaccuracies and a more reliable temperature measurement method is desirable (further discussion in the outlook).

Chapter 6

Summary of Papers & Results

6.1 Paper I: Configurable thermoacoustic streaming by laser-induced temperature gradients

Laser light induces a temperature gradient in the fluid of an acoustofluidic microchannel and causes, in addition to the boundary-driven acoustic streaming, a thermoacoustic streaming due to a localized, temperature-related density and compressibility gradient. A green dye (ICG) was added to the liquid to allow tunable absorption of the near-infrared light. The specialized setup and experimental procedure are presented in detail and the gathered experimental data analysed in 3D and compared to simulation results. The thermoacoustic streaming is benchmarked for two different temperature gradients, at different locations along the width of the channel (fig.6.1), and for five different absorptivities of the light in the liquid.

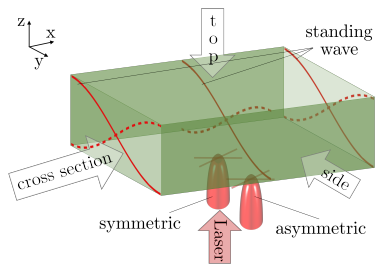

Figure 6.1: Channel orientation and laser spot positions at channel center (symmetric) and at channel side (asymmetric).

If the temperature changes, the compressibility of water changes more drastically than its density. Consequently, the first term of the acoustic body force considering the pressure becomes more important than the second term with density and velocity (eq.4.18). The density term is not negligible, but for the understanding we can focus on the compressibility distribution. A centred, localized temperature gradient with a hot spot in the center (as in fig.6.2 a) decreases the compressibility at its peak to a distribution as in (b). In combination with a pressure gradient with a node in the center and maximum values at the side, as in (c), the acoustic body force will point towards the heat source and is the strongest at the high-pressure wall region in the section where the temperature gradient is the steepest (d). The body force as in (d) leads to a thermoacoustic streaming pattern as in fig. 6.3 B (shown in topview at top, mid and bottom height of the channel, for sideview and cross-section, see paper I). To investigate another constellation of pressure field and temperature gradient, the laser spot position, i.e. the heat source, was shifted to near the side wall of the channel cavity in a second experiment. In the asymmetric temperature distribution, compared to the pointsymmetric, centred case, the overall streaming velocity was slightly lower and the pattern changed to be centred around the heat source at the side of the channel (fig.6.3 D). For the corresponding simulations, where the laser light was modelled as a Gaussian beam, and the resulting temperature distribution was used as an input for the flow computation, the acoustic field has not been simulated but

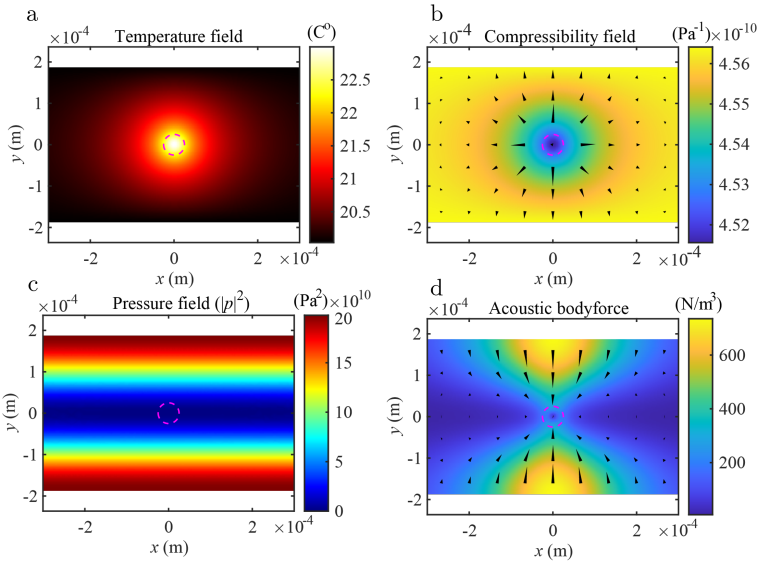

Figure 6.2: Illustration of the components of the acoustic body force for the laser spot positioned in the center (red dashed circle) and a half standing wave with pressure node in the center: a) temperature gradient, b) compressibility field c) pressure field and c) the resulting acoustic body force. Reproduced, with permission, from [93].

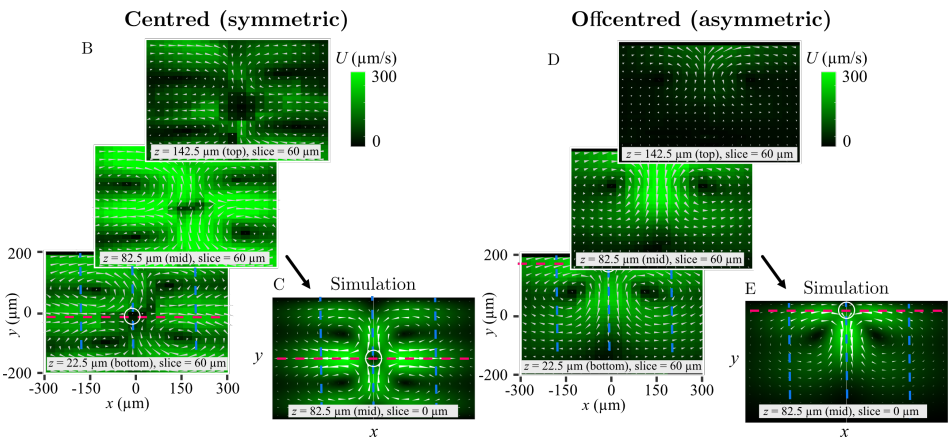

Figure 6.3: B) Centred (symmetric) vs D) offcentered (asymmetric) heat source position, experiments and simulation (C, E), topview, at different channel heights. Reproduced, with permission, from [93].

was implemented using analytical expressions for the acoustic pressure and velocity fields and as no-slip sliding walls for the velocity of Rayleigh streaming. The channel walls were given a no-slip boundary condition with exception of the inlet and outlet of the geometry. The simulation results depict a good match to the experimental results.

The second experiment investigated thermoacoustic streaming for different degrees of absorption of laser light in the fluid. Here, we observe an increase in streaming velocity, the higher the amount of absorbed dye (fig.6.4) with the goal to influence the penetration depth of the light to shorter distances for higher absorption. In contrast to the results presented by Qiu et al. [7], where an LED functioned as a light source for heating, we observe no full streaming rolls in the $y-z$-cross-section. The reason lies in the temperature distribution: the gradient induced by the laser is 16 times higher, because it is more compact in the y-direction compared to the broad gradient induced by the LED. Heating with the LED creates a broad gradient, that reaches to the channel walls, where the pressure amplitude is the high and two streaming rolls form in the $y-z$ plane. Fluid is pushed inwards, away from the walls, where the z-component of the acoustic body force is weak and the fluid can move upwards. While heating with a laser the inward force is less pronounced compared to the opposing downward force and the fluid escapes along x.

A custom setup was presented to create laser-induced temperature gradients in an acoustofluidic cavity. We could show that the thermoacoustic streaming has an approximately 10 times higher streaming velocity than boundary-induced streaming has without the presence of a temperature gradient and that the position of the heat source with respect to the pressure field can change the shape of the streaming pattern, both in experiments and stimulation. We demonstrated the effect the localised gradient has on the streaming pattern for different absorption depths along the height of the channel and compared it to previous experiments with a less localized heat source.

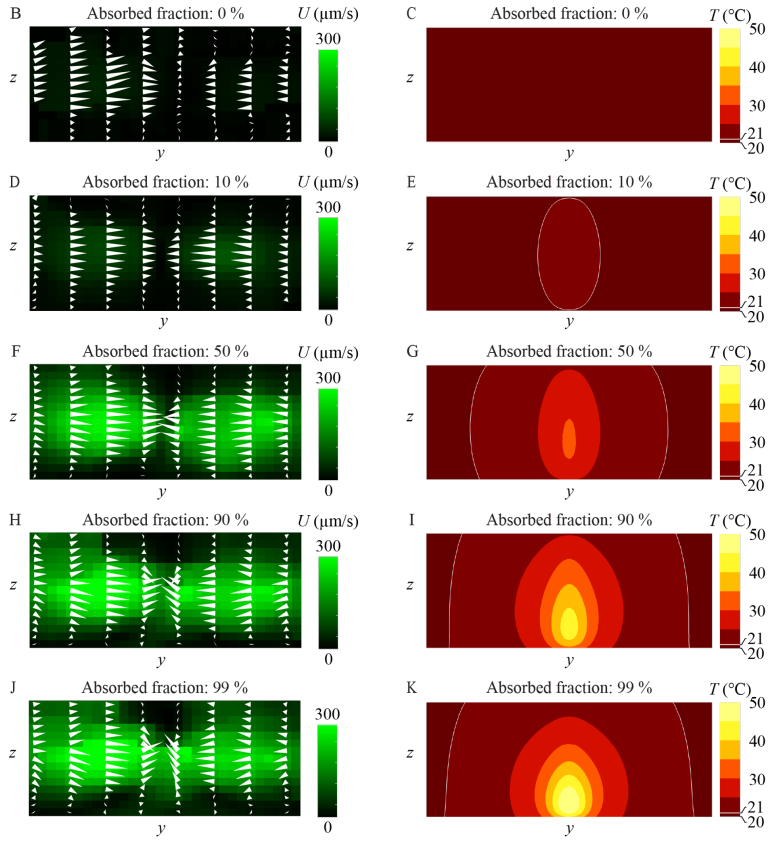

Figure 6.4: ICG is added to the liquid in the channel to enable absorption of the laser light. Increasing amounts of dye (left column, B-J, cross-sectional view) lead to decreasing penetration depth and higher temperatures until a threshold of 50°C is reached. Reproduced, with permission, from [93].

6.2 Paper II: Temporal evolution of thermoacoustic streaming around spatially confined temperature gradient

This publication measures the timescales of buildup and decay of thermoacoustic streaming and shows a temperature increase of 20°C during actuation, in experiments and simulations. We also show in a video that a single, 1 µm sized particle can be moved from the side of the channel to the center with a pulse of thermoacoustic streaming, while a nearby particles trajectory remains unaffected.

The setup configuration is nearly the same as in paper I, except for an additional trigger unit to realise the precise temporal control of imaging, light and sound field. The laser spot is positioned near the side wall of the channel, as in the asymmetric temperature gradient in the previous publication. Two scenarios were tested: toggling on and off the laser light with an already established sound field or toggling on and off the sound field with an already established temperature gradient. Moreover, the temperature was measured in the channel using a temperature sensitive fluorophore, BCECF.

At a frame rate of 100 Hz, the maximum possible imaging speed was reached at which the particles were still detectable by the processing algorithm. For an existing temperature gradient and a triggered sound field, that was not fast enough to capture the buildup or decay. Simulations show that the buildup time for this scenario is around 2 ms. Nevertheless, the buildup for an already established sound field and triggered laser, was 10 times slower and could be measured experimentally and also shown in simulations. The reason lies in the comparably slow thermal diffusion process: while the sound pressure field builds up in less than 1 ms, thermal diffusion takes about 8 ms for the presented system. The decay of the two scenarios is not a reversal

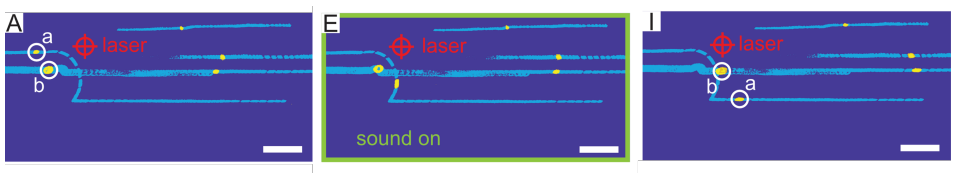

Figure 6.5: Frames of exemplary sorting application video. A (left) before activation of thermoacoustic streaming. The two particles a and b (marked with white circles) flow close to each other from left to right. E (middle) during trigger. Particle a moves from the side of the channel to the center, moving in a bow around particle b. I (right) after trigger ended. Particle b remained on its trajectory, as indicated by blue streamlines while particle a has moved and is now more centred in the channel.

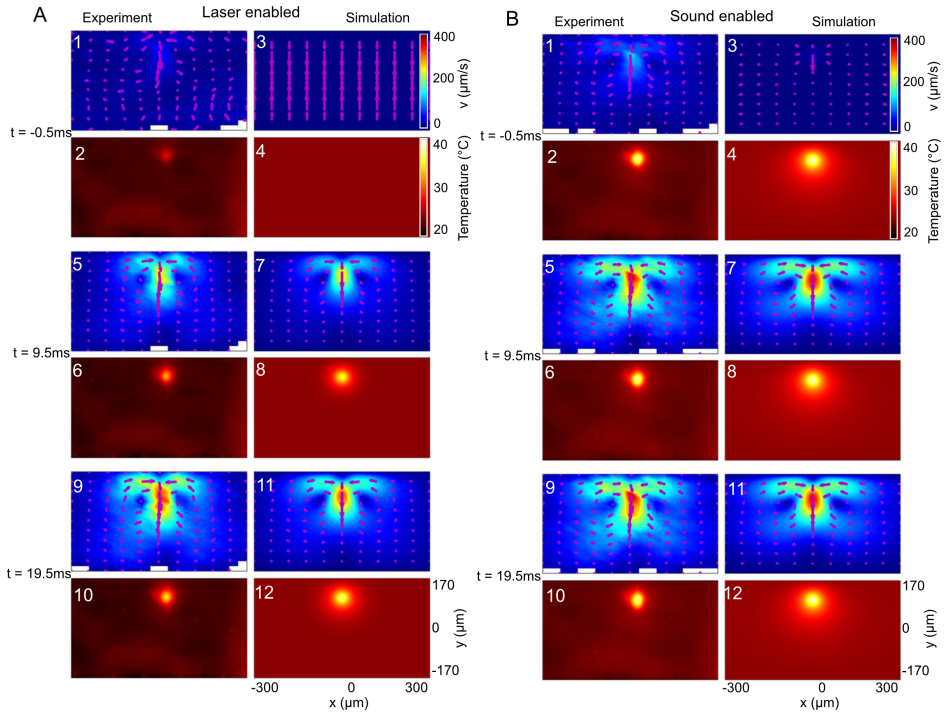

Figure 6.6: Buildup of thermoacoustic streaming for the two different configurations: (A) laser ON at $t = 0\,\mathrm{s}$ and (B) sound ON at $t = 0\,\mathrm{s}$. The left columns of A and B show experimental results of thermoacoustic streaming and temperature at three different times t. The right columns show the corresponding simulation results for thermoacoustic streaming and temperature. All arrows are normalized to their respective frame.

of the buildup since the laser builds up from a small source but decays evenly which enlarges the streaming rolls rather than decreasing their size. One open question depict arc-shaped streaks of higher temperature in the experimental temperature results that so not appear in the simulations. The streaks could come from artefacts of the sensitive temperature measurement or some unaccounted-for effect in the simulation or both.

Fig.6.8(a) shows the velocity amplitude of the whole cycle with two zoom-ins on buildup (b) and decay (c), for a small region of interest (black box in (d)) around the laser spot. After the initial increase, we can see a dip in streaming velocity which we cannot yet fully explain and that we did not observe in simulations. We could exclude that the effect originates from advection, where heat is transported away and the temperature and velocity drops until a stable temperature distribution is reached by calculating the Peclet number to be in the creeping range (cf. chapter 3). The

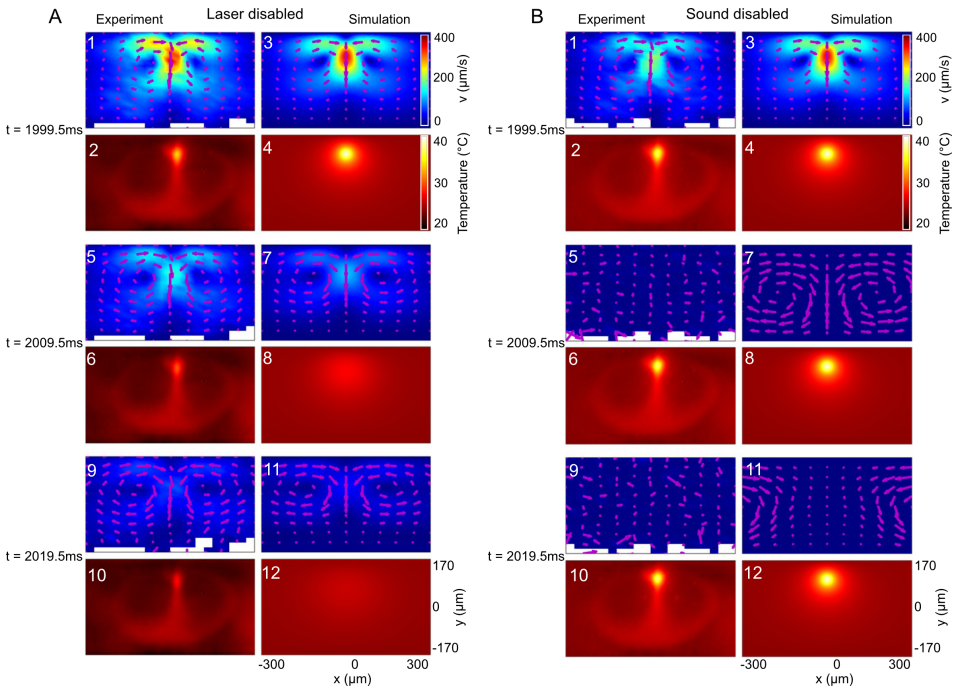

Figure 6.7: Decay of thermoacoustic streaming for the two different configurations: (A) laser OFF at $t = 2\,\mathrm{s}$ and (B) sound OFF at $t = 2\,\mathrm{s}$. The left columns of A and B show experimental results of thermoacoustic streaming and temperature at three different times t. The right columns show the corresponding simulation results for thermoacoustic streaming and temperature. All arrows are normalized to their respective frame.

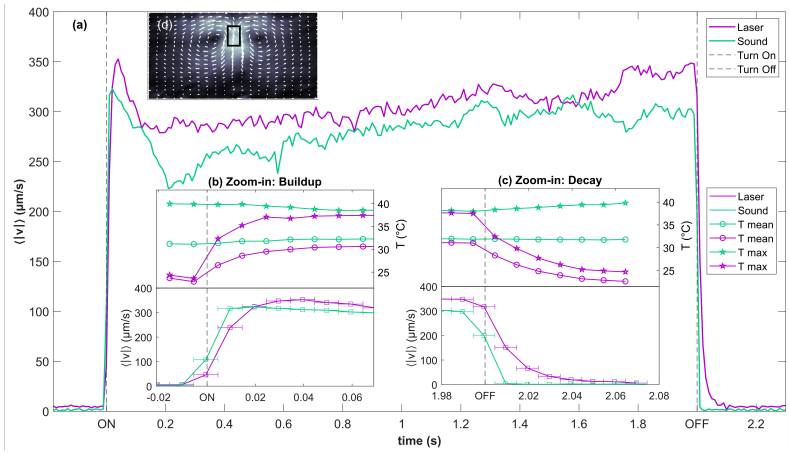

Figure 6.8: Measured streaming velocity (a) and temperature (b,top) in the laser spot for laser (pink) or sound (green) enabled at 0 s and disabled at 2 s. The velocity is extracted only from the ROI (d, black rectangle). Insets (b) and (c) show details for buildup and decay velocity evolution as well as the measured temperature in the ROI, as mean (circles) or max (stars). The dashed lines indicate when the laser or sound was en- or disabled.

video included in the publication demonstrates the use of thermoacoustic streaming for cell separation applications, cf. fig.6.5. It shows two particles flowing through the channel with a distance of 25 µm to each other. As the one particle reaches the laser point of incidence, the laser is triggered, causing the particle to move from the side to the center of the channel with a speed of 350 µm/s, while the other particle, further away from the laser spot, remains on its trajectory. After the trigger ends, both particles continue to follow the parabolic flow profile of the laminar flow. We think that thermoacoustic streaming, triggered in short bursts, has the potential to sort specific micro- or nano-objects contact- and label-free.

6.3 Paper III: Reversal of thermoacoustic streaming direction through compressibility and density tuning

This work shows that the thermoacoustic streaming direction can be reversed by manipulating the density and compressibility through the concentration of a solute molecule in the fluid or the temperature in the channel at a specific concentration, in experiment and simulation.

In the thermoacoustic body force equation we can observe the two terms: $\mathcal{F}_\kappa = -\frac{1}{4}|p_1|^2\left(\frac{\partial \kappa_s}{\partial T}\right)_{T0}$ and $\mathcal{F}_\rho = -\frac{1}{4}|\underline{\mathbf{v}}_1|^2\left(\frac{\partial \rho}{\partial T}\right)_{T0}$. The sign and magnitude of the acoustic body force depends on the temperature derivates of $\mathcal{F}_\kappa$ and $\mathcal{F}_\rho$. Both components can be altered by varying the concentration of DMSO molecules, and through adjustments of the background temperature. The density of DMSO has a negative slope throughout the biocompatible range (fig.6.9) and can consequently not contribute to the reversal of the thermoacoustic streaming. Contrary, the compressibility of DMSO has a local minimum at a concentration of 2.3 Mol and 30°C, unlike water, which reaches its minimum above 50°C (fig.6.9). The positive slope above 30°C enables $\mathcal{F}_\kappa$ to compete with $\mathcal{F}_\rho$ and lead to the reversal of thermoacoustic streaming. Alternatively, by altering the concentration of DMSO, we can reach the local compressibility minimum at a constant temperature and change the dominating contributor (see also chapter 4 as well as fig.4.6 and fig.4.7).

Fig. 6.10 shows the acoustic body force for different concentrations and temperatures. While it is not intuitive to see which combination results in reversal, since the bodyforce points to the heat source (center of the channel) for all combinations, we can observe the isolines (white) to make a qualified guess: The middle plot in the right column shows three isolines from center to side wall, over a distance that corresponds to 187.5 µm, while such a steep decay in force does not appear in any other direction. We can conclude, that the streaming along x (at $y = 0$) should dominate due to the higher forcing. Comparing to the middle plot in the left column, we can see a decrease in force across the width for $x = 0$ while the force across the length at $y = 0$ seems largely unchanged. Consequently, for this combination, the streaming along y (at $x = 0$) should dominate. This can also be seen in fig.6.11, which shows the corresponding simulated velocity fields.

The experimental results of streaming plots at 20°C, 25°C and 30°C at a concentration of 2.3 mol are shown as topview in fig.6.12. Looking at the insets A2 and C2, we can see a clear change in streaming direction between the top and bottom. The transitional

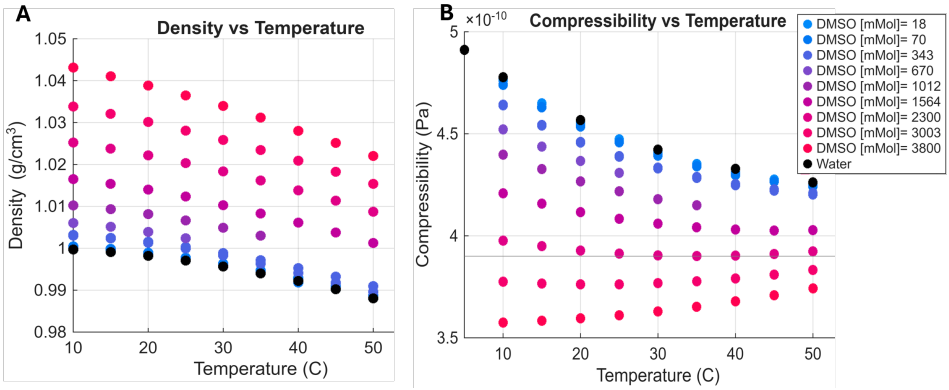

Figure 6.9: Density and Compressibility for water and DMSO solutions. The density curves are shifted to higher values for lower concentrations. The compressibility changes from a negative to a positive slope within the biocompatible temperature range for solutions with concentrations of 1.5 mol and higher.

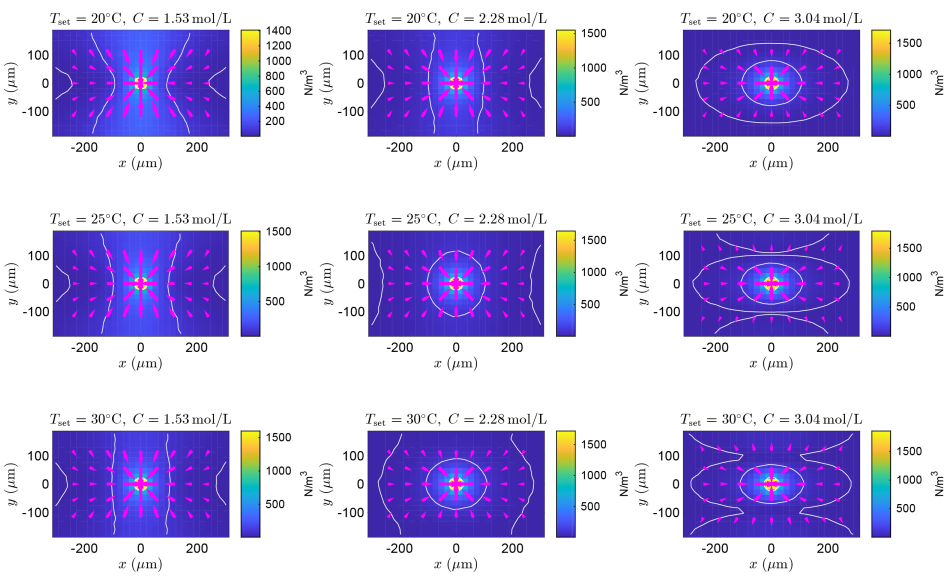

Figure 6.10: Simulation plots of acoustic body force for different concentrations of DMSO (1.5 mol, 2.3 mol, 3 mol) and varying temperatures (20, 25 and 30°C). Isolines in white, the force is the same along those lines.

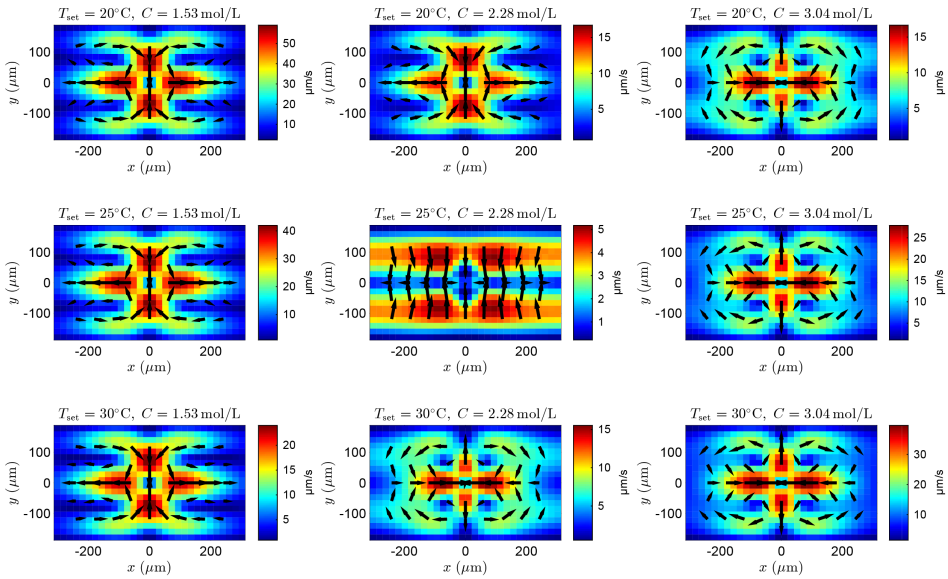

Figure 6.11: Modelled thermoacoustic streaming plots for different concentrations of DMSO and background temperatures.

regime is shown in B1 and B2 and we can see that the streaming pattern is some variation between A1 and C1. However, comparing to streaming patterns for water and a centred laser, the typical four-roll streaming pattern does not appear as clearly in A1 and not at all in C1, which has two streaming rolls that resemble the streaming pattern with the heat source closer to the side wall.
Fig.6.13 shows the streaming at three different DMSO concentrations. Here, the four roll streaming pattern is clearly visible in A1 and C1. The zoom-ins A2 and C2 show that the streaming reverses and B2 indicates a similarly unclear in-between state as seen in the figure for varying temperature.
The unexpected two role streaming pattern could be caused by an changes in the resonance frequency of the system, which varies with temperature. During the measurements, it was clearly noticeable, that the alignment of the laser spot in the channel center was more sensitive than for previous experiments, which, in combination with a slightly different acoustic field could explain the discrepancy. For future experiments, choosing the heat source location on the side of the channel could make the results clearer since the alignment is less sensitive.

We imagine that the ability to reverse the direction of the thermoacoustic streaming opens new possibilities for nano- and microparticle sorting. Investigating other

molecules could lead to exciting, yet unknown effects on the thermoacoustic streaming pattern.

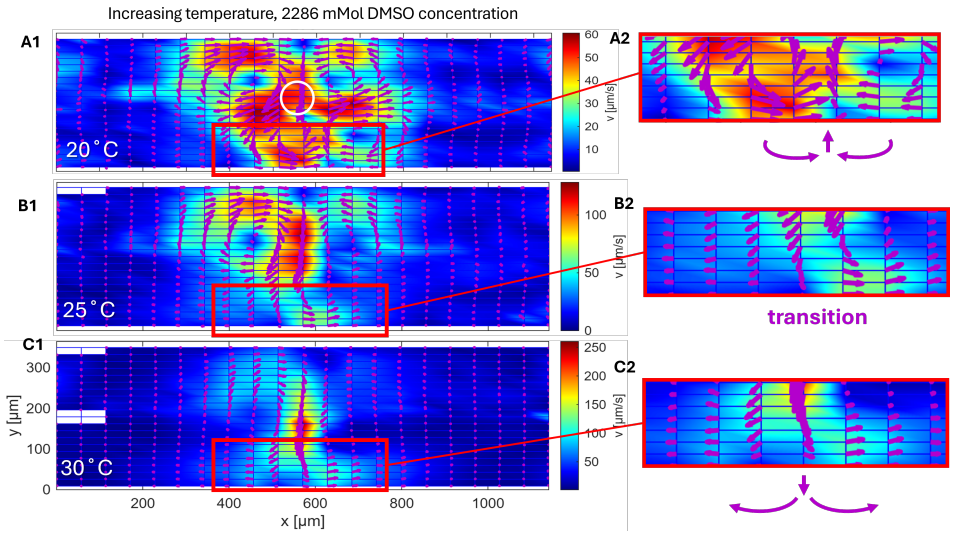

Figure 6.12: Thermoacoustic streaming pattern for a concentration of ≈2.3 mol and varying background temperatures (topview, experimental data plots).

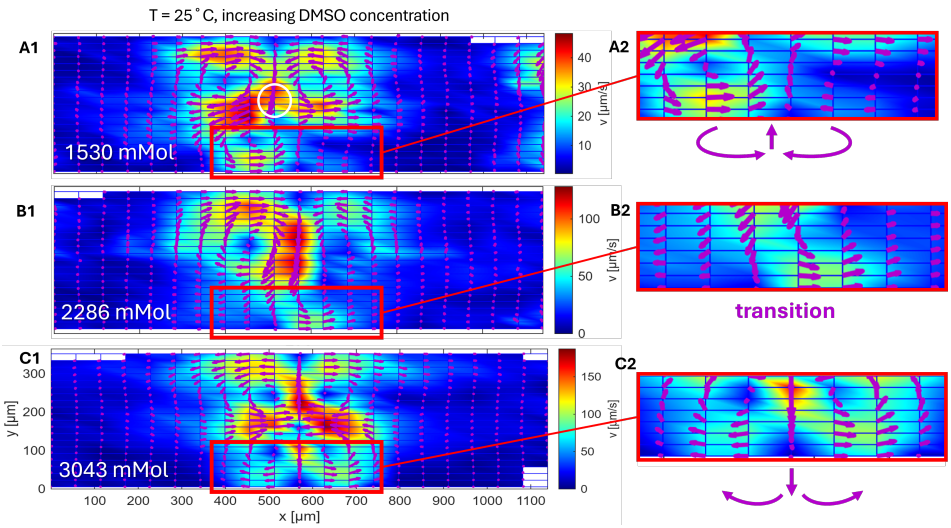

Figure 6.13: Thermoacoustic streaming patterns for varying concentrations of DMSO at a constant background temperature of 25°C (topview, experimental data plots).

Chapter 7
Conclusion

7.1 Discussion and Outlook

After having classified the thermoacoustic streaming and demonstrated it's shape in 3D, measured its time scales and played around with the fluid's material properties to reverse it, there are still many more open questions worth researching.

7.1.1 Cells vs. particles

First of all, all experiments were demonstrated with polystyrene particles. Biological cells are different from particles in many respects, most importantly temperature tolerance but also absorption of light and acoustic contrast factor due to compressibility and density.
How resistant a cell is to a temperature of 40°C, depends on the cell type. Human cells thrive in 37°C and can tolerate the increase to 40°C, especially considering the short time they are exposed to it in the microchannel. However, for higher absorptions than the 30 % used in most experiments, or higher laser powers, the temperature at the laser area of incidence can easily increase well above 40°C which was registered in paper II. That means, if faster streaming is realised by increasing the amount of absorbed laser light, a temperature range harmful to cells could be reached. However, for such fast streaming the exposure to the elevated temperature would be short.
Most cell types contain so much water that their light absorption is close that of water, being mostly transparent to the 785 nm laser light. However, cells can be stained and their absorption properties manipulated. The green-fluorescent polystyrene particles were specifically selected to absorb and emit optically far away from the laser wavelength so that the two mechanisms "imaging of streaming" and "heating of ICG" would be disconnected. Staining cells with an IR absorbing dye, for example ICG, could lead

to the cells heating up or becoming small heat sources. Could a temperature increase inside the objects in the channel have an effect on the streaming pattern around the individual object? What that effect looks like would depend on the objects position in the acoustic field, so cells in the channel center would have a different behaviours to cells near the wall.
Further, we can compare particles and cells with respect to their behaviour in the acoustic field. The compressibility and density varies depending on cell type but generally, the compressibility of cells is higher than that of polystyrene, while their density is similar to that of polystyrene [100]. An increase in compressibility leads to a decrease in acoustic contrast factor (compare equ.4.13), which shifts the limits of where acoustic streaming dominates radiation. That means, if a particle is very compressible it needs to be smaller to stream instead of being focused by the radiation force.
Generally, biological cells are awfully unreliable, their culturing is a substantial, time consuming effort which is why the use of polystyrene beads for these first studies was a good option. Eventually, cells need to be introduced to the systems to demonstrate its use for biotechnology.

7.1.2 Modifying the laser light

In terms of modifying the laser light, two aspects come to mind: the wavelength as well as the spot size and shape.
Which wavelength of light to use was one of the first decisions of the project. The choice of 785 nm wavelength, which is not absorbed by water, forced the addition of the absorbing dye, which allowed to tune light absorption. The absorption of light is essential for the temperature increase in the sample which translates to the velocity of the thermoacoustic streaming. The less light is allowed to be absorbed by the liquid, the slower the streaming will be, as demonstrated in publication II. So if the laser is supposed to remain an unchanged variable, the amount of dye grants more flexibility to affect the streaming. An obvious choice depicts the use of 1.5 µm or 3 µm wavelength laser light because they are absorbed by water (fig.2.1).

Coming back to the use of cells, using a wavelength absorbed by water would mean that cells, which are optically mostly water, would experience a temperature increase as large as the water they are in. An exception to this are red blood cells due to their shape, scattering properties and the fact that they contain about 30% haemoglobin. Fluorescent dyes are often toxic to cells and ICG is not commonly used for imaging of cells in culture but rather as a visualisation aid in heart or eye surgery or for tumour removal. Presumably, the amount of time and concentration of ICG, the cells would be exposed to, is low enough to avoid damage. Nevertheless, a study of cell viability,

after having been sorted with thermoacoustic streaming, would be interesting.
Another idea in using the ICG dye was to laminate absorbing and not-absorbing liquid in a channel to only heat specific parts of the liquid. It would be possible to heat only one small region near the wall or in the centre of the channel. Entirely new combinations of temperature gradient and acoustic pressure field would be possible. However, if that leads to new and relevant streaming patterns still needs to be determined. For the sake of biocompatibility, to ensure a more cell-friendly temperature at high laser powers, the ICG dye was the better option.
Thinking about modifying the laser light itself, changing the beam size and shape come to mind. In the experiments for this thesis, the intensity distribution of the beam is Gaussian and the spot round and about 50 µm in diameter. One major advantage of using laser light compared to non-coherent light sources is that it is highly focusable and shapeable. For a 785 nm light source, the smallest spot size possible, can be found by calculating the diameter d_{Airy} of the airy disk:

$$d_{\text{Airy}} = \frac{1.22 \cdot \lambda}{sin(\theta)} \tag{7.1}$$

$$\text{NA} = n \cdot sin(\theta) \tag{7.2}$$

$$sin(\theta) = \theta \text{ (for small angles)} \tag{7.3}$$

$$\Rightarrow \; d_{\text{Airy}} = \frac{1.22 \cdot \lambda}{\text{NA}} \tag{7.4}$$

with $\theta =$ opening angle of the beam (see fig.7.1), NA = numerical aperture and $n = 1$ refractive index of air.
The Rayleigh length z_R describes the distance from the beam waist w_0 to where its area has doubled (fig.7.1).

$$z_R = \frac{\pi \cdot w_0^2}{\lambda} \tag{7.5}$$

Generally, the smaller the beam waist, the shorter the Rayleigh length, which means for larger numerical apertures, the shorter the length of how far into the channel the laser spot will maintain the same size.

It would be interesting to see how an even smaller beam size, meaning a smaller heat source would influence the thermoacoustic streaming. The Rayleigh length of the setup used in this thesis is about 1.5 mm, so about 10 times the channel height. Focussing to a smaller beam size while maintaining a similar spot size throughout the hole channel is possible but one should consider that the alignment becomes more difficult when

NA	d [µm]	z_R [µm]
0.1 (typically 4x)	9.6	56.8
0.3 (10x, used here)	3.2	6.3
1.4 (oil immersion)	0.68	0.28

Table 7.1: Diffraction limit of 785 nm laser light for different numerical apertures and Rayleigh length

the Rayleigh length approaches the channel height. Practically, a better way to position the chip holder in the microscope would be necessary as well as custom alignment tools.

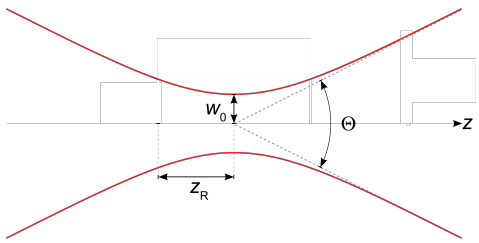

Figure 7.1: The Rayleigh length indicates the distance along the optical axis, until which the spot area has doubled compared to its area at the beam waist w_0. θdenotes the opening angle of the focused beam. Graphic adapted, with permission, from [101].

In addition to the beam size, the beam shape can be altered. Altering the shape of a laser beam can be achieved with an SLM. An SLM can manipulate amplitude, phase and polarization of a laser beam. With a liquid crystal element, certain areas of the beam experience a change in phase or polarization depending on the crystals orientation. That means, light patterning is highly flexible because the crystals can be arranged in many different ways. A typical SLM setup contains an beam expander (a combination of lenses) to match the beam size to the LCD panel. The closer the beam size is to the size of the panel, the better the resolution. The LCD panel is placed in the object plane of the first lens in a 4f-arrangement. The first lens performs a Fourier transformation of the beam pattern and the second transforms from the frequency plane back to the image plane. At the focal point (the Fourier plane) a filter can be placed to clean up the beam and remove frequency artefacts. Because of the high level

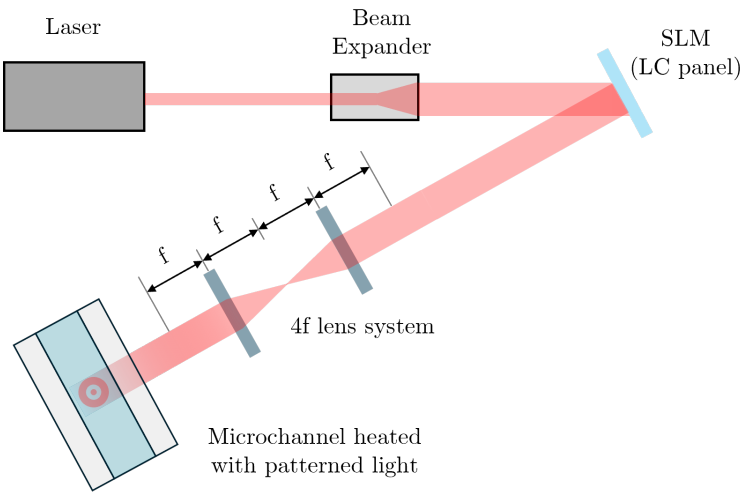

Figure 7.2: SLM example setup

of flexibility of the liquid crystal element, and their fast reaction time, an SLM would add uncountable options of beam shaping to the setup. Any kind of pattern can be created, resulting in any desirable temperature gradient pattern. The resolution limit is the resolution of the liquid crystal panel. Simulations have shown that two spots of laser light, that are placed on opposite sides at the channel walls create entirely new streaming patterns. To give one example, figure 7.3 shows the streaming velocity for the two spots with the first panel having the spots positioned at the same x-position while their offset increases to the last panel.
With respect to timing, liquid crystals react within milliseconds, depending on the system and automation of it. That allows to change between temperature gradient shapes quickly, opening up to include a time component into the temperature gradient studies for thermoacoustic streaming. For example, a path could be programmed to scan over the sample with the laser. Another option could be to quickly change between different streaming patterns, like side vs. center, allowing more control over particle streaming motion.

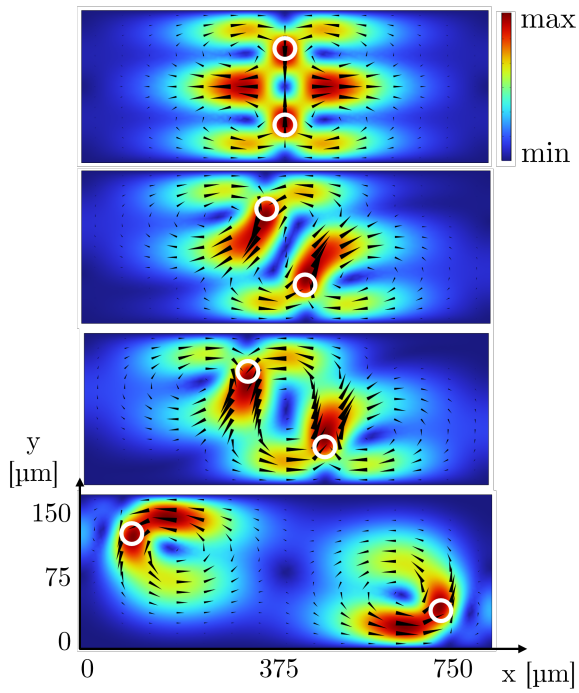

Figure 7.3: Simulated streaming velocity field, if two laser spots (white circle) are positioned on opposite sides of the channel (x-y view, topview). From top to bottom, the offset between the two spots increases from 0 to 750 µm (double the channel width).

7.1.3 Temperature Measurements

One major challenge of the project has been to measure the temperature inside the channel. Two approaches were tested: a temperature sensitive dye, using intensity measurements and temperature sensitive particles, using fluorescence lifetime imaging.

The temperature sensitive dye, namely BCECF, has been used in publication II. It's fluorescence decreases with increasing temperature and therefore, in theory, with a calibration curve of fluorescence at a known temperature, the temperature during the measurement can be calculated. However, the required calibration curves needed to be collected pixel wise because the background illumination is never perfectly even and small deviations decrease the accuracy of the sensitive measurement. Moreover, the BCECF dye bleaches so fast, that each temperature measurement point for each time instance had to be calibrated individually. That results in many repeats, high material use and additional variation in between measurements. Nevertheless, the measurement succeeded and a temperature difference of 20°C could be measured. An unexplained effect of the temperature measurements depict the circular streaks, as discussed in publication II. A more practical and reliable measurement technique is desirable.

Fluorescence lifetime imaging is a possible way to extract temperature information at different locations inside microchannels using molecular tracers or microparticles [102]. After excitation, the decay time of the fluorescence is temperature dependent. For example, a warmer particle will in general have a lower fluorescence intensity than a colder particle after the same amount of time has passed. We explored this possibility and the idea for these measurements was that temperature and thermoacoustic streaming could be measured simultaneously and that the temperature would be mapped throughout the whole volume in the region of interest [103]. One challenge with this technique was that the blue light, exciting the particles had a heating effect on the liquid. Therefore, the excitation time was reduced to a minimum which decreased the temperature increase from 0.15 K to 0.01 K. Detailed calibration curves were necessary to account for uneven background illumination and photobleaching of the particles. Eventually, the rolling shutter of the camera became a problem that we were not able to account for in the time frame of the project. The rolling shutter caused one area of the sample to be illuminated for longer than other areas. For example, the shutter starts to close row by row from the top left corner of the field of view. By the time it reaches the bottom right corner, the particles there have been exposed to the fluorescence excitation light for longer than the ones in the top left corner. A pixel-wise calibration could aid that or the use of a camera with global shutter. Nevertheless, we found that by technical improvements of the optical system we should be

able to measure the temperature with a high precision in the whole volume of the cavity.

Moreover, on-chip sensors to measure the temperature could be an option like a temperature probe that is integrated into the chip's substrate, for example as an additional layer or inside the walls. The difficulty here is to ensure that the resonance of the channel i.e. the acoustic field is not disturbed and that the channel remains transparent for imaging and laser light absorption. The cavity's resonance is sensitive to channel size, which is the reason for high precision requirements in terms of the production of the chips. Practically, the acoustic field inside the channel is never perfect and one major reason is that the channel walls and ceiling are not perfectly smooth and symmetric. The actuation frequency always needs to be tuned to match the specific channel section of interest. Introducing temperature probes into the substrate introduces a material with different acoustic properties than the chip material which will influence the resonance. However, it needs to be tested if the disturbance is small enough to not affect the streaming. In terms of transparency for imaging and heating, the probe would need to be in the wall and not in the floor or ceiling.
Werr et al. have reported a device that measures the temperature of an acoustic trap using integrated thin film resistors that are placed on the side of the acoustic trap on the floor substrate of the chip. They could show successful trapping and achieved a precise temperature measurement [104]. Having a temperature measurement technique that is closer to the cavity could give a better representation of the actual temperature inside the chip than the current placement of the temperature probe. However, such probes on the channel boundaries would not achieve mapping the temperature in 2D or 3D but it could improve the accuracy of the background and reference temperature measurements.

Another way to measure temperature in microfluidic chips is using a holographic microscope. It uses temperature induced refractive index changes to determine the temperature. A resolutions up to 1°C can be achieved, which is about the same range as the temperature sensitive dye used in our experiments. One downside to it is, that it requires an additional optical branch in the setup, that can detect the phase changes induced by the refractive index changes. Moreover, the processing of the data is complex and a good calibration of refractive index and temperature of the liquid is essential.

Lastly, an IR camera could be used to optically measure the temperature. It is feasible to measure high temperature resolution [27]. However, an IR transparent chip material (e.g. Zinc Sulfide) would be necessary, since the glass that the channels are currently fabricated with, absorbs thermal radiation. As of now, fabricating chips out of a material that is transparent both in the visible range and for long-wave thermal radiation has not been achieved.

7.1.4 Faster buildup and decay measurements

In publication II, the transient development of the thermoacoustic streaming has been measured. However, one result was, that a frame rate of 10 Hz is not fast enough to capture the effect in detail. A high-speed camera that can achieve higher frame rate than the 100 fps could give more insights into how fast the thermoacoustic streaming builds up and decays. A challenge with short frame rates is to achieve sufficient image quality for post processing since the exposure time must be very short. With the current setup, the particle brightness is just still resolvable with 2D particle identification algorithms, while it is not sufficient for 3D. A more sensitive camera that can also image with sufficient frame rates and/or an improved optical setup with perhaps more intense illumination and lower losses between sample and camera could allow faster imaging.

7.1.5 Automated particle or cell sorting

In publication II we showed that the laser-induced temperature field can be used to accelerate individual particles to the channel side while nearby particles remain in their position. That answered the research question, if thermoacoustic streaming can be used for particle sorting to some degree: yes, specific particles can be individually moved. However, selecting a particle and moving it to a specific location automatically is a more elaborate task. Ideally, if a particle or cell of interest approaches the heat source, the object would be detected, its location determined and the required temperature gradient and illumination duration calculated to move that object to a desired location in the channel.

For this ambitious goal, many challenges must be overcome: First of all, the microchannel's acoustic field would need to be well mapped, ideally for different frequencies. This is a goal that probably the entire acoustofluidic community desires, since the acoustic field is the fundamental driving mechanism. Secondly, a detection mechanism is necessary, such as an optical element detecting the desired object, like a fluorescently marked cell. Next, several temperature gradients and their effect on the thermoacoustic streaming would have to be tested and mapped. Also, the straight channel used here would need to be replaced with a trifurcated channel, to allow the positioned object to take a specific exit. Lastly, these various elements, detection, calculation of where the particle should be moved to and which combination of acoustic and temperature field that requires, would have to be automated.

Concludingly, approaching each challenge individually and simplifying certain elements, for example the acoustic mapping or choosing easily detectable objects at first, could lead to a thermoacoustic lab on a chip sorting device.

References

[1] R. M. Lequin, "Enzyme immunoassay (eia)/enzyme-linked immunosorbent assay (elisa)," Clinical chemistry, vol. 51, no. 12, pp. 2415–2418, 2005.

[2] A. Urbansky, F. Olm, S. Scheding, T. Laurell, and A. Lenshof, "Label-free separation of leukocyte subpopulations using high throughput multiplex acoustophoresis," Lab on a Chip, vol. 19, no. 8, pp. 1406–1416, 2019.

[3] V. R. Misko, L. Baraban, D. Makarov, T. Huang, P. Gelin, I. Mateizel, K. Wouters, N. De Munck, F. Nori, and W. De Malsche, "Selecting active matter according to motility in an acoustofluidic setup: self-propelled particles and sperm cells," Soft Matter, vol. 19, no. 44, pp. 8635–8648, 2023.

[4] Z. Wang, H. Wang, R. Becker, J. Rufo, S. Yang, B. E. Mace, M. Wu, J. Zou, D. T. Laskowitz, and T. J. Huang, "Acoustofluidic separation enables early diagnosis of traumatic brain injury based on circulating exosomes," Microsystems & nanoengineering, vol. 7, no. 1, p. 20, 2021.

[5] P. B. Muller and H. Bruus, "Theoretical study of time-dependent, ultrasound-induced acoustic streaming in microchannels," Physical Review E, vol. 92, no. 6, p. 063018, 2015.

[6] E. Corato, D. van Assche, O. Jakobsson, W. Qiu, and P. Augustsson, "Thermoacoustic streaming in a linear temperature gradient," Physical Review E, vol. 112, no. 2, p. 025102, 2025.

[7] W. Qiu, J. H. Joergensen, E. Corato, H. Bruus, and P. Augustsson, "Fast microscale acoustic streaming driven by a temperature-gradient-induced nondissipative acoustic body force," Physical Review Letters, vol. 127, no. 6, p.

064501, 2021. [Online]. Available: https://www.ncbi.nlm.nih.gov/pubmed/34420350

[8] A. Kundt, "Über eine neue art akustischer staubfiguren und über die anwendung derselben zur bestimmung der schallgeschwindigkeit in festen körpern und gasen," Annalen der Physik, vol. 127, no. 4, pp. 497–523, 1866. [Online]. Available: http://onlinelibrary.wiley.com/doi/10.1002/andp.18662030402/abstract

[9] J. P. Zymny, in Best of Unisinn. Lektora, 2020, ch. Physik ist schön. Niemand braucht Physik.

[10] Jan Phillip Zymny. (2013) *Physik ist doof*, 5. bielefelder hörsaal slam. https://www.youtube.com/watch?v=lIh55O7wqAQ. [Accessed 2025-11-26].

[11] S. Prahl. (2018) Optical absorption of water compendium. [Online]. Available: https://omlc.org/spectra/water/abs/index.html

[12] D. J. Segelstein, "The complex refractive index of water," 1981.

[13] R. Barnkob, "Acoustofluidics in microsystems: investigation of resonances," Ph.D. dissertation, Master's thesis, DTU Nanotech, Department of Micro and Nano technology, 2009.

[14] P. Augustsson, "On microchannel acoustophoresis - experimental considerations and life science applications," Doctoral Thesis (compilation), Division for Biomedical Engineering, 2011.

[15] R. Shiell and I. McNab, Pedrottis' Introduction to Optics, 4th ed., with contributions by Matthew Romerein, Ed. Cambridge, UK: Cambridge University Press & Assessment, 2024, fourth edition.

[16] D. L. Pavia, G. M. Lampman, G. S. Kriz, J. R. Vyvyan et al., Introduction to Spectroscopy. Cengage learning Stamford, CT, 2015.

[17] W. Demtröder, Laser Spectroscopy 1: Basic Principles. Springer, 2014, vol. 4.

[18] E. J. G. Peterman, F. Gittes, and C. F. Schmidt, "Laser-induced heating in optical traps," Biophysical Journal, vol. 84, no. 2, pp. 1308–1316, 2003. [Online]. Available: <GotoISI>://WOS:000183123700055

[19] H. Bruus, Theoretical Microfluidics. Oxford: Oxford University Press, 2007.

[20] COMSOL Blog, "Tears of wine and the marangoni effect," https://www.comsol.com/blogs/tears-of-wine-and-the-marangoni-effect, 2020, accessed: 2026-01-01.

[21] J. Enger, M. Goksör, K. Ramser, P. Hagberg, and D. Hanstorp, "Optical tweezers applied to a microfluidic system," Lab on a Chip, vol. 4, no. 3, pp. 196–200, 2004.

[22] A. Ashkin, J. M. Dziedzic, J. E. Bjorkholm, and S. Chu, "Observation of a single-beam gradient force optical trap for dielectric particles," Opt Lett, vol. 11, no. 5, p. 288, 1986. [Online]. Available: https://www.ncbi.nlm.nih.gov/pubmed/19730608

[23] X. Wang, S. Chen, M. Kong, Z. Wang, K. D. Costa, R. A. Li, and D. Sun, "Enhanced cell sorting and manipulation with combined optical tweezer and microfluidic chip technologies," Lab on a Chip, vol. 11, no. 21, pp. 3656–3662, 2011.

[24] I. A. Favre-Bulle and E. K. Scott, "Optical tweezers across scales in cell biology," Trends in Cell Biology, vol. 32, no. 11, p. 932–946, 2022, 7v6sn Times Cited:30 Cited References Count:137. [Online]. Available: <GotoISI>://WOS:000912944600005

[25] J. P. Brody and P. Yager, "Diffusion-based extraction in a microfabricated device," Sensors and Actuators A: Physical, vol. 58, no. 1, pp. 13–18, 1997.

[26] H. Schlichting and K. Gersten, Boundary-layer theory. springer, 2016.

[27] L. Li, E. Wu, K. Jia, and K. Yang, "Temperature field regulation of a droplet using an acoustothermal heater," Lab on a Chip, vol. 21, no. 16, pp. 3184–3194, 2021.

[28] M. A. Burguillos, C. Magnusson, M. Nordin, A. Lenshof, P. Augustsson, M. J. Hansson, E. Elmér, H. Lilja, P. Brundin, T. Laurell, and T. Deierborg, "Microchannel acoustophoresis does not impact survival or function of microglia, leukocytes or tumor cells," PLoS ONE, vol. 8, no. 5, p. e64233, 2013. [Online]. Available: https://doi.org/10.1371/journal.pone.0064233

[29] M. Wiklund, "Acoustofluidics 12: Biocompatibility and cell viability in microfluidic acoustic resonators," Lab Chip, vol. 12, no. 11, pp. 2018–28, 2012. [Online]. Available: http://www.ncbi.nlm.nih.gov/pubmed/22562376

[30] E. F. F. Chladni, Entdeckungen über die Theorie des Klanges. Zentralantiquariat der Deutschen Demokratischen Republik, 1787. [Online]. Available: https://archive.org/details/entdeckungenuber00chla/page/n9/mode/2up

[31] W. H. Stone, Elementary Lessons on Sound. Macmillan & Company, 1879.

[32] M. Savart, "Recherches sur les vibrations normales," Anns Chim. Phys, vol. 36, pp. 187–208, 1827.

[33] M. Faraday, "On a peculiar class of acoustical figures, and on certain forms assumed by groups of particles upon vibrating elastic surfaces," Philosophical Transactions of the Royal Society of London, vol. 121, pp. 299–340, 1831. [Online]. Available: http://rsta.royalsocietypublishing.org/content/325/1583/local/back-matter.pdfhttp://www.jstor.org/stable/10.2307/107936

[34] L. Rayleigh, "On the circulation of air observed in kundt's tubes, and on some allied acoustical problems," Philosophical Transactions of the Royal Society of London, vol. 175, no. 0, pp. 1–21, Dec. 1884. [Online]. Available: http://www.jstor.org/stable/10.2307/109434

[35] H. Schlichting, "Berechnung ebener periodischer grenzschichtstromungen," Physikalische Zeit., vol. 33, pp. 327–335, 1932.

[36] G. G. Stokes et al., "On the effect of the internal friction of fluids on the motion of pendulums," 1851.

[37] W. M. Nyborg, "Acoustic streaming, physical acoustics," Academic Press, vol. 2, pp. 265–331, 1965.

[38] C. Eckart, "Vortices and streams caused by sound waves," Physical review, vol. 73, no. 1, pp. 68–76, 1948. [Online]. Available: http://prola.aps.org/abstract/PR/v73/i1/p68_1

[39] J. Lighthill, "Acoustic streaming," Journal of sound and vibration, vol. 61, no. 3, pp. 391–418, 1978.

[40] J. Rufo, F. Cai, J. Friend, M. Wiklund, and T. J. Huang, "Acoustofluidics for biomedical applications," Nature Reviews Methods Primers, vol. 2, no. 1, p. 30, 2022.

[41] P. Li and T. J. Huang, "Applications of acoustofluidics in bioanalytical chemistry," Analytical chemistry, vol. 91, no. 1, pp. 757–767, 2018.

[42] W. Li, Z. Yao, T. Ma, Z. Ye, K. He, L. Wang, H. Wang, Y. Fu, and X. Xu, "Acoustofluidic precise manipulation: Recent advances in applications for micro/nano bioparticles," Advances in Colloid and Interface Science, vol. 332, p. 103276, 2024.

[43] R. Soller, O. Jakobsson, and P. Augustsson, "In-line enrichment of cancer cells from whole blood by cell self-organization in acoustic fields," Analytical Chemistry, 2025.

[44] Z. Saeidpour, M. Bouloorchi, S. Javadizadeh, Z. Habibi, and M. Badieirostami, "Acoustofluidic-based motile sperm isolation using microvortices," in 2023 30th National and 8th International Iranian Conference on Biomedical Engineering (ICBME). IEEE, 2023, pp. 115–120.

[45] J. Gai, "Acoustofluidics for assisted reproductive technologies," Ph.D. dissertation, Monash University, 2022.

[46] A. Lenshof, C. Johannesson, M. Evander, J. Nilsson, and T. Laurell, "Acoustic cell manipulation," Microtechnology for cell manipulation and sorting, pp. 129–173, 2016.

[47] J. Friend and L. Y. Yeo, "Microscale acoustofluidics: Microfluidics driven via acoustics and ultrasonics," Reviews of Modern Physics, vol. 83, no. 2, pp. 647–704, 2011.

[48] M. Hossein and P. Angeli, "A review of acoustofluidic separation of bioparticles," Biophysical Reviews, vol. 15, no. 4, pp. 511–528, 2023. [Online]. Available: https://link.springer.com/article/10.1007/s12551-023-01112-2

[49] M. Wu, A. Ozcelik, J. Rufo, Z. Wang, R. Fang, and T. Jun Huang, "Acoustofluidic separation of cells and particles," Microsystems & Nanoengineering, vol. 5, no. 1, 2019. [Online]. Available: https://doaj.org/article/9aeaa58817fb44ce90de985fa6b04ed2

[50] M. Evander, L. Johansson, T. Lilliehorn, J. Piskur, M. Lindvall, S. Johansson, M. Almqvist, T. Laurell, and J. Nilsson, "Noninvasive acoustic cell trapping in a microfluidic perfusion system for online bioassays," Anal Chem, vol. 79, no. 7, pp. 2984–91, 2007. [Online]. Available: http://www.ncbi.nlm.nih.gov/entrez/query.fcgi?cmd=Retrieve&db=PubMed&dopt=Citation&list_uids=17313183

[51] M. Evander and J. Nilsson, "Acoustofluidics 20: applications in acoustic trapping," Lab Chip, vol. 12, no. 22, pp. 4667–76, 2012. [Online]. Available: http://www.ncbi.nlm.nih.gov/pubmed/23047553

[52] B. Hammarström, M. Evander, H. Barbeau, M. Bruzelius, J. Larsson, T. Laurell, and J. Nilsson, "Non-contact acoustic cell trapping in disposable glass capillaries," Lab on a chip, vol. 10, no. 17, pp. 2251–7, 2010. [Online]. Available: http://pubs.rsc.org/en/content/articlehtml/2010/lc/c004504ghttp://pubs.rsc.org/en/content/articlepdf/2010/lc/c004504g

[53] B. Hammarstrom, T. Laurell, and J. Nilsson, "Seed particle-enabled acoustic trapping of bacteria and nanoparticles in continuous flow systems," Lab Chip, vol. 12, no. 21, pp. 4296–304, 2012. [Online]. Available: https://www.ncbi.nlm.nih.gov/pubmed/22955667

[54] A. Ku, H. C. Lim, M. Evander, H. Lilja, T. Laurell, S. Scheding, and Y. Ceder, "Acoustic enrichment of extracellular vesicles from biological fluids," Analytical Chemistry, vol. 90, no. 13, pp. 8011–8019, 2018. [Online]. Available: <GotoISI>://WOS:000438008600032

[55] M. Havers, "Sowing the seeds of acoustic trapping: Towards rapid isolation of extracellular vesicles," Ph.D. dissertation, Lund University, 2025.

[56] M. Gerlt and T. Laurell, "Acoustofluidic chromatography for extracellular vesicle enrichment from 4 µl blood plasma samples," Analytical Chemistry, vol. 97, pp. 6049 – 6058, 2025.

[57] P. Augustsson, J. T. Karlsen, H.-W. Su, H. Bruus, and J. Voldman, "Iso-acoustic focusing of cells for size-insensitive acousto-mechanical phenotyping," Nature Communications, vol. 7, no. 1, p. 11556, Sep. 2016. [Online]. Available: https://www.nature.com/articles/ncomms11556

[58] P. Augustsson, C. Magnusson, M. Nordin, H. Lilja, and T. Laurell, "Microfluidic, label-free enrichment of prostate cancer cells in blood based on acoustophoresis," Analytical Chemistry, vol. 84, no. 18, pp. 7954–7962, 2012. [Online]. Available: <GotoISI>://WOS:000308829700054

[59] X. Ding, Z. Peng, S.-C. S. Lin, M. Geri, S. Li, P. Li, Y. Chen, M. Dao, S. Suresh, and T. J. Huang, "Cell separation using tilted-angle standing surface acoustic waves," PNAS, vol. 111, no. 36, pp. 12 992–12 997, 2014. [Online]. Available: http://www.pnas.org/content/111/36/12992.abstracthttp://www.pnas.org/content/111/36/12992.full.pdf

[60] C. Magnusson, P. Augustsson, E. Undvall Anand, A. Lenshof, A. Josefsson, K. Welén, A. Bjartell, Y. Ceder, H. Lilja, and T. Laurell, "Acoustic enrichment of heterogeneous circulating tumor cells and clusters from metastatic prostate

cancer patients," Analytical Chemistry, vol. 96, no. 18, p. 6914–6921, 2024. [Online]. Available: https://doi.org/10.1021/acs.analchem.3c05371

[61] M. Antfolk, S. H. Kim, S. Koizumi, T. Fujii, and T. Laurell, "Label-free single-cell separation and imaging of cancer cells using an integrated microfluidic system," Sci Rep, vol. 7, p. 46507, 2017. [Online]. Available: https://www.ncbi.nlm.nih.gov/pubmed/28425472

[62] M. X. Wu, Y. S. Ouyang, Z. Y. Wang, R. Zhang, P. H. Huang, C. Y. Chen, H. Li, P. Li, D. Quinn, M. Dao, S. Suresh, Y. Sadovsky, and T. J. Huang, "Isolation of exosomes from whole blood by integrating acoustics and microfluidics," Proceedings of the National Academy of Sciences of the United States of America, vol. 114, no. 40, pp. 10 584–10 589, 2017. [Online]. Available: <GotoISI>://WOS:000412130500047

[63] X. He, F. Ren, Y. Wang, Z. Zhang, J. Zhou, J. Huang, S. Cao, J. Dong, R. Wang, M. Wu et al., "Acoustofluidic-based microscopic examination for automated and point-of-care urinalysis," Lab on a Chip, vol. 24, no. 15, pp. 3679–3689, 2024.

[64] J. Gai, R. Nosrati, and A. Neild, "High dna integrity sperm selection using surface acoustic waves," Lab on a Chip, vol. 20, no. 22, pp. 4262–4272, 2020.

[65] S. Abbasi, B. Barahimi, S. Darbari, I. Halvaei, M. Zabetian, R. Nosrati, A. Neild, and M. K. Moravvej-Farshi, "Acoustotaxis-based pump-less separation of highly motile human sperm by a saw-in-capillary acoustofluidic platform," Sensors and Actuators A: Physical, vol. 381, p. 116069, 2025.

[66] T. Franke, S. Braunmüller, L. Schmid, A. Wixforth, and D. a. Weitz, "Surface acoustic wave actuated cell sorting (sawacs)," Lab on a chip, vol. 10, no. 6, pp. 789–94, 2010. [Online]. Available: http://www.ncbi.nlm.nih.gov/pubmed/20221569http://pubs.rsc.org/en/content/articlepdf/2010/lc/b915522h

[67] O. Jakobsson, C. Grenvall, M. Nordin, M. Evander, and T. Laurell, "Acoustic actuated fluorescence activated sorting of microparticles," Lab on a Chip, vol. 14, no. 11, pp. 1943–1950, 2014. [Online]. Available: <GotoISI>://WOS:000335925400020

[68] L. Ren, S. Yang, P. Zhang, Z. Qu, Z. Mao, P. H. Huang, Y. Chen, M. Wu, L. Wang, P. Li, and T. J. Huang, "Standing surface acoustic wave (ssaw)-based fluorescence-activated cell sorter," Small, vol. 14, no. 40, p. e1801996, 2018. [Online]. Available: https://www.ncbi.nlm.nih.gov/pubmed/30168662

[69] M. Wiklund, R. Green, and M. Ohlin, "Acoustofluidics 14: Applications of acoustic streaming in microfluidic devices," Lab on a Chip, vol. 12, no. 14, p. 2438, 2012.

[70] B. G. Winckelmann and H. Bruus, "Theory and simulation of electroosmotic suppression of acoustic streaming," The Journal of the Acoustical Society of America, vol. 149, no. 6, pp. 3917–3928, 2021.

[71] J. S. Bach and H. Bruus, "Suppression of acoustic streaming in shape-optimized channels," Physical Review Letters, vol. 124, no. 21, 2020. [Online]. Available: <GotoISI>://WOS:000535679100022

[72] D. Van Assche, E. Reithuber, W. Qiu, T. Laurell, B. Henriques-Normark, P. Mellroth, P. Ohlsson, and P. Augustsson, "Gradient acoustic focusing of sub-micron particles for separation of bacteria from blood lysate," Scientific Reports, vol. 10, no. 1, p. 3670, 2020. [Online]. Available: https://www.ncbi.nlm.nih.gov/pubmed/32111864

[73] J. T. Karlsen, W. Qiu, P. Augustsson, and H. Bruus, "Acoustic streaming and its suppression in inhomogeneous fluids," Physical Review Letters, vol. 120, no. 5, p. 054501, 2018. [Online]. Available: https://www.ncbi.nlm.nih.gov/pubmed/29481204

[74] L. Capretto, W. Cheng, M. Hill, and X. Zhang, "Micromixing within microfluidic devices," Microfluidics: technologies and applications, pp. 27–68, 2011.

[75] C. Zhang, X. Guo, P. Brunet, M. Costalonga, and L. Royon, "Acoustic streaming near a sharp structure and its mixing performance characterization," Microfluidics and Nanofluidics, vol. 23, no. 9, p. 104, 2019.

[76] N. Garg, T. M. Westerhof, V. Liu, R. Liu, E. L. Nelson, and A. P. Lee, "Whole-blood sorting, enrichment and in situ immunolabeling of cellular subsets using acoustic microstreaming," Microsystems & Nanoengineering, vol. 4, no. 1, pp. 1–9, 2018.

[77] P.-H. Huang, C. Y. Chan, P. Li, Y. Wang, N. Nama, H. Bachman, and T. J. Huang, "A sharp-edge-based acoustofluidic chemical signal generator," Lab on a Chip, vol. 18, no. 10, pp. 1411–1421, 2018.

[78] L. P. Gor'kov, "On the forces acting on a small particle in an acoustical field in an ideal fluid," Soviet Physics Doklady, vol. 6, no. 9, pp. 773–775, 1962. [Online]. Available: http://adsabs.harvard.edu/abs/1962SPhD....6..773G

[79] H. Bruus, "Acoustofluidics 7: The acoustic radiation force on small particles," Lab on a chip, vol. 12, no. 6, pp. 1014–21, 2012. [Online]. Available: http://www.ncbi.nlm.nih.gov/pubmed/22349937http://pubs.rsc.org/en/content/articlepdf/2012/lc/c2lc21068a

[80] L. Johansson, S. Johansson, F. Nikolajeff, and S. Thorslund, "Effective mixing of laminar flows at a density interface by an integrated ultrasonic transducer," Lab on a chip, vol. 9, no. 2, pp. 297–304, 2009. [Online]. Available: http://www.ncbi.nlm.nih.gov/pubmed/19107288http://pubs.rsc.org/en/content/articlepdf/2009/lc/b815114h

[81] S. Deshmukh, Z. Brzozka, T. Laurell, and P. Augustsson, "Acoustic radiation forces at liquid interfaces impact the performance of acoustophoresis," Lab on a Chip, vol. 14, no. 17, pp. 3394–3400, 2014. [Online]. Available: <GotoISI>://WOS:000340204300034

[82] J. T. Karlsen, P. Augustsson, and H. Bruus, "Acoustic force density acting on inhomogeneous fluids in acoustic fields," Physical Review Letters, vol. 117, no. 11, p. 114504, Sep. 2016. [Online]. Available: https://www.ncbi.nlm.nih.gov/pubmed/27661695

[83] A. Aleksandrov, A. Kochetkov, and I. Demin, "Speed of sound in ethyl alcohol," Thermophysical Properties of Substances and Materials [in Russian], Izd. Standartov, Moscow, no. 14, pp. 92–96, 1980.

[84] J. Resa, C. Gonzalez, J. Goenaga, and M. Iglesias, "Influence of temperature on ultrasonic velocity measurements of ethanol+ water+ ethyl acetate mixtures," Physics and Chemistry of Liquids, vol. 43, no. 1, pp. 65–89, 2005.

[85] Engineering ToolBox. (2018) Ethanol - density and specific weight vs. temperature and pressure. https://www.engineeringtoolbox.com/ethanol-ethyl-alcohol-density-specific-weight-temperature-pressure-d_2028.html. [Accessed 2025-12-02].

[86] "Ethanol speed of sound: Datasheet from "dortmund data bank (ddb) – thermophysical properties edition 2014" in springermaterials (https://materials.springer.com/thermophysical/docs/sos_c11)," copyright 2010-2014 Springer-Verlag Berlin Heidelberg & DDBST GmbH, Oldenburg, Germany. [Online]. Available: https://materials.springer.com/thermophysical/docs/sos_c11

[87] Engineering ToolBox. (2004) Water - speed of sound vs. temperature. https://www.engineeringtoolbox.com/sound-speed-water-d_598.html. [Accessed 2025-12-02].

[88] Engineering Toolbox. (2004) Water - density and specific weight. https://www.engineeringtoolbox.com/water-density-specific-weight-d_595.html. [Accessed 2025-12-02].

[89] B. G. Winckelmann and H. Bruus, "Acoustic radiation force on a heated spherical particle in a fluid including scattering and microstreaming from a standing ultrasound wave," Physical Review E, vol. 108, no. 3, p. 035108, 2023.

[90] Fluoro-Max Dyed Green Aqueous Fluorescent Particles, 1.1µm, [Accessed 2026-01-11]. [Online]. Available: https://www.thermofisher.com/order/catalog/product/G0100

[91] I. AAT Bioquest. (2025) Quest graph™ spectrum [icg (indocyanine green)]. https://www.aatbio.com/fluorescence-excitation-emission-spectrum-graph-viewer/icg_indocyanine_green. [Accessed 2025-09-29].

[92] C. A. Sweden, "Software for multiphysics simulations," 2024, [Accessed: (11-March 2025)]. [Online]. Available: www.comsol.com

[93] F. Martens, W. Qiu, O. Jakobsson, C. Cierpka, A. Ehn, and P. Augustsson, "Configurable thermoacoustic streaming by laser-induced temperature gradients," Phys. Rev. Appl., vol. 23, p. 024043, Feb 2025. [Online]. Available: https://link.aps.org/doi/10.1103/PhysRevApplied.23.024043

[94] C. Cierpka, R. Segura, R. Hain, and C. J. Kähler, "A simple single camera 3c3d velocity measurement technique without errors due to depth of correlation and spatial averaging for microfluidics," Measurement Science and Technology, vol. 21, no. 4, p. 045401, 2010.

[95] R. Barnkob, C. J. Kähler, and M. Rossi, "General defocusing particle tracking," Lab on a Chip, vol. 15, no. 17, pp. 3556–3560, 2015. [Online]. Available: <GotoISI>://WOS:000359555400015

[96] R. Barnkob and M. Rossi, "General defocusing particle tracking: fundamentals and uncertainty assessment," Experiments in Fluids, vol. 61, no. 4, p. 110, Apr. 2020.

[97] R. Barnkob, C. Cierpka, M. Chen, S. Sachs, P. Mäder, and M. Rossi, "Defocus particle tracking: a comparison of methods based on model functions, cross-correlation, and neural networks," Measurement Science and Technology, vol. 32, no. 9, p. 094011, 2021.

[98] R. Barnkob and M. Rossi, "Defocustracker v2.0.0," 2024, https://defocustracking.com/ [Accessed: (10-June-2024)]. [Online]. Available: https://defocustracking.com/

[99] N. López-Gil, F. J. Rucker, L. R. Stark, M. Badar, T. Borgovan, S. Burke, and P. B. Kruger, "Effect of third-order aberrations on dynamic accommodation," Vision research, vol. 47, no. 6, pp. 755–765, 2007.

[100] D. Hartono, Y. Liu, P. L. Tan, X. Y. S. Then, L.-Y. L. Yung, and K.-M. Lim, "On-chip measurements of cell compressibility via acoustic radiation," Lab on a chip, vol. 11, no. 23, p. 4072, 2011. [Online]. Available: http://www.ncbi.nlm.nih.gov/pubmed/22020269http://pubs.rsc.org/en/content/articlepdf/2011/lc/c1lc20687g

[101] R. Hermans, "Gaussian beam waist diagram," Wikimedia Commons, 2009, based on work by Bob Mellish. Licensed under CC BY-SA 3.0. [Online]. Available: https://commons.wikimedia.org/wiki/File:GaussianBeamWaist.svg

[102] Z. Deng, J. König, and C. Cierpka, "A combined velocity and temperature measurement with an led and a low-speed camera," Measurement Science and Technology, vol. 33, no. 11, p. 115301, 2022.

[103] F. Martens, W. Qiu, P. Augustsson, and C. Cierpka, "On the characterization of the velocity and temperature fields in an acoustically driven microchannel with non-uniform temperature distribution," in Proceedings of the 30th Fachtagung Experimentelle Strömungsmechanik. München, Germany: Deutsche Gesellschaft für Laser-Anemometrie (GALA e.V.), Sep. 2023, pp. 15–1–15–7.

[104] G. Werr, Z. Khaji, M. Ohlin, M. Andersson, L. Klintberg, S. S. Searle, K. Hjort, and M. Tenje, "Integrated thin film resistive sensors for in situ temperature measurements in an acoustic trap," Journal of Micromechanics and Microengineering, vol. 29, no. 9, p. 095003, 2019.

Printed by Tryckeriet i E-huset, Lund 2026

About the author

Instead of becoming a high school teacher, as her bachelor's degree had intended, Franziska Martens was captivated by biomedical engineering during her thesis at the University of Hannover which conveniently aligned with her passion for lasers perfectly.
Her master's thesis on Raman spectroscopy and laser-assisted bioprinting at the Fraunhofer Institute for Laser Technology in Aachen wasn't quite finished when she embarked on the first steps of her next journey: a PhD in biomedical engineering about laser heating of acoustofluidic microchannels at Lund University in Sweden.

This work is about how laser light can be utilized to heat a fluid in an acoustofluidic microchannel, what effect that has on the acoustic streaming pattern in the fluid and how that synergy of light and ultrasound can be useful to the field of biotechnology.

LUND UNIVERSITY

ISBN: 978-91-8104-812-4 (print)
ISBN: 78-91-8104-813-1 (electronic)
ISRN: LUTEDX/TEEM–1150–SE
Report-nr: 1/26